CHARACTERIZATION OF GULF OF MEXICO CLAY USING AUTOMATED TRIAXIAL TESTING

A Thesis

by

MADHURI MURALI

Submitted to the Office of Graduate Studies of
Texas A&M University
in partial fulfillment of the requirements for the degree of

MASTER OF SCIENCE

December 2011

Major Subject: Civil Engineering

Characterization of Gulf of Mexico clay using Automated Triaxial testing.

CHARACTERIZATION OF GULF OF MEXICO CLAY USING AUTOMATED TRIAXIAL TESTING

A Thesis

by

MADHURI MURALI

Submitted to the Office of Graduate Studies of
Texas A&M University
in partial fulfillment of the requirements for the degree of

MASTER OF SCIENCE

Approved by:

Chair of Committee,	Giovanna Biscontin
Committee Members,	José M. Roësset
	Frederick Chester
Head of Department,	John M. Niedzwecki

December 2011

Major Subject: Civil Engineering

ABSTRACT

Characterization of Gulf of Mexico clay using Automated Triaxial testing. (December 2011)

Madhuri Murali, B.Tech, National Institute of Technology, Tiruchirapalli

Chair of Advisory Committee: Dr. Giovanna Biscontin

With increasing development in the oil and gas industry, exploration and production is continuously moving deeper off the continental shelf and onto the continental slopes. This increases the risk of submarine slope failures leading to damage of offshore structures. Thus there is a need to study and understand properties of offshore marine clays on slopes. This study was undertaken in order to understand better the characteristics of a sub-marine clay deposit taken from the Gulf of Mexico.

This thesis presents the results of SHANSEP triaxial testing performed on undisturbed samples of Gulf of Mexico clay. Background information is given about the clay, the sampling program and the laboratory testing program. The GEOTAC Truepath automated stress path triaxial apparatus implemented for this research and the laboratory procedures used are described in detail. Data is summarized from the various types of tests run on the clay ($\mathrm{CK_oU}$ compression and extension, CIU compression and extension tests, consolidations tests) and the stress history of the deposit is evaluated.

The SHANSEP reconsolidation technique was used for a comprehensive program of $\mathrm{K_o}$consolidated-undrained ($\mathrm{CK_oU}$) triaxial compression and extension tests at over-consolidation ratios (OCR) ranging from one to eight. Eighteen tests were run on jumbo piston core samples from one particular core. The consolidation phase of these SHANSEP tests provided most of the preconsolidation pressure values used to establish the stress history at the test site. These tests were used to estimate the in situ Ko and how it varies with OCR. The undrained shear phase of the tests provides detailed information on the values

of S and m for use in the SHANSEP undrained strength equation, $S_u/\sigma'_{vo} = S(OCR)^m$, effective stress failure envelopes, etc.

ACKNOWLEDGMENTS

The author wishes to acknowledge the following people:

Dr. Giovanna Biscontin, my thesis advisor, for her unwavering support and guidance throughout the course of this project.

Dr. José M. Roësset and Dr. Frederick Chester, my committee members, for their valuable comments and assistance.

Cassandra Rutherford, my Ph.D. mentor, for giving me advice, company in the laboratory and for making me laugh when nothing was working.

I would like to thank all my friends within this department, for making geotechnical engineering the best field to study in. I would also like to thank my friends outside of the department, for making life a whole lot easier when I really needed it.

Lastly I would like to express gratitude to my family for all their love and support: mama, papa, Mayuri and Varenya Kumar.

TABLE OF CONTENTS

Page

ABSTRACT iii

ACKNOWLEDGMENTS v

TABLE OF CONTENTS vi

LIST OF TABLES ix

LIST OF FIGURES x

1. INTRODUCTION 1

1.1 Need for testing 1
1.2 Submarine landslides 2
1.3 Research objectives 4
1.4 Methodology 5
1.4.1 Equipment setup 5
1.4.2 Experimental plan 7
1.4.3 Marine soil samples 7
1.5 Organization 8

2. LITERATURE REVIEW 10

2.1 Introduction 10
2.2 Shear strength 10
2.3 Triaxial tests 11
2.3.1 Consolidated drained 14
2.3.2 Consolidated undrained 14
2.3.3 Unconsolidated undrained 15
2.4 Stress paths 15
2.5 Controlling stress paths during consolidation and shear 19
2.6 Saturation and back pressure 19
2.7 Consolidation in triaxial tests 24
2.8 Triaxial shear 28
2.9 Sample disturbance 30
2.10 Reconsolidation procedures for mitigating sample disturbance: SHANSEP and recompression 31

3. CHARACTERISTICS OF GULF OF MEXICO CLAY 37

Page

3.1 Introduction . . . 37
3.2 Geology and provenance . . . 37
3.3 Multi sensor core logging (MSCL) . . . 40
3.4 Classification and index properties . . . 42
3.4.1 Natural water content, atterberg limits, plasticity chart . . . 42
3.4.2 Strength . . . 44
3.4.3 Grain size distribution and specific gravity . . . 44
3.5 Pre-consolidation pressure . . . 46

4. GEOTAC TRUEPATH AUTOMATED STRESS PATH SYSTEM: EQUIPMENT AND TESTING PROCEDURES . . . 49

4.1 Equipment and software . . . 49
4.2 Testing procedures . . . 51
4.3 Data reduction . . . 53
4.4 Comments on testing problems and quality of test data . . . 54
4.4.1 Equipment problems . . . 54
4.4.2 Procedural problems . . . 57
4.4.3 Overall quality of test data . . . 58

5. TEST RESULTS ON GULF OF MEXICO CLAY . . . 59

5.1 $\mathrm{CK_oU}$ tests . . . 59
5.1.1 Stress-strain characteristics . . . 59
5.1.2 Normalized undrained shear parameters from $\mathrm{CK_oU}$ testing . . . 62
5.1.3 Effective stress behavior . . . 67
5.1.4 Undrained moduli . . . 73
5.1.5 Coefficient of earth pressure at rest . . . 77
5.2 Results from CIU tests . . . 78
5.2.1 Stress-strain and excess pore pressure characteristics . . . 78
5.2.2 Effective stress behavior . . . 81

6. CONCLUSION AND RECOMMENDATION . . . 85

6.1 Conclusion . . . 85
6.2 Recommendations for future work . . . 86

REFERENCES . . . 87

APPENDIX A. EQUIPMENT AND PROCEDURES . . . 90

A.1 Components of the GEOTAC TruePath automated stress path system . . . 90
A.1.1 The triaxial cell . . . 90
A.1.2 Load frame . . . 94

Page

A.1.3 DigiFlow pressure-volume pumps . . . 96
A.1.4 Instrumentation . . . 100
A.1.5 Computer, data acquisition system and control software . . . 103
A.2 Control algorithm . . . 106
A.2.1 General operation . . . 106
A.2.2 Reading schedules . . . 108
A.2.3 Pump saturation . . . 109
A.2.4 Uplift calibration . . . 109
A.3 Triaxial testing procedure . . . 110
A.3.1 Specimen preparation and setup . . . 110
A.3.2 Starting a test . . . 114
A.3.3 Seating . . . 117
A.3.4 Back pressure saturation and B value . . . 118
A.3.5 Consolidation . . . 119
A.3.6 Shear . . . 120
A.3.7 Test tear down . . . 121

APPENDIX B. DATA REDUCTION AND CALIBRATION OF SENSORS . . . 122

B.1 Calculation . . . 122
B.2 Corrections . . . 122
B.2.1 Area correction . . . 124
B.2.2 Membrane correction . . . 124
B.3 Calibration of transducers . . . 125
B.3.1 Axial displacement transducer . . . 125
B.3.2 Force transducer . . . 125
B.3.3 Pressure transducer . . . 128

VITA . . . 132

LIST OF TABLES

TABLE Page

1.1 Triaxial testing program 7

3.1 Representative sample testing summary 46

5.1 Normalized undrained strength parameters 63

5.2 Degree of anisotropy 65

A.1 Equipment list 92

A.2 List of Instruments and calibrating factors 104

B.1 Formulae used for data reduction 123

LIST OF FIGURES

FIGURE Page

1.1 Very large slides in the Gulf of Mexico, east of Mississippi canyon, offshore Louisiana. These slides combined encompass over 5,000 km^2 of seafloor. Slides of this magnitude could pose substantial hazard to offshore drilling and/or production infrastructure (Wright and Rathje, 2000). 3

1.2 GEOTAC Truepath automated stress path system used for this research. . . . 6

2.1 Idealized failure criteria for soils (Head, 1998). 12

2.2 Triaxial apparatus for 1.5 inch diameter samples (Head, 1998). 13

2.3 Principles of triaxial tests: (a) Application of stresses; (b) Representation of principal stresses; (c) Usual arrangement for effective stress tests; (d) Representation of total and effective stresses (Head, 1998). 16

2.4 Stress paths of total and effective stresses for an undrained triaxial compression test on normally consolidated clay (Head 1998). 18

2.5 Layout of triaxial apparatus developed by (Bishop and Wesley, 1975). 20

2.6 Effective and total stress paths for undrained compression and extension tests (Bishop and Wesley, 1975). 21

2.7 Relationship between pore pressure coefficient B and degree of saturation (Head, 1998). 23

2.8 Time required for saturation under appropriate back pressure, related to initial degree of saturation (Black and Lee, 1972). 24

2.9 Techniques for anisotropic consolidation to OCR=1 (Germaine and Ladd, 1988). 25

2.10 Scheme of the equipment (Olsen et al., 1988). 27

2.11 Undrained stress-strain behavior for Ko and isotropic consolidation of OCR=1 resedimented boston blue clay (Germaine and Ladd, 1988). 29

2.12 Consolidation procedures for $\mathrm{CK_oU}$ (Ladd and Foott, 1974). 33

2.13 Schematic illustration of variation in undrained shear strength with strain rate (Germaine and Ladd, 1988). 36

3.1 Locations of jumbo piston cores from Gulf of Mexico (Rutherford, 2011). . . 38

3.2 TDI-Brooks International jumbo piston coring system (www.tdi-bi.com). . . . 39

3.3 Details of bulk density, compressional velocity and porosity along the length of core GOM-core1 obtained using MSCL. 41

FIGURE Page

3.4 Natural water content against depth. 43

3.5 Casagrande's plasticity chart showing atterberg limit results for sections from the core GOM-core1. 44

3.6 Plots of minivane shear strength against depth. 45

3.7 Hydrometer analysis for sections from core GOM-core1. 47

3.8 Casagrande's graphical method to find pre-consolidation pressure. 48

4.1 The GEOTAC TruePath system used for testing. 50

4.2 Comparing pressure transducer sensitivity: a) New pressure transducer ; b) Old pressure transducer. 55

4.3 Axial force vs axial strain using old load cell. 56

5.1 Stress-strain relations for $\mathrm{CK_oU}$-C tests. 60

5.2 Stress-strain relations for $\mathrm{CK_oU}$-E tests. 61

5.3 Failure strain with overconsolidation ratio. 62

5.4 Normalized undrained strength data from SHANSEP $\mathrm{CK_oU}$ tests. 64

5.5 Normalized undrained strengths and Ks versus OCR. 66

5.6 Normalized effective stress paths from $\mathrm{CK_oU}$-C/E testing. 69

5.7 Excess pore pressure generated from $\mathrm{CK_oU}$-C testing. 70

5.8 Negative excess pore pressure generated from $\mathrm{CK_oU}$-E testing. 71

5.9 Pore pressure parameter at failure ($\overline{A_f}$) versus OCR from $\mathrm{CK_oU}$-C/E testing. . 72

5.10 Normalized secant moduli versus OCR from $\mathrm{CK_oU}$-C/E testing. 73

5.11 Normalized secant moduli versus OCR from $\mathrm{CK_oU}$-C/E testing. 74

5.12 Secant moduli versus axial strain from $\mathrm{CK_oU}$-C testing. 75

5.13 Secant moduli versus axial from $\mathrm{CK_oU}$-E testing. 76

5.14 Coefficient of earth pressure versus OCR. 77

5.15 Variation of $\mathrm{K_o}$ with vertical effective stress (σ_v). 78

5.16 Stress-strain relations from CIU-C tests.) 79

FIGURE Page

5.17 Stress-strain relations from CIU-E tests. 80

5.18 Excess pore pressure developed in CIU compression tests. 81

5.19 Excess pore pressure developed in CIU extension tests. 82

5.20 Normalized effective stress paths from CIU-C/E testing. 83

A.1 GEOTAC Truepath Automated stress path system. 91

A.2 Layout of the TruePath Automated stress path system for triaxial testing (Trautwein Soil Testing Equipment Co., 2009). 93

A.3 Sketch of water entering and exiting the triaxial cell. 95

A.4 Load frame with triaxial cell inside. 97

A.5 Servo module on the side panel of the load frame. 98

A.6 External ADIO module for the load frame. 99

A.7 Schematic of the DigiFlow pressure volume pump (Guldur, 2010). 101

A.8 Graphical user interface of the GeoTAC TruePath before starting a test. 107

A.9 Hydraulic hand pump along with the extruder. 112

A.10 Sample placed in the triaxial chamber and ready to be tested. 115

B.1 Calibration of the LSCT used for this research. 126

B.2 Calibration of the load cell LCCA-200 used for this research. 127

B.3 Calibration of the cell pressure transducer used for this research. 129

B.4 Calibration of the pore pressure transducer used for this research 130

B.5 Calibration of the back pressure transducer used for this research 131

1. INTRODUCTION

1.1 Need for testing

Oil and gas developments often require placing equipment, such as, subsea wells, pipelines and flowlines, foundation systems for floating structures, in areas with sloping seafloors. Submarine slope failures (occurring beneath many of the world's oceans) could impact all types of offshore and coastal facilities. Analysis and modeling of submarine slope stability has become an important aspect of the risk analysis for offshore structures and seabed infrastructure. This study was undertaken in order to better understand the characteristics of a sub-marine clay deposit from the Gulf of Mexico.

This thesis presents the results of SHANSEP triaxial testing performed on undisturbed samples of Gulf of Mexico clay. Background information is given about the clay, the sampling program and the laboratory testing program. The GEOTAC Truepath automated stress path triaxial apparatus implemented for this research and the laboratory procedures used are described in detail. Data is summarized from the various types of tests run on the clay ($\mathrm{CK_oU}$ consolidated undrained triaxial-compression and extension, isotropically consolidated undrained triaxial-compression and extension tests, consolidations tests) and the stress history of the deposit is evaluated.

Due to the difficulties and costs in exploring the marine environment, published experimental information on offshore clays is limited. Hence there is a lack of information in the literature about the properties of offshore soils in situ. Recently seafloor mapping technology using geographical information systems (GIS) has been developed. The collected data can be used to assess and mitigate potential landslide hazards in offshore regions of similar geology and geomorphology, and perhaps start investigating the triggers for deep water mass movements (Wright and Rathje, 2000). This makes the current study an important piece in understanding all the properties of Gulf of Mexico clay.

This thesis follows the style of Journal of Geotechnical and Geoenvironmental Engineering.

This thesis is presented as a companion to a dissertation where a multi-directional simple shear testing device was developed for the characterization of the cyclic shear response of marine clays (Rutherford, 2011). Although the multi-directional simple shear device (MDSS) will be used to test the clay and apply complex stress or strain paths, it is important for constitutive modeling and to fully study and understand the response of the marine clay in many different shearing modes. The traditional triaxial test does exactly that and completes our understanding of the offshore deposit. The data resulting from the triaxial tests along with the MDSS test data, helps provide insight into the behavior of marine soils. This high quality laboratory data will be used in constitutive and finite element model development for analysis of submarine slopes.

1.2 Submarine landslides

Although many submarine slides occur in the deepwater, far offshore, their influence can be substantial. A submarine landslide triggered by an earthquake on the Grand Banks in 1929 created a turbidity current that severed trans-Atlantic communication cables almost 600 km away (Hampton et al., 1996; Heezen and Ewing, 1952). In 1964, the great earthquake in Prince William Sound, Alaska triggered submarine slides that eventually retrogressed past the coastal zone, swallowing the towns of Seward and Valdez, and creating tsunamis that repeatedly washed over low-lying coastal areas (Coulter and Migliaccio, 1966; Hampton et al., 1996). Twenty-meter high waves associated with Hurricane Camille caused slope failures which damaged petroleum platforms on the Texas and Louisiana Gulf of Mexico shelf in August of 1969 (Bea, 1971). Figure 1.1 shows a picture of the Mississippi Canyon in Gulf of Mexico bay where the slide occurred.

Submarine slope failures can affect large areas and volumes of soil. In comparison to aerial landslides, seafloor slides tend to travel much greater distances, with a tremendous sediment transport along its way. They also occur on extremely flat slopes of less than 4^{o} (Lewis, 1971).

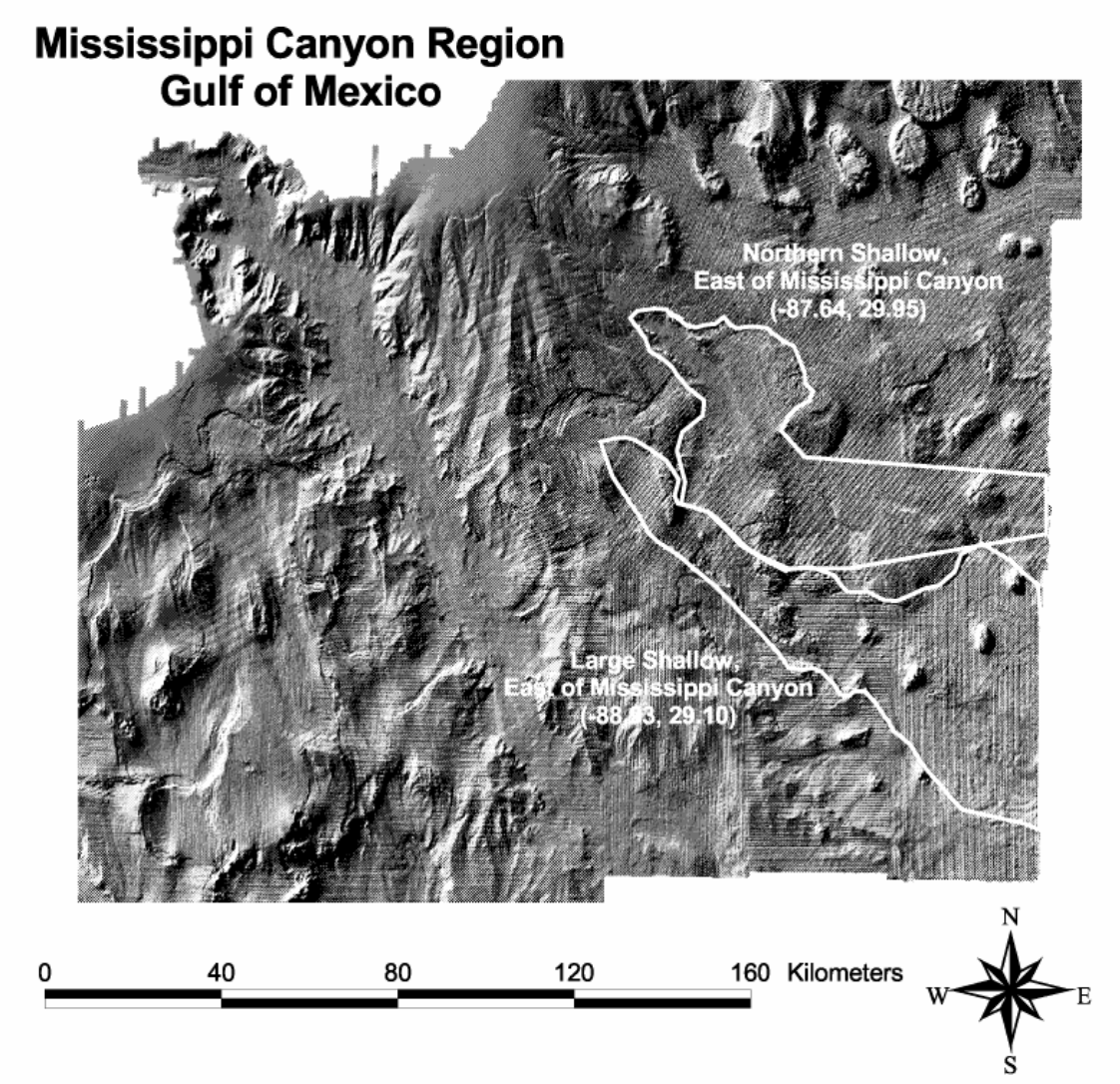

Fig. 1.1. Very large slides in the Gulf of Mexico, east of Mississippi canyon, offshore Louisiana. These slides combined encompass over 5,000 km^2 of seafloor. Slides of this magnitude could pose substantial hazard to offshore drilling and/or production infrastructure (Wright and Rathje, 2000).

According to Hance (2003) who carried out a literature review on case histories of submarine slope failures worldwide, identified a number of causes for seafloor slope failures. These triggering mechanisms include:

- Earthquakes and faulting
- Rapid sedimentation
- Gas and disassociation of gas hydrates
- Ocean storm waves and tidal events
- Mud and magma volcanoes
- Salt diapirism
- Sea-level fluctuations

Since many failures affect fine grained soil, triggers such as earthquakes, ocean waves, rapid sedimentation, rapid erosion, and gas hydrate disassociation develop at a rate faster than the soil can drain, and stability should be evaluated using undrained strengths. On the other hand, triggers such as salt diapirism and faulting tend to increase gradually the inclination of a slope, and the slope tends to be loaded at a rate slow enough to allow for dissipation of excess pore water pressures and full drainage. Thus, for these cases, stability should be evaluated using drained shear strengths.

Since the triggers that cause slope failures under undrained conditions such as earthquakes and storms are more prominent (Hance, 2003), in this research, consolidated undrained compression and extension tests were carried out to obtain the undrained shear response of the marine clay.

1.3 Research objectives

The first objective of this research program was to setup two GEOTAC TruePath Automated Stress Path systems. This phase of the research program represented the most of

the initial work on the project as it was necessary to get high quality data from the tests carried out.

- Perform an experimental program to conduct $\mathrm{K_o}$ consolidated-undrained triaxial compression and extension ($\mathrm{CK_oU}$-TXC and $\mathrm{CK_oU}$-TXE) tests using the SHANSEP approach to obtain undrained stress strain-strength parameters as a function of over-consolidation ratio (OCR) for Gulf of Mexico clay.
- Run conventional isotropically consolidated-undrained triaxial compression and extension (CIU-TXC and CIU-TXE) at varying over consolidation ratios and comparing the results to characterize the marine clay.

1.4 Methodology

1.4.1 Equipment setup

The GEOTAC TruePath Automated Stress Path system (Figure 1.2) was used for the work presented here. This apparatus can be separated into five essential components each with a basic function in the triaxial system.

- Triaxial cell
- Load frame
- DigiFlow pressure-volume pumps
- Sensors
- Computer, data acquisition system and control software

The use of DigiFlow pressure-volume flow pumps enables a feed back loop allowing the system to enforce $\mathrm{K_o}$ conditions by measuring the volume change and varying the cell pressure. Combinations of vertical and volumetric deformation rates can be used to control strain paths.

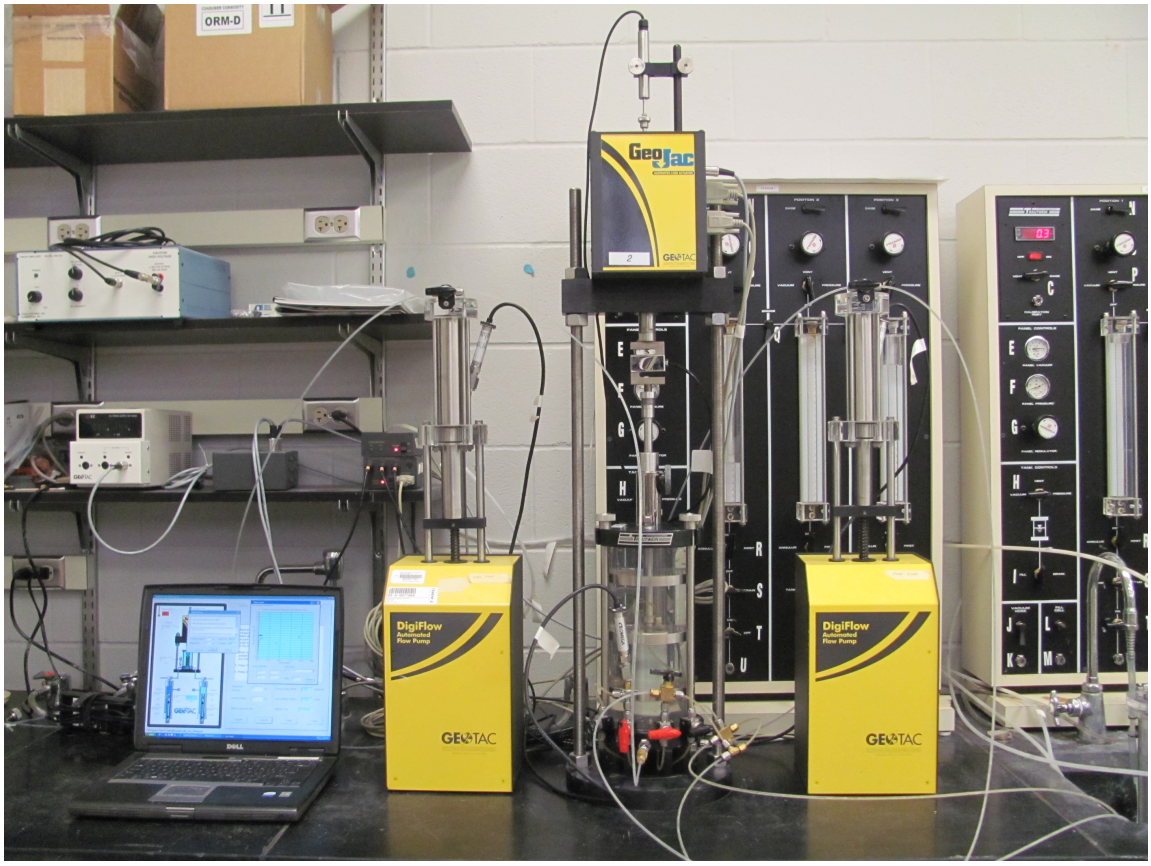

Fig. 1.2. GEOTAC Truepath automated stress path system used for this research.

Table 1.1
Triaxial testing program

OCR	K_o		**Isotropic**	
1	CU-Compression	CU-Extension	CU-Compression	CU-Extension
1.5	CU-Compression	CU-Extension	-	-
2	CU-Compression	CU-Extension	CU-Compression	CU-Extension
4	CU-Compression	CU-Extension	CU-Compression	CU-Extension
8	CU-Compression	CU-Extension	CU-Compression	CU-Extension

1.4.2 Experimental plan

Index tests and soil classification was performed on each soil sample tested. The tests included water content, liquid limit, plastic limit, specific gravity and hydrometer analysis. These tests were required to classify the soil under the Unified Soil Classification system and give general information about the soil's characteristics.

Constant rate of strain (CRS) consolidation tests were carried out on specimens from various depths to determine the maximum past pressure (stress history) and compressibility parameters of the marine clay.

Four different types of tests were used to measure the undrained shear strengths along different stress paths: Isotropically consolidated triaxial compression test (CIU-TXC), Isotropically consolidated triaxial extension test (CIU-TXE), K_o consolidated triaxial compression test (CK_oU-TXC), Ko consolidated triaxial extension test (CK_oU-TXE). The soil samples were consolidated to 2 times the maximum past pressure and swelled to OCR ratios of 1, 1.5, 2, 4 and 8 under both K_o and isotropic conditions (Table 1.1).

1.4.3 Marine soil samples

Marine clays on the continental shelf and slope differ from fine grained sediments in three important aspects: depositional environment, depositional mechanisms, and stress history (Rutherford, 2011). Because the structure of the deposits and the mechanical re-

sponse to loading can be influenced by these aspects, the samples in the proposed experimental plan will be undisturbed marine soils. However, not only is collecting offshore samples expensive and requires specialized equipment, high quality undisturbed samples require great expertise.

Gulf of Mexico clay samples were collected in and around the Green Canyon near the Sigsbee Escarpment on the Research Vessel Brooks-McCall operated by TDI-Brooks International. These samples were collected as part of the multi directional simple shear research project (Rutherford, 2011) in October 2007. The 100 mm (4 in) diameter cores were taken using the jumbo piston core system at approximately 1,000-1,300 meters of water depth. A jumbo piston corer uses the free fall of the coring rig to achieve a greater initial force on impact than gravity coring. A sliding piston inside the core barrel is used to reduce inside wall friction with the sediment and to assist in the evacuation of displaced water from the top of the corer. The Jumbo Piston Cores utilizes a cantilevered deployment platform over the stern of the vessel with a rail and capture bucket assembly placed on the deck of the vessel directly beneath the stern Aframe. The JPC consists of a 4,000 lb weight stand, a 4" core barrel, a mechanical trigger, standard schedule 40 PVC liner, a cutting shoe, and a foil core catcher.

The core samples were scanned using a GEOTEK multi-sensor core logger (MSCL). A conveyor system moves the sensor array, which scans the core as it passes. The MSCL data will be used to locate samples within the core liner with a minimum amount of disturbance. Both ends of core sections will not used because of possible disturbance, possible oxidation and change in water content during the storage period.

1.5 Organization

Section 2 presents a review of relevant literature. Basic concepts of shear strength and effective stress paths, triaxial tests and its nuances, sample disturbance, SHANSEP and recompression procedures for mitigating sample disturbance in soft clays are covered.

Section 3 gives information about the marine clay, its provenance and geology. All the results of tests including water content, liquid limit, plastic limit, specific gravity and hydrometer analysis are presented in this chapter. The CRS Consolidation test results are also presented here.

Section 4 talks briefly about the test procedure. It also describes all the problems encountered during setup of the triaxial system and while running the tests.

Section 5 is dedicated to the presentation of test data and the analysis of test results.

Section 6 includes the findings and conclusions of the performed research, and provides suggestions for future work.

Appendix A expands on Section 4 and talks about the setup of the GEOTAC Truepath triaxial system and the test procedures followed in detail. Appendix B presents the data reduction and corrections on the raw data and the calibration of all the sensors used in this research.

2. LITERATURE REVIEW

2.1 Introduction

Unlike other materials such as steel, the strength of soil is not a unique property but varies within wide limits depending on the conditions imposed, whether in-situ or in a laboratory test.

The triaxial apparatus is the principal laboratory shear device used in geotechnical engineering practice for measuring the stress strain strength properties of soils. Triaxial testing is also widely used in research to study basic soil behavior, such as the influence of stress history, strain rate, creep, and cyclic loading (Germaine and Ladd, 1988). It offers the most satisfactory way of measuring the shear strength of soil for many engineering purposes. The triaxial system is versatile and procedures can be related to numerous types of practical problems.

This chapter details all the major principles of the triaxial system and the relevant experimental work carried out using the triaxial apparatus.

2.2 Shear strength

The shear strength of soil is measured in terms of a limiting resistance to deformation offered by a soil mass or a test specimen when subjected to loading or unloading (Head, 1998). This limiting shearing resistance corresponds to the condition generally referred to as ‘failure’ which can be defined in several different ways. Shear strength is not a unique property of a soil, but depends on many factors such as void ratio, water content, stress history. Factors such as rate of loading, shearing mode and especially quality of sampling and specimen preparation affect the measurement of shear strength.

Skempton (1960) defined shear strength as the maximum shear stress the soil could withstand, whereas Hvorslev (1949) defined shear strength as the shear stress on the failure plane of the soil at the moment of failure.

For any failure criterion, the shear stress, τ, on a potential failure surface is related to the normal effective stress, denoted by σ'_n. The Mohr-Coulomb criterion is the most commonly used for soils:

$$\tau'_f = c' + \sigma' \tan \phi' \tag{2.1}$$

According to Head (1998), there are five different criteria for 'failure' from which the shear strength of soil is determined. This is listed below and illustrated in Figure 2.1:

1. Peak deviatoric stress
2. Maximum principal stress ratio
3. Limiting strain
4. Critical state
5. Residual state

2.3 Triaxial tests

The triaxial test was initially developed by A. Casagrande (Casagrande, 1936) in the 1930s to overcome the limitations of the direct shear test. A major advantage of the triaxial test is that drainage can be controlled and the failure plane is not constrained by the design of the apparatus to occur on a specific plane.

One of the earliest effective stress triaxial test procedure was established by Bishop and Henkel (1962) and was later accepted as standard practice in many countries. Figure 2.2 shows details of a triaxial cell used in the laboratory to carry out regular tests. This was later modified to facilitate tests in which no lateral yield was permitted, called $\mathrm{K_o}$ cells. These $\mathrm{K_o}$ cells had a lateral strain indicator around the sample to measure radial deformation.

The soil sample is usually encased in a rubber membrane to prevent the pressurized cell fluid (water or oil) from penetrating the soil. Axial load is applied through a piston.

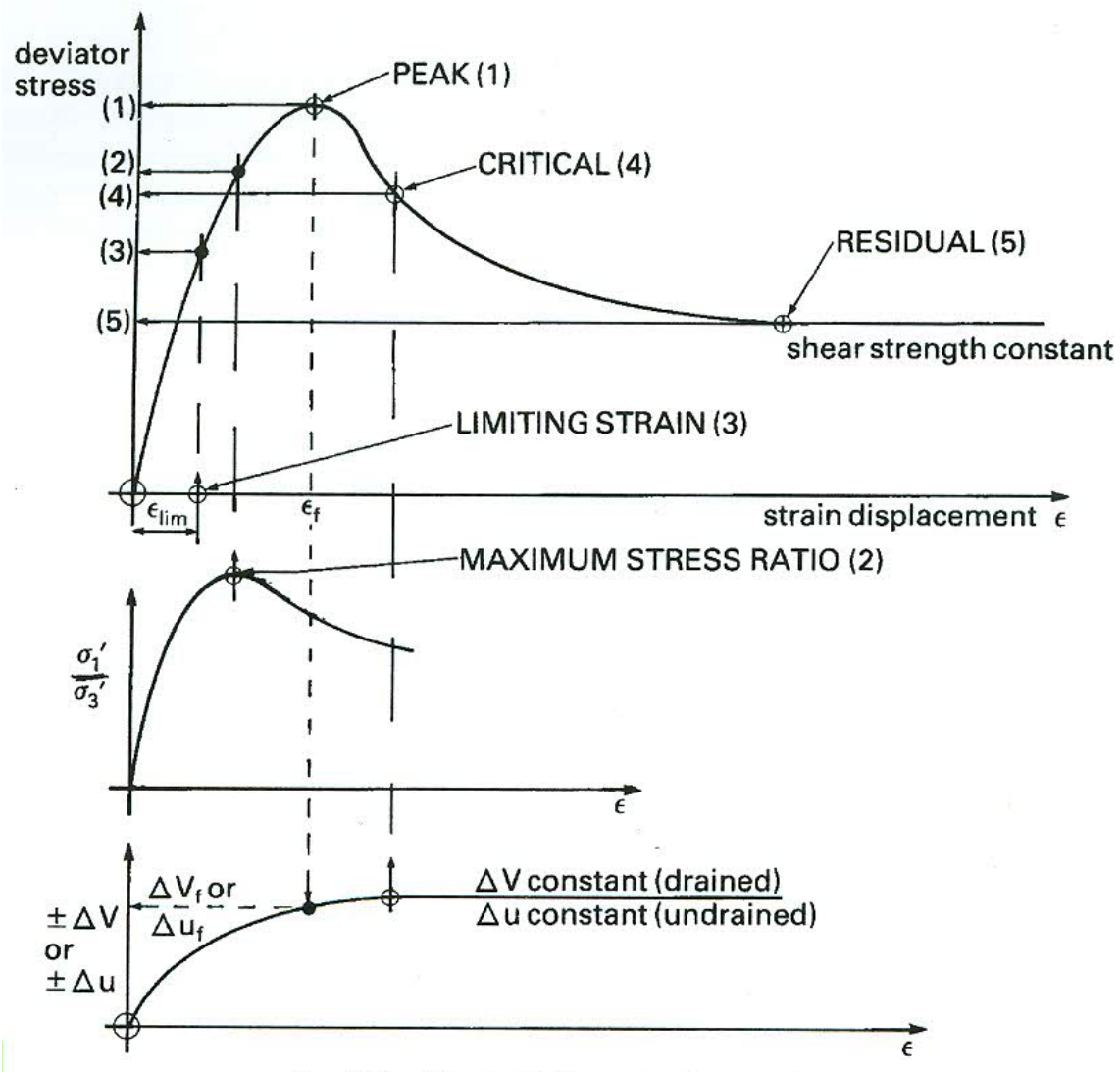

Fig. 2.1. Idealized failure criteria for soils (Head, 1998).

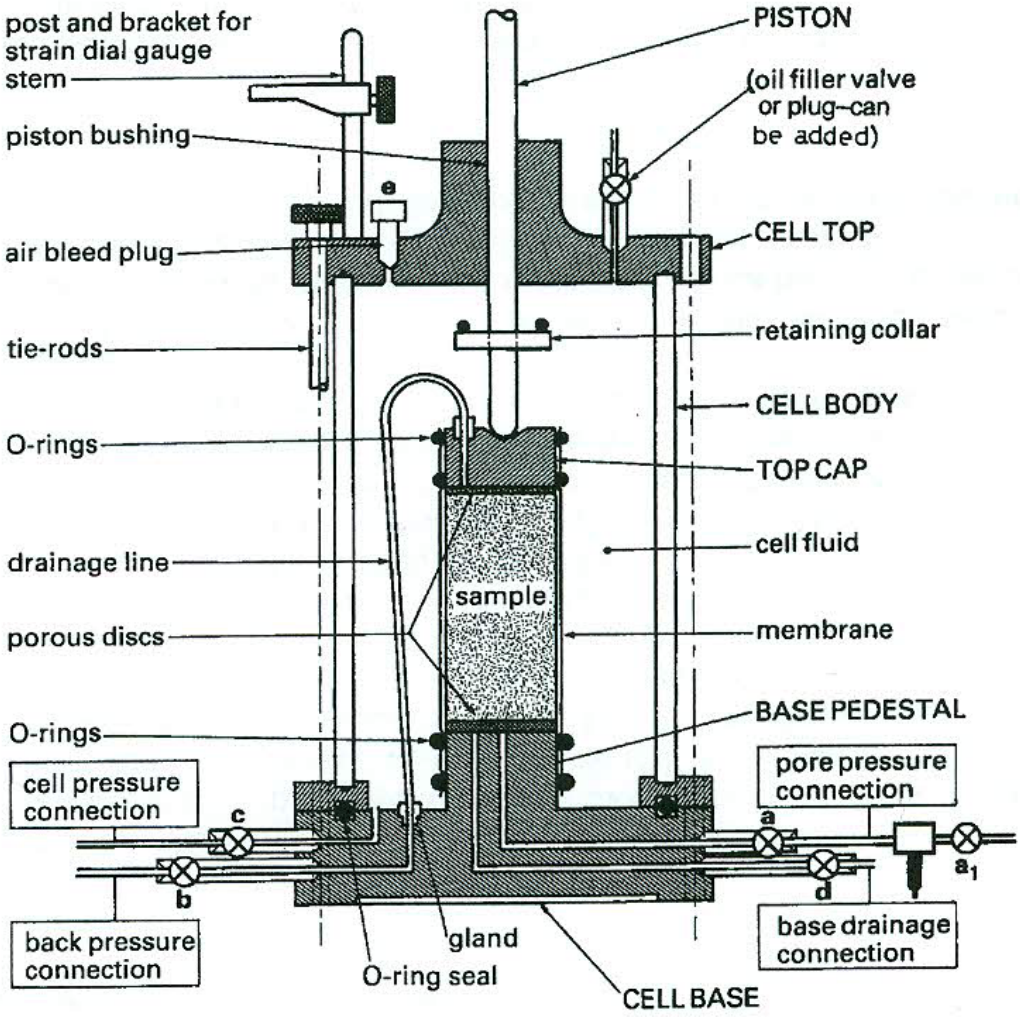

Fig. 2.2. Triaxial apparatus for 1.5 inch diameter samples (Head, 1998).

Often the volume change during a drained test or the pore water pressure induced within the sample during an undrained test is measured.

Two major variables that can be controlled in the triaxial test: the boundary drainage conditions and the imposed stress path. There are limiting conditions of drainage in the triaxial test which model real field situations. Triaxial tests for the determination of shear strength properties of soil can be divided into three main categories: consolidated drained (CD), consolidated undrained (CU), unconsolidated undrained (UU).

2.3.1 Consolidated drained

This procedure involves consolidating the test sample under some state of stress appropriate to the field or design situation. The consolidation stresses can either be hydrostatic (isotropic) or non-hydrostatic (anisotropic). Once the consolidation is over, the drainage valves remain open for the shear phase. Here the stress difference is applied very slowly such that no excess pore water pressure develops during the test. Thus in this test the total stresses are always equal to the effective stresses.

2.3.2 Consolidated undrained

The soil sample is first consolidated under the desired stresses (isotropic or anisotropic). When this phase is complete the drainage valves are closed and the specimen is loaded to failure in undrained shear. This test can be performed with and without the measurement of pore water pressure. If the pore pressure is measured during the undrained stage, the result can be expressed in terms of effective stresses.

The excess pore water developed during shear can either be positive or negative depending on whether the sample tries to contract or expand. Positive pore water pressures occur in normally consolidated clays and negative pore water pressures are developed in lightly over consolidated clays (Holtz and Kovacs, 1981).

2.3.3 Unconsolidated undrained

In this test the specimen is placed in the triaxial cell with the drainage valves closed from the beginning. Thus no consolidation occurs even if a confining pressure is applied and the sample is saturated 100%. The sample is sheared undrained as with the CU test. This is known to be a total stress test and pore water pressures are not measured. This was termed as the Q- test ('quick') by A. Casagrande since the sample is loaded to failure in about 20 minutes.

2.4 Stress paths

The stresses on the sample of a triaxial test are represented in Figure 2.3. The confining pressure (σ_h) or cell pressure is applied by cell fluid within the triaxial chamber. The deviator stress (σ_v-σ_h) is applied by an axial load at the top of the sample. σ_v, σ_h and σ_h acting mutually perpendicular to each other are called the total principal stresses. These stresses acting on a saturated undrained sample generate a pore water pressure, u, which can be positive or negative as mentioned before. The effective stresses (σ'_v and σ'_h) acting on the soil are defined as follows:

$$\sigma'_v = \sigma_v - u \tag{2.2}$$

$$\sigma'_h = \sigma_h - u \tag{2.3}$$

The state of stress of a soil element can be completely defined by the principal stresses, the orientation of these stresses and the pore pressure. A locus of stress points showing the successive states of stress which a specimen undergoes during loading or unloading is called a stress path (Lambe and Whitman, 1969).

One of the most widely used methods of plotting stress paths was developed by Prof. T. W. Lambe, known as the MIT stress path plot (Lambe, 1967). The stress path is the

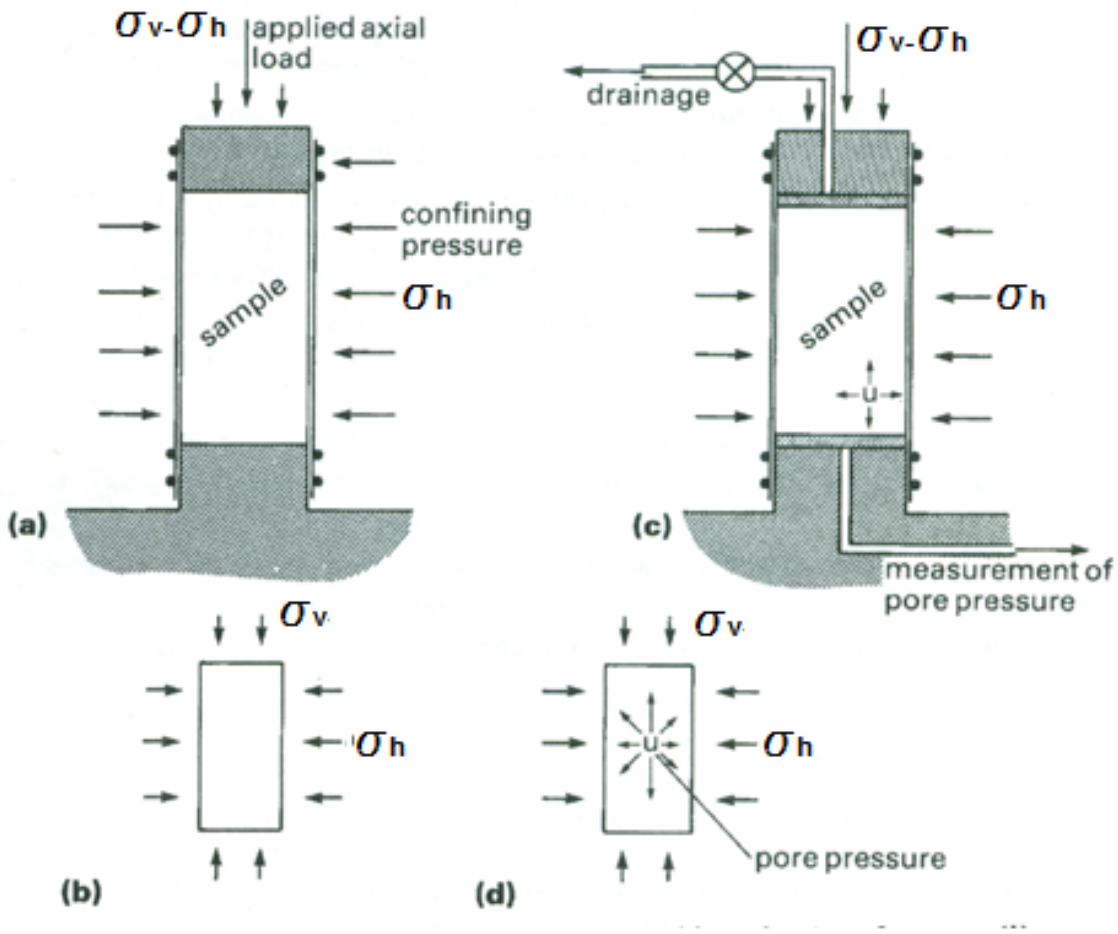

Fig. 2.3. Principles of triaxial tests: (a) Application of stresses; (b) Representation of principal stresses; (c) Usual arrangement for effective stress tests; (d) Representation of total and effective stresses (Head, 1998).

locus of points of maximum shear stress experienced by a soil element as the state of stress varies. The parameters used in this plot are called s and t, they are defined as:

$$s = (\sigma'_v + \sigma'_h)/2 \tag{2.4}$$

$$t = (\sigma'_v - \sigma'_h)/2 \tag{2.5}$$

Another stress path method is the Cambridge stress field developed by Roscoe et al. (1953) at the University of Cambridge, England. This method makes use of the mean of the three principal effective stresses instead of the mean of the major and minor principal stresses. The stress path is plotted on a p-q diagram where:

$$p = (\sigma'_v + \sigma'_h + \sigma'_h)/3 \tag{2.6}$$

$$q = \sigma'_v - \sigma'_h \tag{2.7}$$

A useful aspect of these stress path methods is that they may be used to show both total stress paths (TSP) and effective stress paths (ESP) on the same diagram. For drained loading the total stress path and the effective stress path are identical as the pore pressure induced by loading is approximately equal to zero at all times during shear (Roscoe et al., 1953).

In an undrained test on normally consolidated clay the pore pressure increases as the deviator stress increases. The increasing pore pressure increases the difference between effective stress and total stress, so the effective stress path follows a curve which deviates to the left as shown in Figure 2.4 (Head, 1998). The horizontal distance between the ESP and TSP at any point is equal to the pore pressure u at that instant. Pore pressure u has two components: the initial pore pressure u_o, and the excess pore pressure Δu, generated due to the application of the deviator stress.

The real virtue of the triaxial test lies in the variety of stress paths that can be followed during both consolidation and shearing.

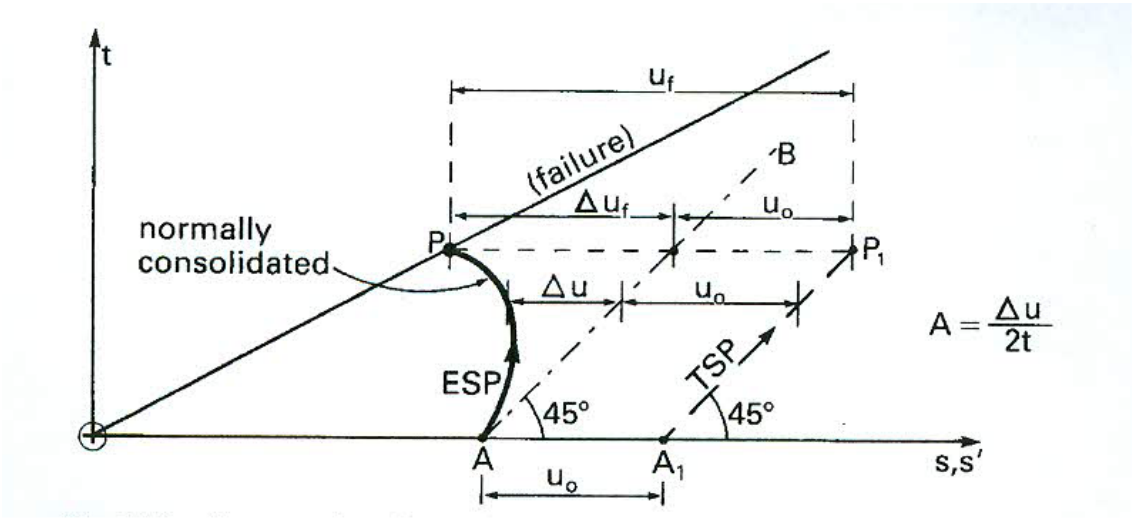

Fig. 2.4. Stress paths of total and effective stresses for an undrained triaxial compression test on normally consolidated clay (Head 1998).

2.5 Controlling stress paths during consolidation and shear

One of the first triaxial apparatus for controlled stress path testing was developed by Bishop and Wesley (1975) (Figure 2.5). Their particular configuration made use of Bellofram rolling seals and was that of mounting the sample on top of the loading ram. The apparatus was well suited for both stress controlled and strain controlled loading. For their Ko consolidation the lateral strain was monitored either indirectly from the volume change and axial strain or directly from a lateral strain indicator as illustrated by Bishop and Henkel (1962), Figure 47 and 48.

They tested four samples a-d cut from the same block and consolidated them to the same estimated values of in situ effective stress, corresponding to a Ko value of 0.56. Samples a and b were then brought to failure in compression, a with σ_r constant and σ_a increasing and b with σ_a constant and σ_r increasing, as shown in Figure 2.6. Its seen that the undrained compression tests a and b have almost identical effective stress paths. The undrained extension tests c and d likewise have almost identical effective stress paths, whilst for each pair of tests the total stress paths are radically different.

The triaxial cell configuration requires that failure occur either in compression (axial compression) with $\sigma_a = \sigma_v > \sigma_r = \sigma_h$ or in extension (axial extension) with $\sigma_r = \sigma_h > \sigma_a = \sigma_v$ (Germaine and Ladd, 1988). These two failure modes involve a change in the direction of the major principal stress at failure (vertical for compression and horizontal for extension) and in the relative magnitude of the intermediate principal stress as reflected by the value of $b = (\sigma_2 - \sigma_3)/(\sigma_1 - \sigma_3)$ (b= 0 for compression tests and b=1 for extension tests).

2.6 Saturation and back pressure

Saturation of the entire system is required for accurate measurements of volume change based on recorded water inflow and outflow during consolidation and shearing, and is essential for reliable data during undrained shear. When pore water fluid is used to control

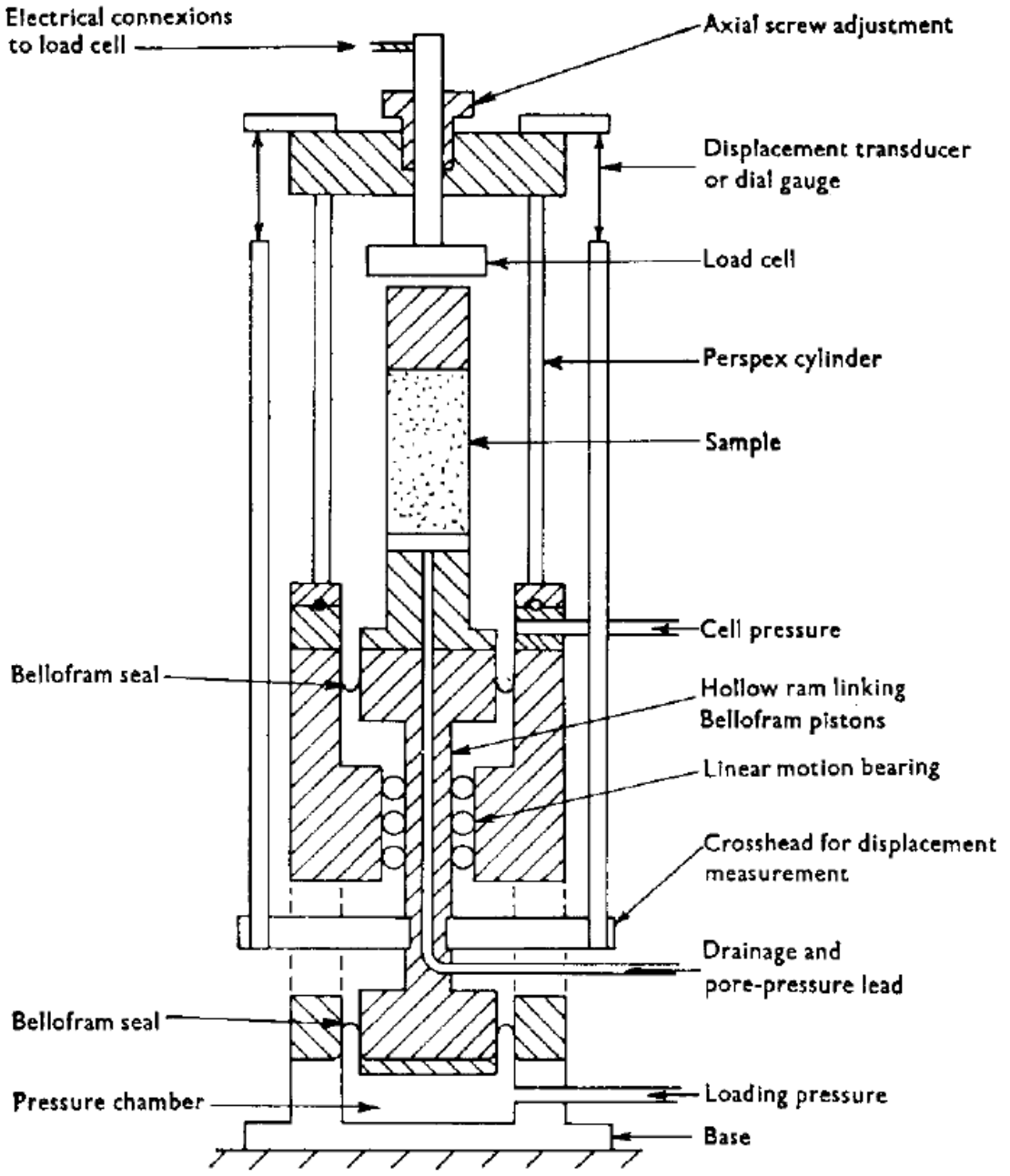

Fig. 2.5. Layout of triaxial apparatus developed by (Bishop and Wesley, 1975).

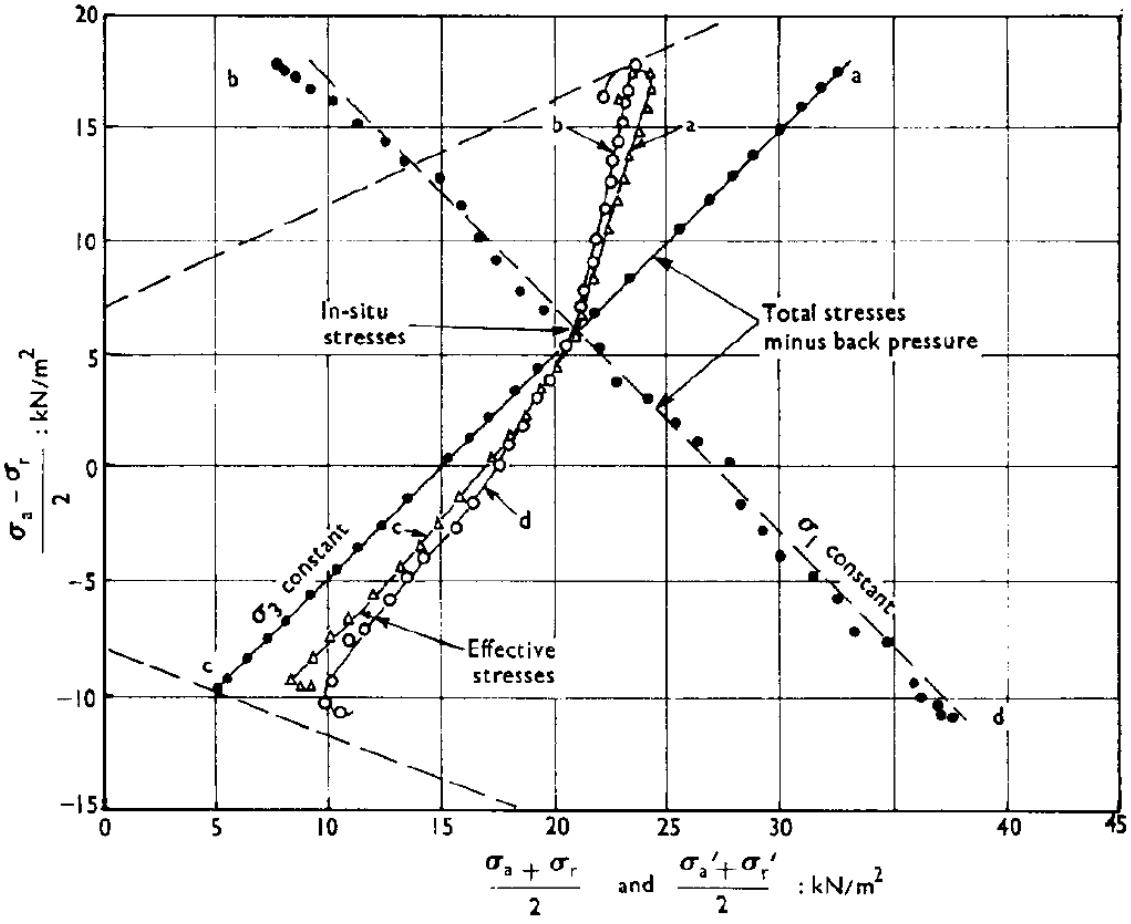

Fig. 2.6. Effective and total stress paths for undrained compression and extension tests (Bishop and Wesley, 1975).

or measure changes in the specimen volume, the presence of macroscopic gas will create errors that depend on test type and specimen stiffness (Rad and Clough, 1984).

Saturation is carried out by raising the pore water pressure to a level high enough for the water to dissolve into the solution all the air originally in the void spaces. At the same time the confining pressure is raised in order to maintain just a small positive effective stress value within the specimen (Black and Lee, 1972).

Ideally the two pressures are raised simultaneously and continuously, maintaining a constant difference between them (Head, 1998). The most common method is to apply a back pressure to the pore fluid incrementally, alternating with increments in the confining pressure, maintaining a constant difference between them. The back pressure is always lesser than the confining pressure to ensure that the effective stress is positive and the sample does not swell.

The excess pore pressure (Δu_{ex}) generated due to an isotropic stress change ($\Delta \sigma_h$) on the sample is related to the stress change by a coefficient, B, defined by the equation:

$$\Delta u_{ex} = B \times \Delta \sigma_h \tag{2.8}$$

If the sample is 100% saturated, any change in σ_h will be reflected by an equal change in u, thus it follows that B=1. The effective stresses remain the same. The value of B is determined to check for 100% saturation in the sample. Figure 2.7 shows how the B value varies with the degree of saturation.

Saturation by application of back pressure not only dissolves air contained in the specimen, but also eliminates air bubbles in the drainage line and pore pressure connections which cannot be flushed out. Any air trapped between the membrane and the specimen is removed as well. Black and Lee (1972) investigated the diffusion of bubbles into the pore water under an applied back pressure. The time required for solution of the bubbles in the tube depends on their length and tube diameter. Large bubbles are reduced to small bubbles before they are absorbed. Bubbles in a smaller bore tube take longer to dissolve than bubbles of similar volume in a large bore tube because there is less surface area of

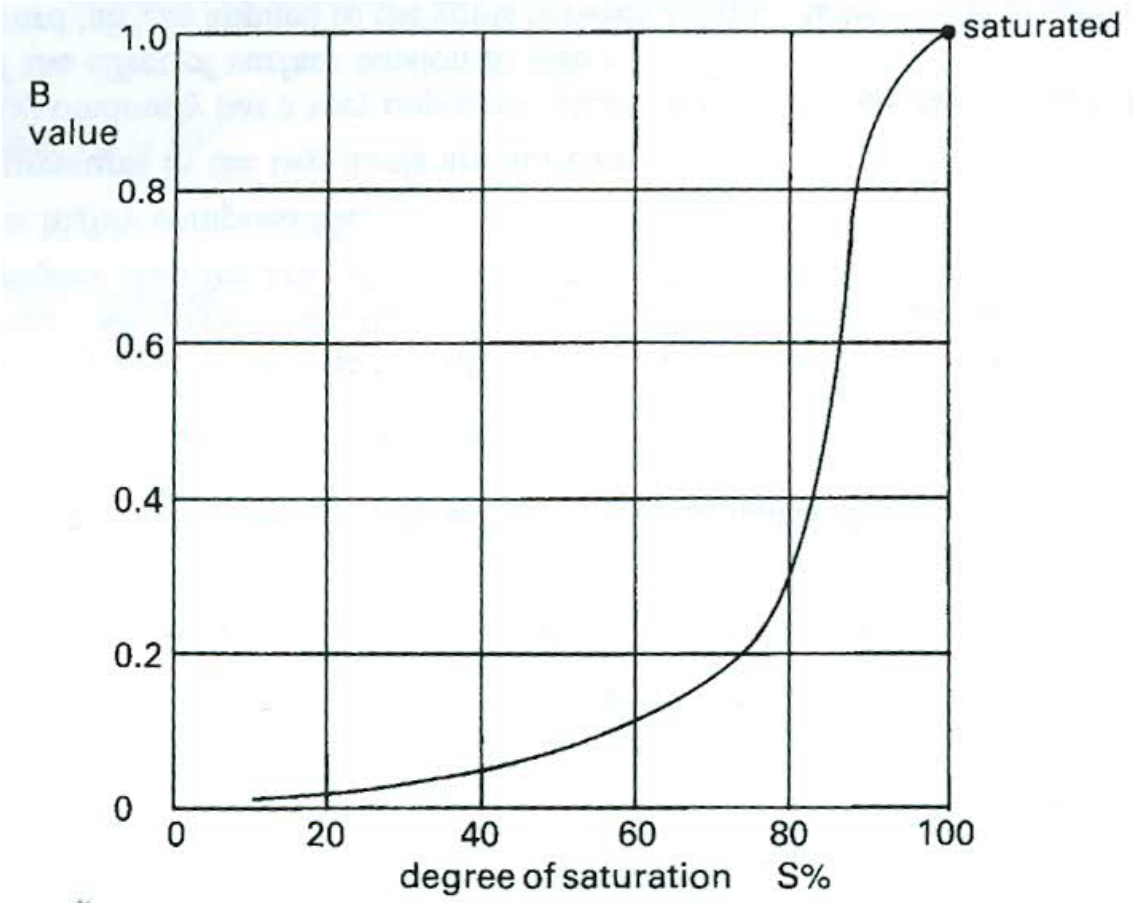

Fig. 2.7. Relationship between pore pressure coefficient B and degree of saturation (Head, 1998).

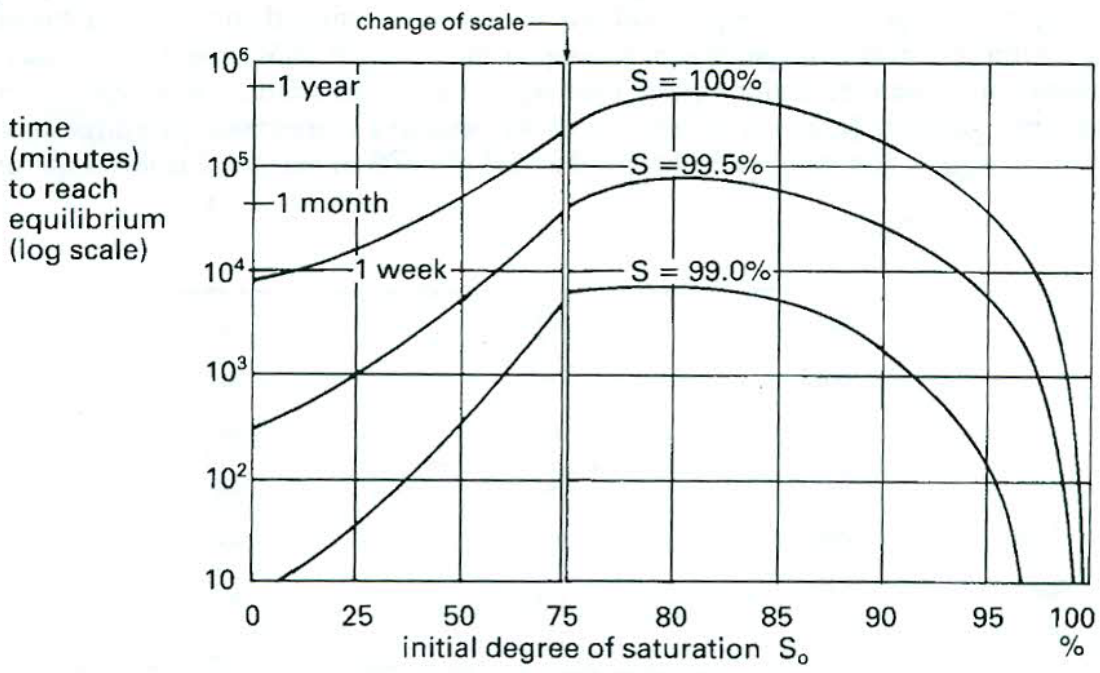

Fig. 2.8. Time required for saturation under appropriate back pressure, related to initial degree of saturation (Black and Lee, 1972).

air in direct contact with water. The Figure 2.8 shows the data derived by Black and Lee (1972) from their tests on specimens of clean sand with similar results observed in clay soils.

The time required for saturation appears to be greatest when the initial saturation lies in the range 75-85%. The time required decreases dramatically when the initial saturation exceeds 95%. It also decreases towards the dry end where the air voids are larger and interconnected and allow easier access for penetration of flowing water.

2.7 Consolidation in triaxial tests

True K_o consolidation requires application of many small increments of vertical and radial stress in order to follow a stress path that is dictated by the specimen deformation.

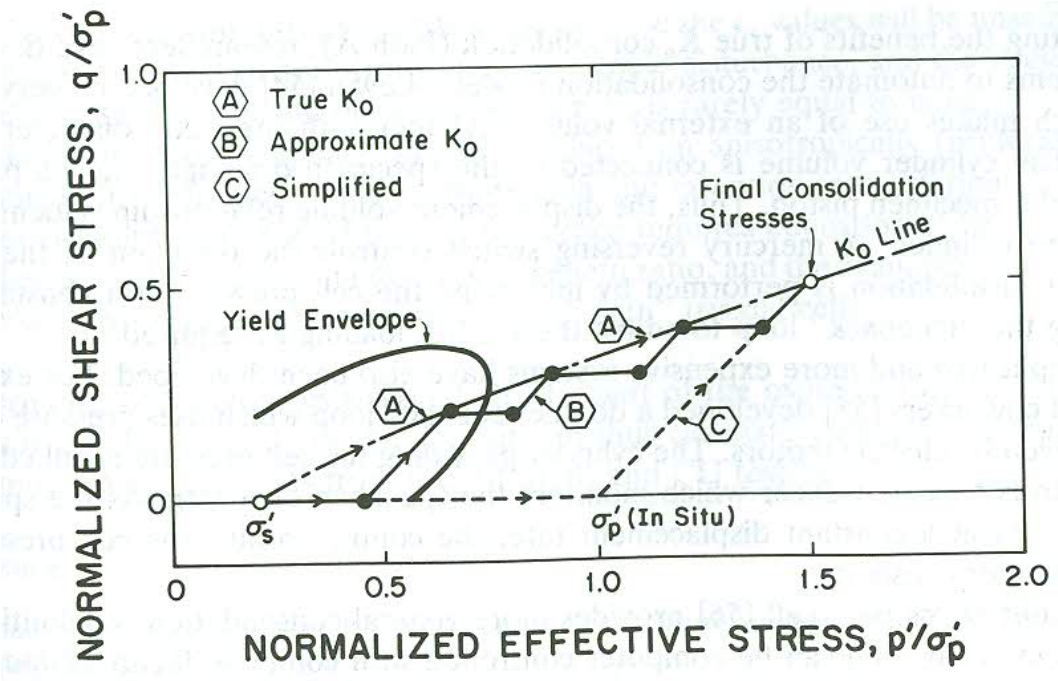

Fig. 2.9. Techniques for anisotropic consolidation to OCR=1 (Germaine and Ladd, 1988).

Germaine and Ladd (1988) discuss a simplified method for manual K_o consolidation. The back pressured specimen is first isotropically consolidated to σ'_s, and then follows a drained stress path of decreasing K_o as it approaches the normally consolidated condition (the true K_o stress path A is shown in Figure 2.9). For actual manual K_o consolidation, increments must be sufficiently small to minimize straining due to undrained shear and must remain long enough to allow full consolidation. At the end of each increment the change in length and volume are used to calculate the present area to determine if the selected K_o is too high or too low. Based on this information a new K_o value is estimated and the next increment is applied.

Berre and Bjerrum (1973) presented the technique shown as stress path C in Figure 2.9 in which the specimen is isotropically consolidated to the final radial effective stress, and then the vertical stress is increased such that K_o equals the estimated K_o value. This stage

is equivalent to drained triaxial compression and must be performed relatively slowly. Once at the K_o value, the vertical stress must be maintained for one cycle of secondary compression prior to undrained shear. This process dramatically decreases the testing period and labor requirements compared to stress path A.

The results of both compression and extension tests on Drammen clay (Berre and Bjerrum, 1973) confirm that the simplified method, while not perfect, yields data comparable to true K_o consolidation. However isotropic consolidation well beyond the yield envelope may cause a significant change in the structure of the soil. Hence a better approach would be to select a path similar to B in Figure 2.9.

Lewin (1971) developed a simple analog which makes use of an external volume cylinder with the same diameter as the specimen. The cylinder volume is connected to the specimen drainage, and its piston is attached to the specimen piston. Thus the displacement volume relationship is identical for both the specimen and cylinder. A mercury reversing switch controls the direction of the piston movement. Consolidation is performed by increasing the cell pressure at a constant rate and allowing the feedback loop to adjust the vertical load.

Olsen et al. (1988) developed their triaxial apparatus by adding a flow pump to control liquid movement to and from the ends of a test specimen. Figure 2.10 presents a scheme of the authors' experimental equipment. A triaxial cell (T) mounted in a loading frame, is equipped with a permeant control manifold which interconnects the base pedestal and top cap of a test specimen (E) with the flow pump (P), the differential transducer (D), the gage transducers (G), and the permeant fluid standpipes (S). The triaxial cell is also connected to the chamber fluid standpipe (C). The left and right of the manifold are symmetric, and they are connected, respectively to the base pedestal and to the top cap of the test specimen within the triaxial cell. The flow pump is connected so that it can infuse liquid into or withdraw liquid from either side of the manifold, or both sides simultaneously.

They found that the flow pump capabilities include measurements of constant rate of deformation consolidation, very small strain compressibility, low gradient permeability,

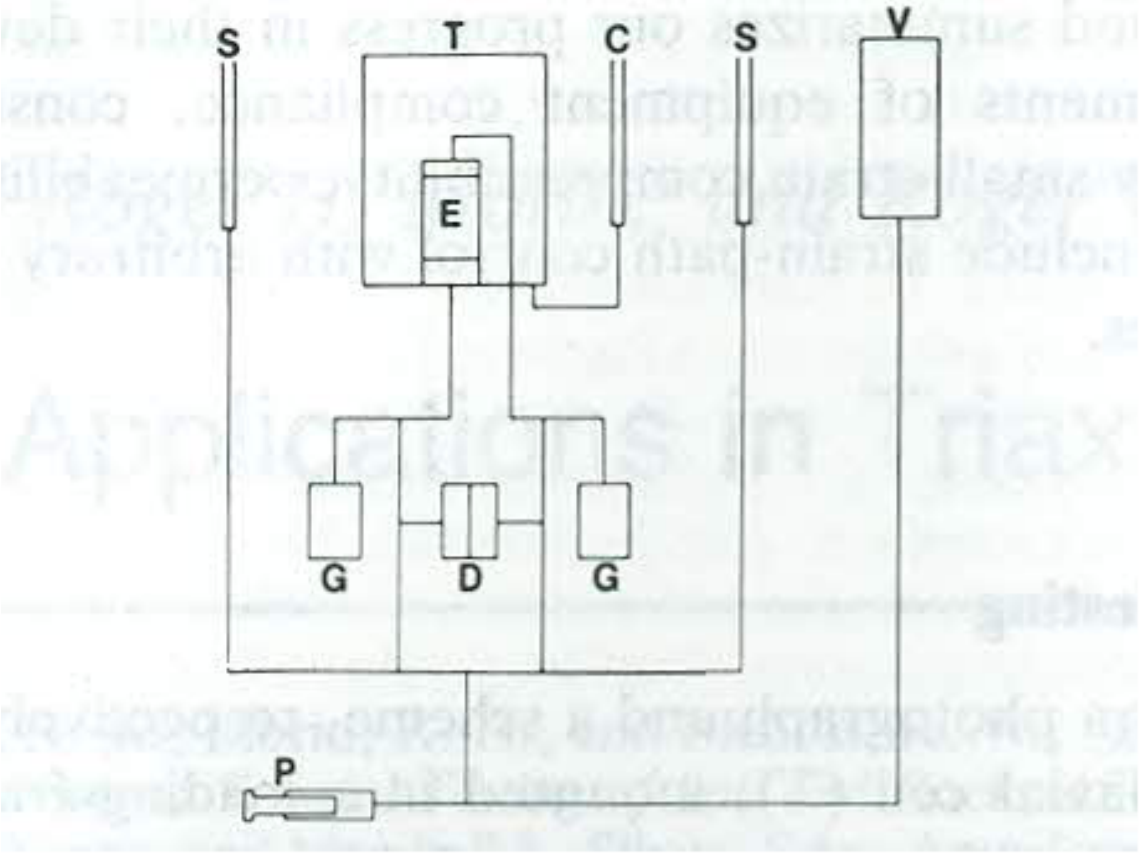

Fig. 2.10. Scheme of the equipment (Olsen et al., 1988).

and coefficient of consolidation. Combinations of vertical and volumetric deformation rates can be used to control strain paths. Use of the flow pump also reduces the equipment and the number of replicate specimens needed for determining the permeability, compressibility, and strength of a given soil.

Anisotropy can also have a significant effect on undrained stress strain behavior, as shown by Germaine and Ladd (1988) from $\mathrm{CK_oU}$-TC and TE tests on OCR=1 resedimented boston blue clay (Figure 2.11). Shearing in compression produces a very high peak strength at a very low strain (Ea=0.3%) followed by pronounced strain softening as the effective stresses decrease and finally reach the maximum obliquity failure envelope. In contrast the effective stress path is always decreasing during shear in extension, which produces a much lower strength at a very large axial strain. Figure 2.11 also plots results from CIU tests, which show that isotropically consolidated specimens give completely different behavioral trends. This occurs because anisotropic consolidation causes most of the anisotropy observed in typical low OCR soils. Hence, CIU testing will generally give a highly misleading picture of soil behavior when the in situ $\mathrm{K_o}$ is less than about 0.7 to 0.8.

Ladd et al. (1977) pointed out that soil anisotropy has two components, one being inherent anisotropy reflecting the depositional characteristics of the soil and the other being a stress system induced component whenever the coefficient of earth pressure at rest is not equal to unity. Hansen and Gibson (1949) predicted that theoretically for truly isotropic materials stress system induced anisotropy leads to different shear strengths under different modes of shear. This anisotropy results from the fact that different increments of shear stress are required to produce failure as the major principal stress at failure varies between the vertical and horizontal direction.

2.8 Triaxial shear

As first presented by Bishop and Henkel (1962) in their book, the triaxial test results are sensitive to the rate of loading for two reasons: the time required for the flow of water

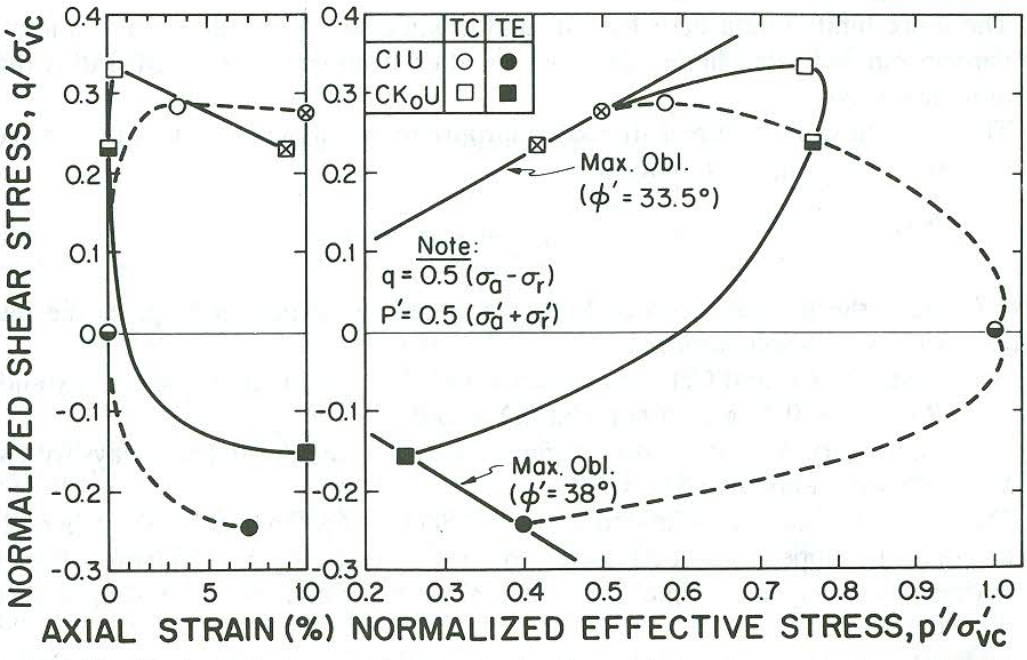

Fig. 2.11. Undrained stress-strain behavior for Ko and isotropic consolidation of OCR=1 resedimented boston blue clay (Germaine and Ladd, 1988).

and the inherent viscosity of the soil skeleton. The major concern while selecting a rate of loading should be the time required for the pore pressure to equilibrate throughout the specimen under the requisite drainage conditions.

They also reported an approximate theoretical relationship between the degree of calibration and the time which can be used to compute a loading rate.

$$t_s = 1.7h^2/c_a \qquad \text{without drains} \tag{2.9}$$

$$t_s = 0.07h^2/c_a \qquad \text{with fully effective drains} \tag{2.10}$$

where

t_s = time to failure

C_a = Coefficient of consolidation

The displacement rate will then depend on some selected fraction of the strain to failure which is a function of the type of consolidation, type of loading and OCR. A problem with using these equations occurs if the permeability of the specimen is greater than 10^{-8} cm/s as the filter strips do not provide a free draining boundary. Bishop and Henkel (1962) recommended an extension of the initial slope of the volume change versus square root of time curve to obtain t_{100} and the use of the following equations:

$$t_f = 16t_{100} \qquad \text{without drains} \tag{2.11}$$

$$t_s = 2t_{100} \qquad \text{with fully effective drains} \tag{2.12}$$

2.9 Sample disturbance

During retrieval of the sample from the ground and installation of the soil specimen into the testing device, the soil undergoes changes in stress, water content and structure which are generally referred to as sample disturbance effects. The quality of a sample is the result of many actions before, during and after the actual sampling operation: drilling,

penetration and retrieval of the sampling tube, transportation, storage, extrusion, trimming and other operation required to prepare the specimen for the experiment (Santagata, 1994).

Jamiolkowski et al. (1985) identifies three sources of sample disturbances arising from the stress relief, sampling techniques and handling procedures. He also suggests ways of assessing the degree of sample disturbance via radiography, measurement of the sample's effective stress and evaluation of one dimensional compression curves.

Ladd (1991) states that sample disturbance from conventional tube sampling alters the in situ soil structure, causes internal migration of water, frequently leads to substantial reduction in the effective stress of the sample, and often produces highly variable strengths from unconsolidated-undrained (UU) type testing. He advocates the use of consolidated-undrained (CU) tests to minimize these adverse effects. However, CIU tests are deemed inappropriate since shearing starts from isotropic rather than the in situ $\mathrm{K_o}$ stress conditions. Therefore, $\mathrm{CK_oU}$ tests using a consolidation stress ratio, K_c=$\sigma'_{hc}/\sigma'_{vc}$, approximating the in situ $\mathrm{K_o}$ are needed, both to help restore the in situ soil structure and to give more meaningful stress-strain-strength data. The two distinct reconsolidation techniques used for $\mathrm{CK_oU}$ tests, the SHANSEP (Ladd and Foott, 1974) and Recompression (Bjerrum, 1973) methods, are now discussed.

2.10 Reconsolidation procedures for mitigating sample disturbance: SHANSEP and recompression

The restoration of soil structure and the elimination or mitigation of the effects of sample disturbance on soft soils using laboratory testing methods has always been a challenge for researchers. There are two widely used reconsolidation methods that attempt to achieve this goal: the Stress History and Normalized Soil Engineering Parameters method (SHANSEP; Ladd and Foott (1974)) and the Recompression method Bjerrum (1973). These two methods were developed independently and each has its advantages and disadvantages as related to sample disturbance.

The SHANSEP method was introduced in Massachussetts Institute of Technology in the early 1970s by Ladd and Foott (1974). This technique attempts to do the following: minimize adverse effects of sample disturbance, recognize the importance of stress history, consider the effects of stress induced anisotropy, and use the normalized stress behavior to predict undrained shear strength. The laboratory tests includes triaxial Ko consolidated undrained compression and extension tests ($\mathrm{CK_oU}$-TC/TE) as well as direct simple shear tests.

Bjerrum (1973) believed that mechanical disturbance was a minor problem when compared to internal swelling, and the original objective of the Recompression method was to eliminate the adverse effects of internal swelling by reconsolidating the soil specimens to the exact in situ stress state that the soil experienced prior to being sampled. As a result, volume changes incurred during sampling should ideally be reversed as the specimen is recompressed.

Both the SHANSEP method and the Recompression methods use the reconsolidation technique to minimize the effect of sample disturbance. The reconsolidation technique is illustrated in Figure 2.12. Point 1 in Figure 2.12 designates the in situ stress state. Point 2 indicates the stress state of the sample after sampling as the stresses decrease. When the sample is reloaded to the effective insitu vertical stress it will have a lower void ratio than the insitu sample due to disturbance. As the sample is loaded beyond the maximum past pressure, it follows the virgin consolidation curve, the further the soil is loaded along the virgin consolidation curve the closer it approaches along the insitu consolidation curve (shown by the dashed line in Figure 2.12). Thus loading beyond the maximum past pressure tends to erase the effects of sample disturbance. The soil specimen can then be sheared to failure in a normally consolidated state (point B) or swelled and sheared to failure at a known OCR (points C and D). In the Recompression technique, the test specimen is reconsolidated (ideally at $\mathrm{K_o}$) to $\sigma'_{vc} = \sigma'_{vo}$ shown by point 3.

The SHANSEP method accounts for the effects of stress history on undrained shear strength. Consolidation testing is first needed to determine the stress history of the soil.

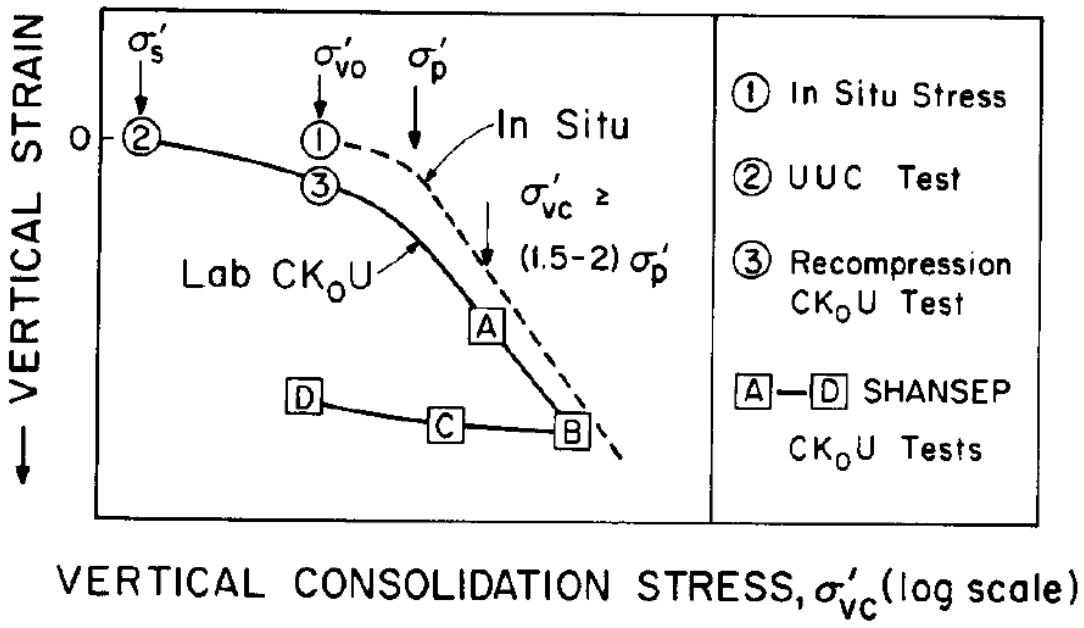

Fig. 2.12. Consolidation procedures for CK_oU (Ladd and Foott, 1974).

During $\mathrm{CK_oU}$ triaxial testing the soil is consolidated under $\mathrm{K_o}$ conditions beyond the maximum past pressure, thus making it normally consolidated; the soil is then swelled under $\mathrm{K_o}$ conditions making it overconsolidated. Normally consolidated soils and overconsolidated soils have different undrained shear strength.

The results are expressed in terms of normalized soil parameters (NSP), and the NSP vs. OCR relationships need to be established (e.g., log C_u/σ'_{Vc} vs. log OCR to obtain values of S and m in equation 2.13).

$$\tau/\sigma'_{vc} = S(OCR)^m \tag{2.13}$$

These relationships can then be used to along with the stress history to compute Cu profiles as a function of time.

Much has been debated about the relative merits of the two reconsolidation techniques. Ladd (1991) opinion can be summarized as follows.

The Recompression technique:

1. Is clearly superior for highly structured deposits (e.g. brittle, sensitive Canadian clays), and for strongly cemented soils.

2. Is preferred whenever block quality samples are available and for testing weathered and highly overconsolidated deposits where SHANSEP is often difficult to apply.

3. Should always be accompanied by a thorough evaluation of the in situ stress history.

The SHANSEP technique:

1. Is strictly applicable only to mechanically overconsolidated and truly normally consolidated deposits exhibiting normalized behavior.

2. Is probably preferred for testing tube samples from deep deposits of low OCR "ordinary" clays.

3. Has the distinct advantage of forcing the user to assess the in situ history, and of developing normalized stress-strain strength parameters that can be used on subsequent projects.

Two types of time effects influence the behavior of $\mathrm{CK_oU}$ tests Ladd and Foott (1974): the time allowed for consolidation prior to shear and the strain rate used during shear. The first affects behavior due to the well known fact that "aging" at constant effective stress (i.e. secondary compression) increases the stiffness and pre-consolidation pressure and, hence, the undrained strength of normally loaded soils. 'Aging' effects are most important with low OCR specimens, thus the amount of aging should be controlled in order to obtain consistent $\mathrm{CK_oU}$ data. Ladd (1991) recommends one log cycle as the ideal amount of time allowed for consolidation. If $\log(t/t_p)$ is much less than one, significant pore pressures may develop during undrained shear due to preventing secondary compression and a $\log(t/t_p)$ much greater than one will take too long and the strength data will require a correction for the increased σ'_p.

Laboratory undrained tests on cohesive soils show that strength increases with increasing strain rate and hence decreasing time to failure (t_f). Although no rational framework exists to select strain rates to replicate in situ behavior, laboratory triaxial tests on cohesive soils show higher strengths with increasing strain rate (Germaine and Ladd, 1988), this is shown in Figure 2.13. Thus general practice by many leading research-consulting laboratories is to use an axial strain rate of 0.5-1% per hour for triaxial tests.

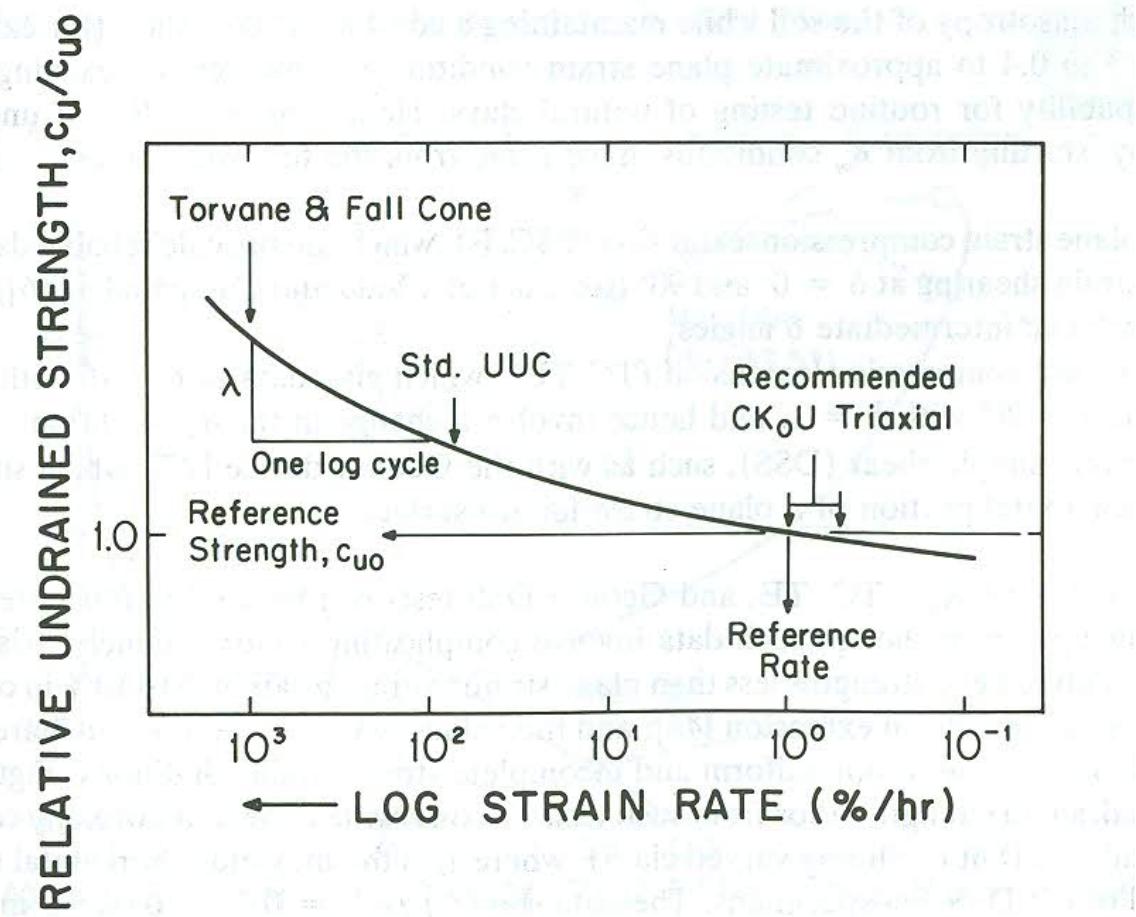

Fig. 2.13. Schematic illustration of variation in undrained shear strength with strain rate (Germaine and Ladd, 1988).

3. CHARACTERISTICS OF GULF OF MEXICO CLAY

3.1 Introduction

In order to understand and assess the likelihood of seafloor slope failures in the Gulf of Mexico, studying the properties of the sub-marine deposit is of utmost importance. The biggest challenge is that the offshore soil sampling is extremely expensive and mostly proprietary, resulting in limited publicly available information. Obtaining offshore samples is not only expensive, requiring the use of specialized equipment but also needs great expertise in handling and producing high quality undisturbed samples. This makes the available offshore samples of Gulf of Mexico clay extremely valuable.

This chapter explains the origin and provenance of Gulf of Mexico clay and how it was sampled. It also lists and summarizes all the preliminary tests and characteristics of the clay.

3.2 Geology and provenance

Gulf of Mexico clay samples were collected in and around the Green Canyon near the Sigsbee Escarpment by the Research Vessel Brooks-McCall operated by TDI-Brooks International. These samples were collected as part of the multi directional simple shear (MDSS) research project (Rutherford, 2011) in October 2007. Approximately 30 sites were sampled for the cores as shown in Figure 3.1, some of the cores were sampled on flat ground but most were sampled on slopes of varying degrees.

The 100 mm (4 in) diameter cores were taken using the jumbo piston core (JPC) system at 1,000-1,300 meters of water depth. The JPC consists of a 4,000 lb weight stand, a 4" core barrel, a mechanical trigger, standard schedule 40 PVC liner, a cutting shoe, and a foil core catcher. The jumbo piston corer (www.tdi-bi.com) uses the free fall of the coring rig to achieve a greater initial force on impact than gravity coring. A sliding piston inside the core barrel is used to reduce inside wall friction with the sediment and to assist in the

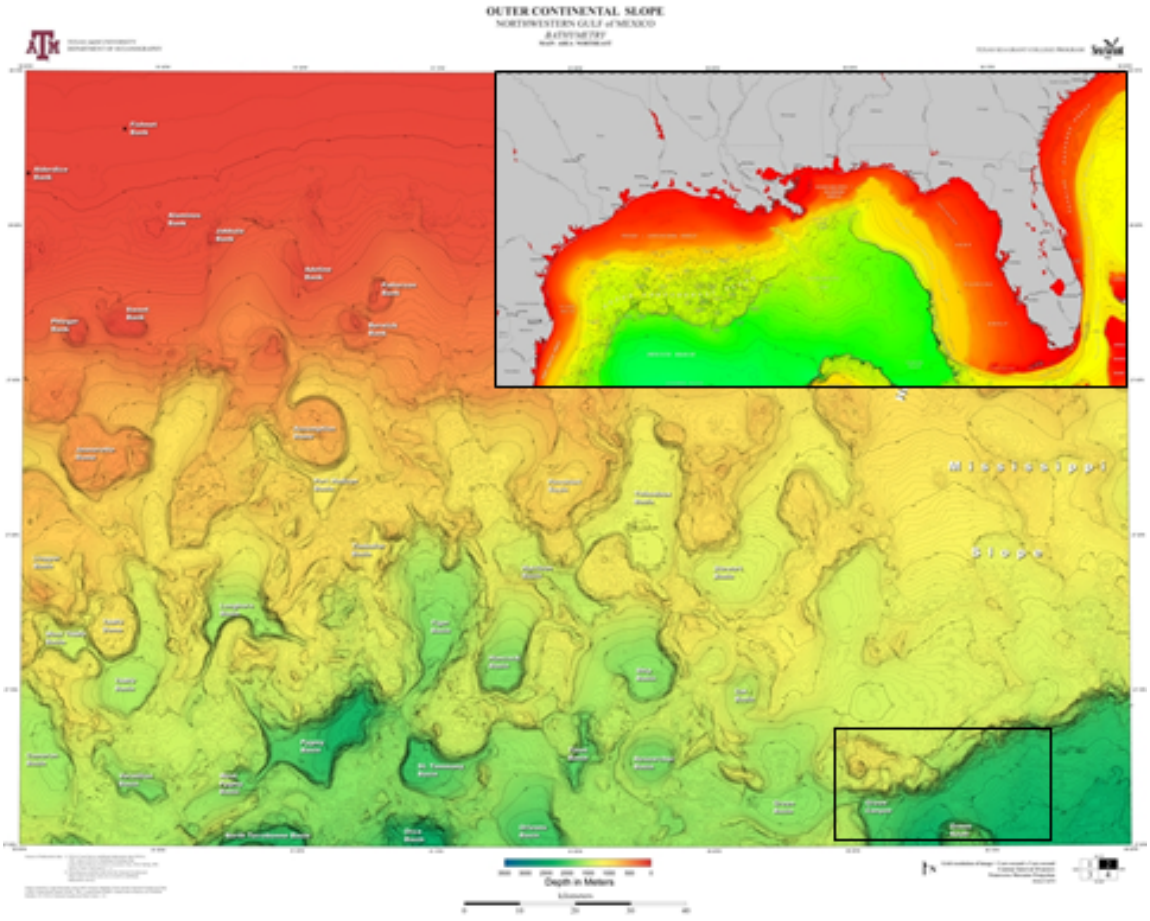

Fig. 3.1. Locations of jumbo piston cores from Gulf of Mexico (Rutherford, 2011).

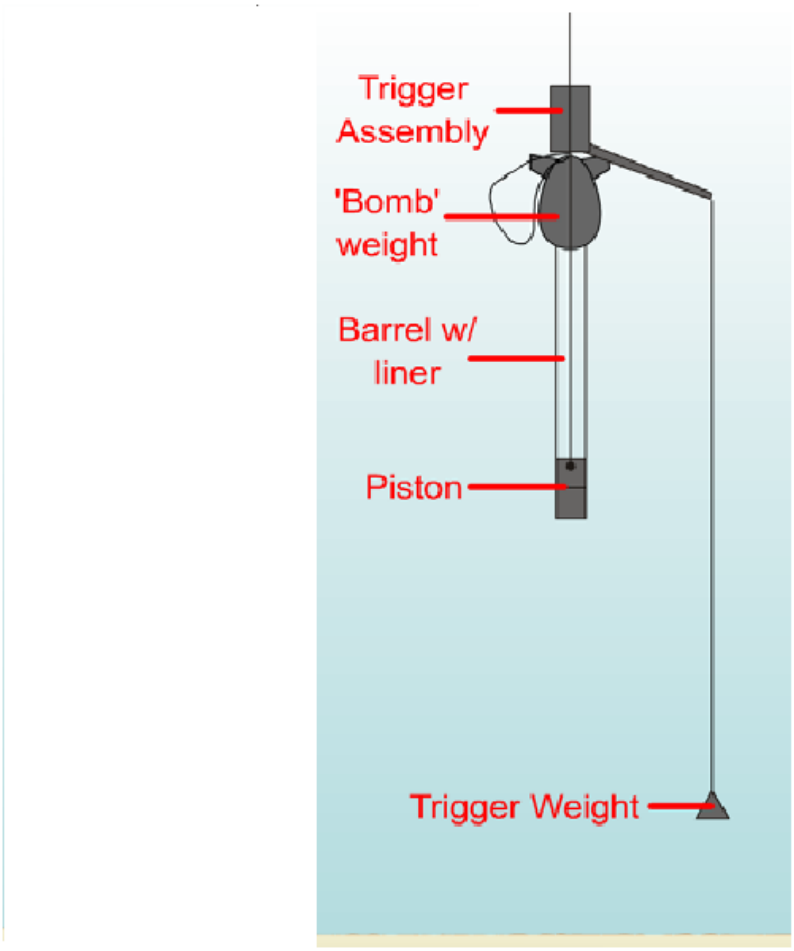

Fig. 3.2. TDI-Brooks International jumbo piston coring system (www.tdi-bi.com).

evacuation of displaced water from the top of the corer. TDI-BI vessels are equipped with 30 meter 4" Jumbo Piston cores that can be collected at depths in excess of 4,000 meters. The JPC utilizes a cantilevered deployment platform over the stern of the vessel with a rail and capture bucket assembly placed on the deck of the vessel directly beneath the stern Aframe. The jumbo piston cores were cut into 1 meter long sections, labeled, wax sealed, capped and stored vertically. Some cores were tested with a laboratory miniature vane on the vessel and the top 7-8 cm (3 in) were bagged for additional geotechnical testing onshore.

3.3 Multi sensor core logging (MSCL)

The core samples were scanned using a GEOTEK Multi-sensor core logger (MSCL). A conveyor system moves the sensor array, which scans the core as it passes. The conveyor is driven by a stepper motor which can position a core to an accuracy of better than 0.5 mm. The computer controlling the conveyor also controls the sensors, so that all data is automatically correlated. The computer also measures the length of each core section and can automatically subtract the thickness of the end caps, allowing the sections to follow sequentially, producing a profile for the full core (Rutherford 2011).

The MSCL can log core sections up to 1.5 m long and 15 cm in diameter, and can sample at 1 mm intervals. The logger is equipped with a 137 Cs gamma source in a lead shield for determining bulk density, with a resolution better than 1%. The logger is also equipped with 250-500 kHz piezo-electric ceramic transducers for measuring P-wave velocity. The sensors which are spring-loaded against the sample and accurate to about 0.2%. Core diameter measurements are taken using rectilinear displacement transducers, with a resolution of 0.05 mm. Data recorded includes p-wave velocity, bulk density, porosity and moisture content.

Figure 3.3 shows the MSCL data of core GOM-core1 which was used for testing. This core was taken from a depth of 1,310 m beneath mean sea level. The p-wave velocity was used to locate samples within the core liner with a minimum amount of disturbance. Only sections with no or very low disturbance were tested in the triaxial apparatus (depths 6.5 m-7.7 m and 8.3 m-11 m). Both ends of core sections were not used because of possible disturbance, oxidation and change in water content during the storage period. Compared to other clays the p-wave velocity measured is quite low (1050 m/s). The porosity at the depths tested appears to remain constant.

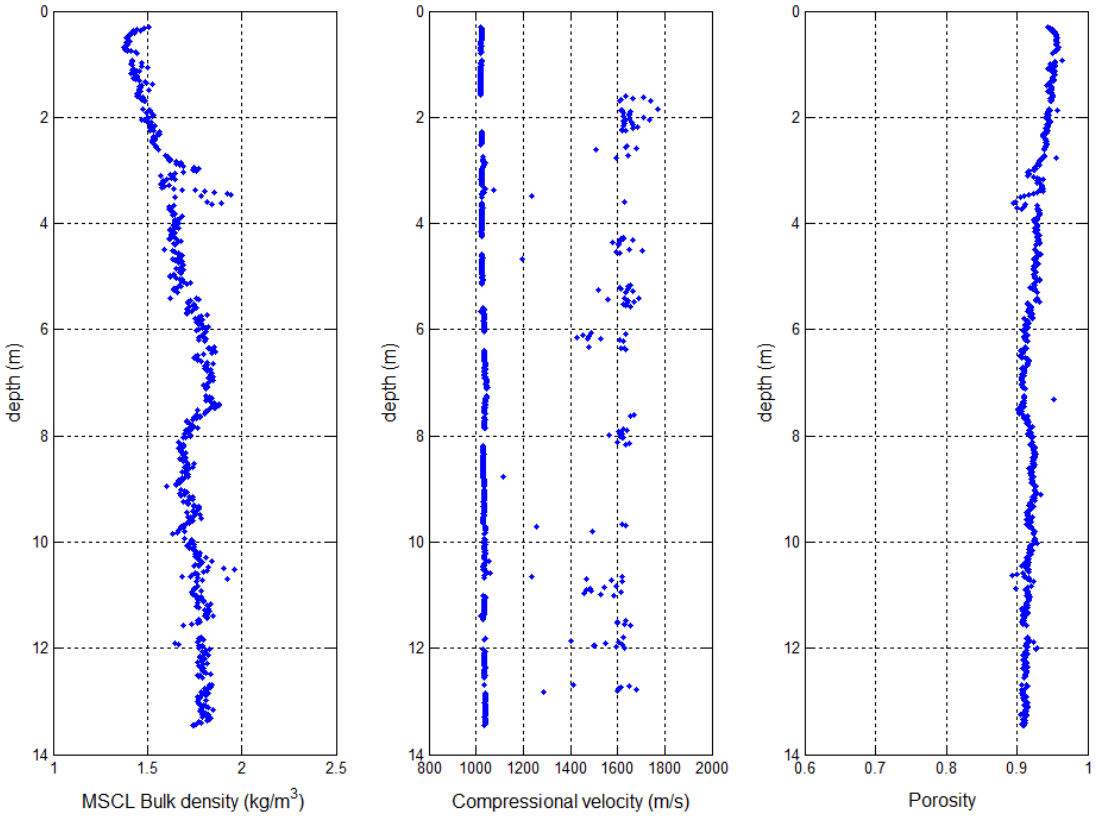

Fig. 3.3. Details of bulk density, compressional velocity and porosity along the length of core GOM-core1 obtained using MSCL.

3.4 Classification and index properties

Following the MSCL radiography process, classification and index tests were carried out on samples from core GOM-core1. The natural field water contents and minivane strengths were determined from the ends of each tube section. Additional water content measurements along the length of the core were obtained from every sample used for the engineering tests, both before and after performing the test. Atterberg limits, grain size analysis and specific gravity tests were also performed on representative samples.

3.4.1 Natural water content, atterberg limits, plasticity chart

Figure 3.4 presents core depth versus natural water content for core GOM-core1. As seen from the figure, the water contents in the top 4 m is more than 100%. Along the depth of 4 m to 7 m the water content is seen to slowly decrease from 100% to around 60%. Beyond 7 m the water content appears to be quite stable ranging from 60% to 80%. This trend is physically noticable in the stiffness of the clay. The clay at shallow depths was found to be extremely soft but stiffness increased with depth. Most of the tests for this research were carried out at depths below 6 m as the sample was too soft to handle and could not be placed in the triaxial chamber without considerable disturbance.

Figure 3.4 shows the liquid and plastic limits for the clay core. The tests were carried out from the trimmings of the engineering tests. The plastic limit is approximately 29 + 1 SD from the depths 4 m to 14 m, for the depth 0-4 m the plastic limit appears to be 36 + 1 SD. The liquid limit gradually decreases from 100 to 60 from depths of 0 m to 6 m and ranges from 60 to 80 at depths below 7 m. It should be observed that the natural water content is more than the liquid limit until a depth of 6 m.

The plasticity chart is presented in Figure 3.5. The results show that each section is close to the A-Line, as is typical of marine illitic clays, meaning that each soil could be classified as either MH or CH. The classification was carried out only at certain represen-

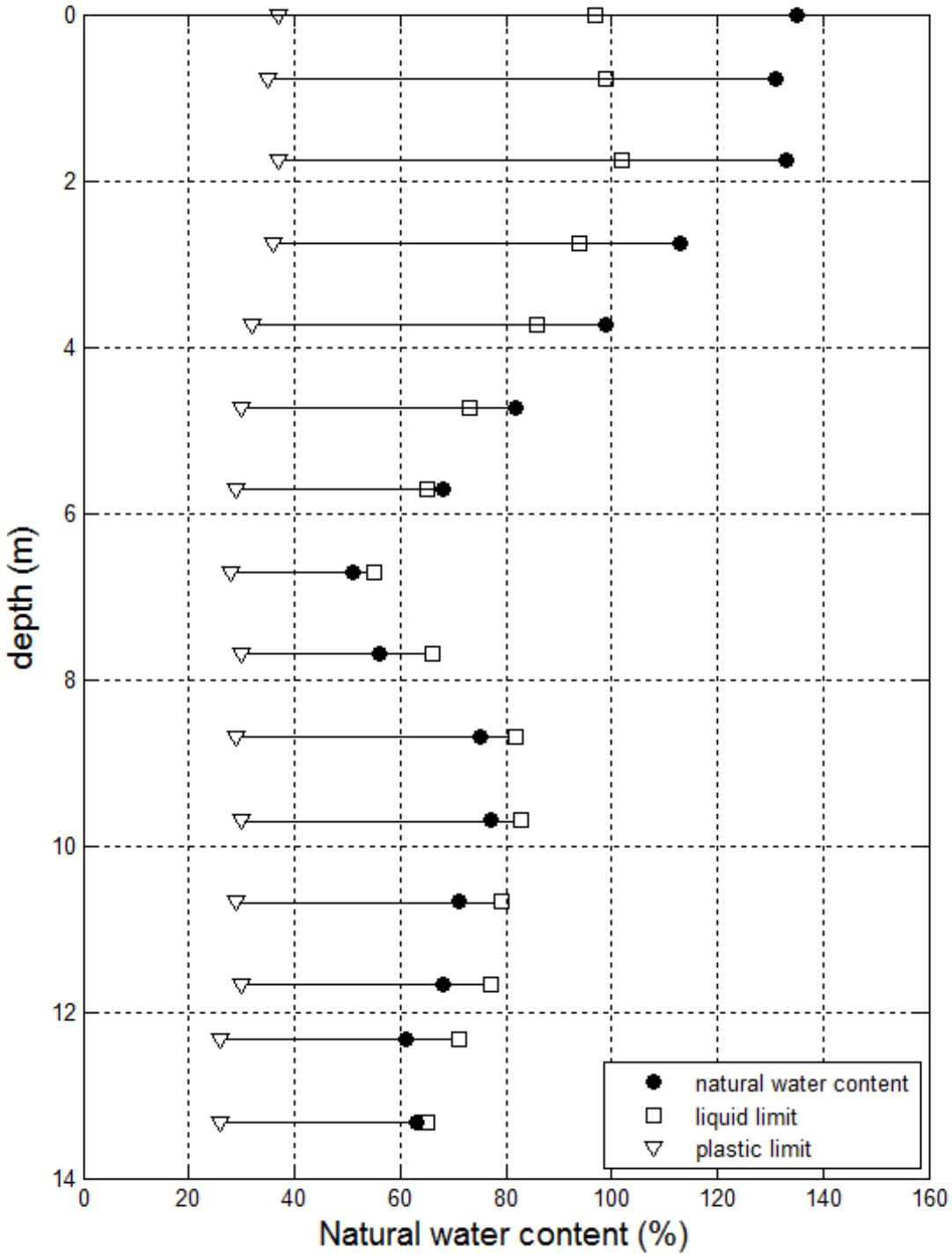

Fig. 3.4. Natural water content against depth.

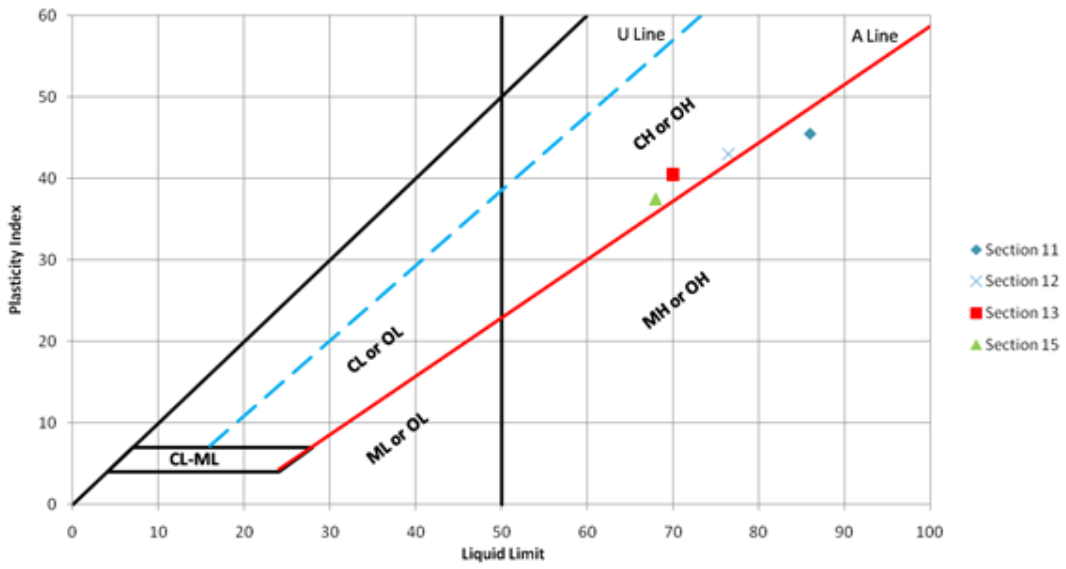

Fig. 3.5. Casagrande's plasticity chart showing atterberg limit results for sections from the core GOM-core1.

tative sections close to the samples that resulted in high quality data during testing. The depth of these sections are given in Table 3.1.

3.4.2 Strength

Figure 3.6 shows the minivane strengths for the clay deposit (Rutherford, 2011). The strength increases gradually with depth as expected. The range of the strength shows that the clay is extremely soft with a maximum shear strength of only 22 kPa at depths of 12-14 m.

3.4.3 Grain size distribution and specific gravity

Grain size curves (Figure 3.7) obtained from four hydrometer tests are very consistent throughout the clay core. Results show that all soils present are composed of 84-99%

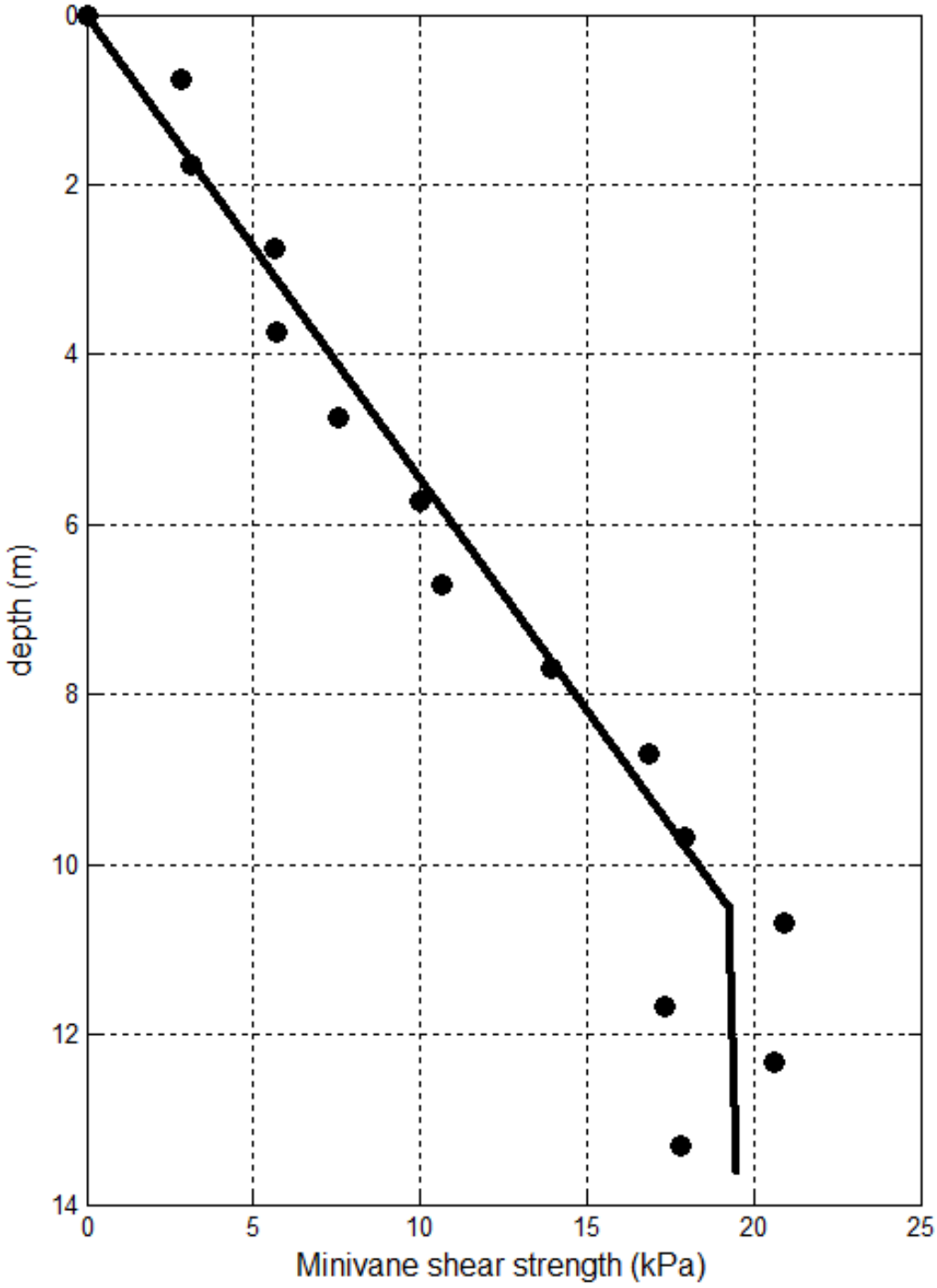

Fig. 3.6. Plots of minivane shear strength against depth.

Table 3.1
Representative sample testing summary

Section	Depth (m)	Specific gravity	Soil type
11	9-9.7	2.74	MH
12	9.7-10.6	2.76	CH
13	10.6-11.5	2.76	CH
15	12.2-13.5	2.76	CH

fine particles, 51-72% of which were clay size. Atterberg limits tests were used for classification purposes as they capture more accurately the behavior of the soil in practice. Specific Gravity tests were also performed in accordance with ASTM D854. The results are reported in the representative samples test results summary shown in Table 3.1.

3.5 Pre-consolidation pressure

The pre-consolidation pressure was determined from the consolidation phase of the triaxial test. Presented in Figure 3.8 is Casagrande's graphical method used to obtain the value of pre-consolidation pressure (σ'_p). The consolidation curve in this figure is from a depth of 11.5 m (38 ft). As seen from the figure the pre-consolidation pressure is found to be 72 kPa. Following the SHANSEP technique (reconsolidate to twice the past maximum pressure), all the samples were consolidated to a vertical effective stress of 140 kPa.

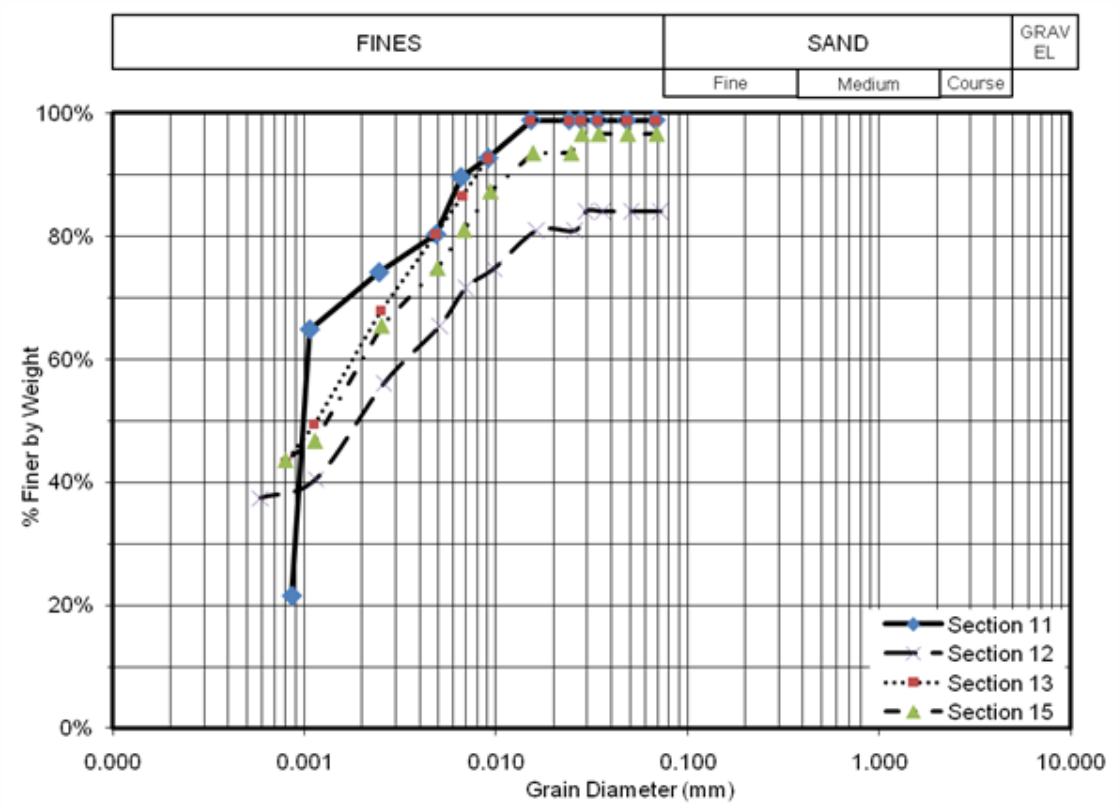

Fig. 3.7. Hydrometer analysis for sections from core GOM-core1.

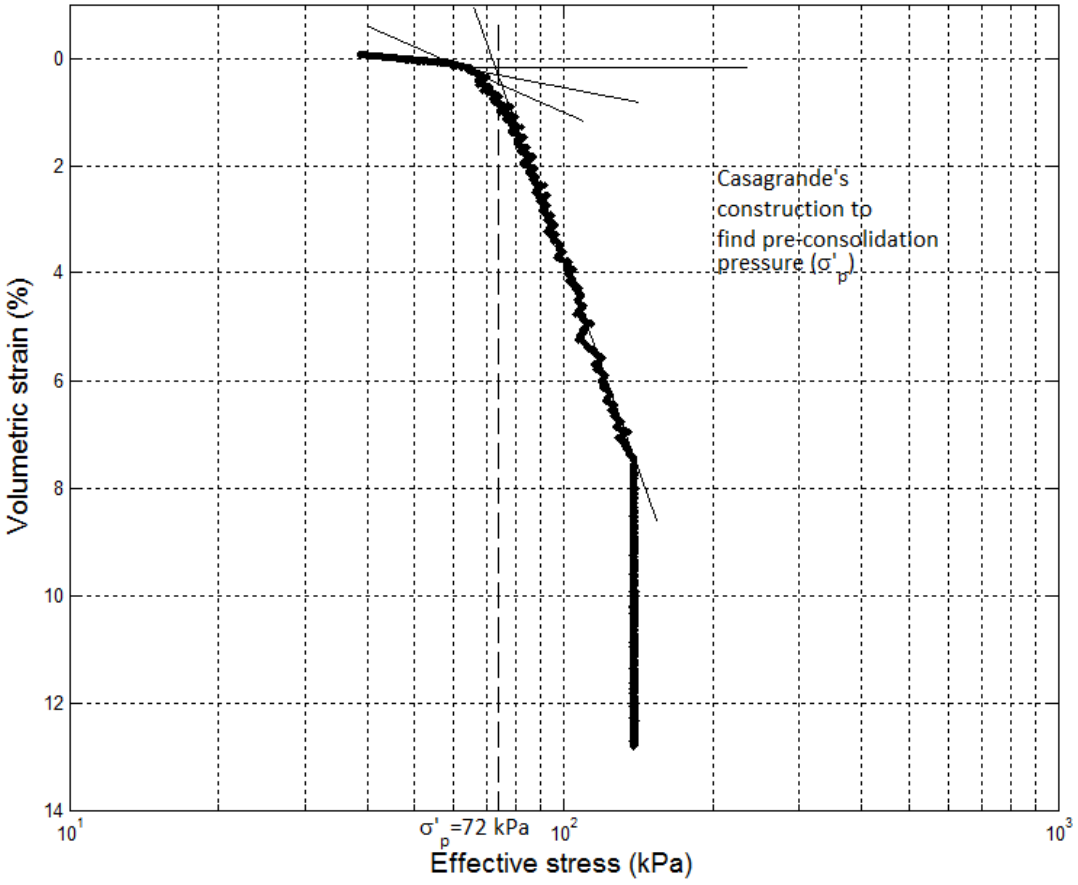

Fig. 3.8. Casagrande's graphical method to find pre-consolidation pressure.

4. GEOTAC TRUEPATH AUTOMATED STRESS PATH SYSTEM: EQUIPMENT AND TESTING PROCEDURES

Improving the current testing equipment and procedures was an integral part of the project in keeping with the goal of obtaining high quality test data during the course of this research. Emphasis was placed on developing consistent laboratory and data reduction techniques in order to remove as much operator-induced uncertainty in the results as possible. Also, special care was taken in the handling of the samples, to avoid causing additional disturbance.

This chapter describes the GeoTAC TruePath Automated Stress Path System, its components and their functions, and how the system was improved to give reliable and consistent test data. The equipment and setup of the triaxial system is explained in greater detail in Appendix A.

4.1 Equipment and software

The triaxial testing system used for this research was the GEOTAC TruePath system (Figure 4.1), which consists of the axial load frame, cell and pore pressure-volume flow pumps, instrumentation, data acquisition and control hardware and software.

The axial load frame has a capacity of 4.45 kN (1,000 lb), and also provides deformation control with a calibrated screwjack. The position of the platen is recorded when the test is started and the change in platen position used to calculate deformation.

There are two DigiFlow pressure-volume pumps (PVP) in the system: a cell PVP and a sample (pore) PVP that are filled with deaired water. The cell PVP controls the confining pressure applied on the sample and pore PVP leads into the lines that are located at the bottom and top of the specimen. These lines are used for backpressure saturation of the soil specimen and pore fluid drainage/supply during consolidation and drained shear test phases. The pore pressure-volume pump measures the volume change in the sample during consolidation and by knowing the initial area of the sample, a feed back loop can

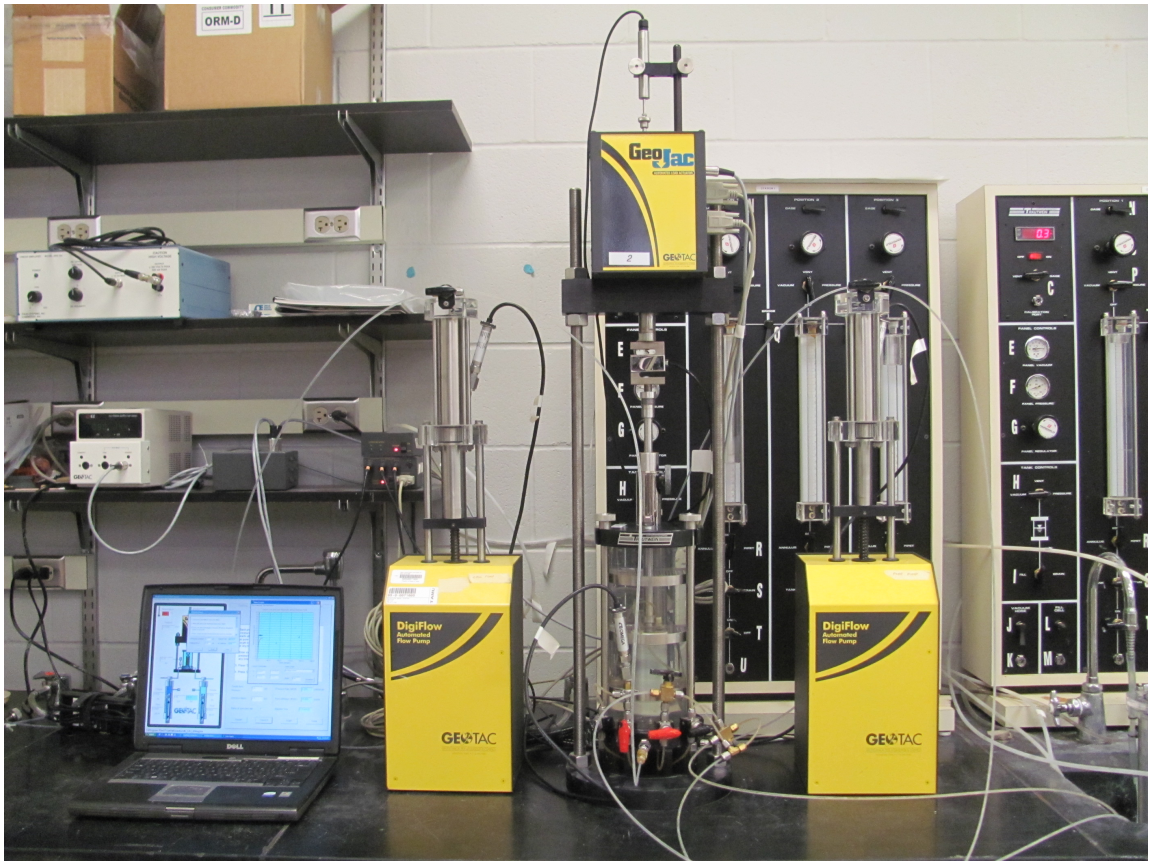

Fig. 4.1. The GEOTAC TruePath system used for testing.

automatically enforce K_o conditions by varying the cell pressure. Combinations of vertical and volumetric deformation rates can be used to control strain paths.

Transducers which are monitored by the data acquisition system and recorded using the GeoTAC system software, are used for monitoring and controlling the test progress. The sensors used in this setup include: a linear strain conversion transducer (LSCT) for axial displacement; force transducer for axial force; and three pressure transducers, one each for cell pressure at the cell PVP, back pressure at the pore PVP and pore pressure within the sample.

The system is operated by a control and data acquisition software which has a graphical user interface to enable the user to input test parameters and monitor the test. A standard Windows-style menu is located at the top of the main user interface window. The available menu items enable users to enter and edit test parameters, sensor calibration information, reading schedules, and hardware settings. The software displays instrumentation readings on the screen as follows: temperature (C), position of axial load platen (inches), specimen displacement (inches), axial force (lbf), fluid pressures (psi), and platen deformation rate (inches/min) values. If any of the instrumentation readings go beyond the minimum or maximum limits set by the user , the corresponding display field turns red, an alarm sounds, and the relevant device component stops moving (Trautwein Soil Testing Equipment Co., 2009).

The program is flexible and user-friendly. It performs all phases of a triaxial test: initial application of a cell pressure to establish a positive pore pressure in the specimen; back pressure saturation; B value check; isotropic or K_o consolidation along any stress path; and shear in either compression or extension.

4.2 Testing procedures

A detailed description of the triaxial system setup procedure is found in appendix A.

Once the sections of the core with low disturbance are identified using the MSCL data, they are cut into shorter lengths of 4 in using a telescopic pipe cutter. These 4 in sections

are then extruded and trimmed very carefully so as to not disturb the sample or change the water content of the specimen. The sample is cut into dimensions of 1.5 in diameter and 3-3.75 in length.

Once the sample is prepared, it is enclosed in a rubber membrane and installed in the triaxial chamber. The preliminary steps for both compression and extension tests are common. A seating pressure of 2 psi (13.78 kPa) and a seating load of 1-2 lbs (4.4-8.8 N) is applied to the sample. An important step is to make sure no air bubbles are trapped in the pore pressure system. This is done by flushing the drain lines multiple times in both directions to remove all visible air bubbles. Each specimen is back pressured to about 5 psi (34.4 kPa) for 12 to 15 hrs, after which the B-value is checked. The test proceeds to the consolidation phase if the B-value is greater than 0.95. Otherwise the sample is again back pressured for another 12 hrs and its B-value is rechecked.

The laboratory tests carried out in the testing program consist of both $\mathrm{CK_oU}$-C and $\mathrm{CK_oU}$-E tests. $\mathrm{K_o}$ consolidation is specified to model the existing conditions in the field. Tests were carried out at selected elevations with OCRs of 1, 1.5, 2, 4 and 8. The samples for these tests were taken as closely spaced as possible to each other so that they had similar pre-consolidation pressures. Isotropic consolidation was also carried out at OCRs of 1, 2, 4 and 8. Each test consists of two main parts - consolidation and shear - but only the consolidation phase is significantly different between isotropic and $\mathrm{K_o}$ tests. Both parts are controlled automatically by the computer, as previously mentioned. The amount of water leaving the sample is measured by the pore PVP and $\mathrm{K_o}$ consolidation is achieved by controlling the rate of axial deformation and the rate of increase of cell pressure so that the volumetric strain always remains equal to the axial strain, thus maintaining no radial strain conditions.

Another requirement of the SHANSEP method is to reconsolidate the sample to twice the in situ preconsolidation pressure, σ'_p, which experience has shown, can usually be achieved by straining the specimens to at least 7% (Ladd et al., 1977). For this research the sample is reconsolidated to a vertical effective stress of 20 psi (140 kPa) which is two

times the preconsolidation pressure as determined by both constant rate of strain (CRS) consolidation tests and the consolidation phase of the triaxial tests. The specimen at the end of consolidation, is then normally consolidated (NC), and the resulting K_o corresponds to the in-situ, one-dimensional normally consolidated value. The strain rate used is approximately 1%/ hr, which results in consolidation times of 3 (NC) to 5 (OC) days. At this point in the test, the specimen is allowed to sit for 24 hours at the final stress state for the sample to reach equilibrium, to allow some secondary compression to take place and restore a bit of the structure of the clay which was altered during consolidation (Ladd and Foott, 1974). The sample can then either be sheared, or rebounded to a chosen overconsolidation ratio (OCR), allowed to sit for another 24 hours, and sheared then. The undrained shearing is also carried out at a rate of 1%/hr to a maximum strain of 15%, and this takes 15 hrs to complete.

4.3 Data reduction

The data reduction is carried out using Microsoft excel and Matlab.

The instrumentation signals and input voltage are stored at user-defined time intervals during all test phases. The data sheet created by the user includes the details specific to each test such as initial specimen dimensions and zero recordings of each measurement instrument. The raw data is converted into engineering quantities such as force, pressure, displacement, and pore water volume change (refer Appendix B).

The data file appears in four sections in the spreadsheet: seating, back pressure, consolidation and shear. The data for each phase is extracted from each section and imported into a matlab code, where data reduction and plotting is carried out. Although an LSCT was present, it was not used to calculate the axial strain, the platen position within the load frame was used.

4.4 Comments on testing problems and quality of test data

As may be expected for any experimental program, a certain number of problems were encountered. The problems can be roughly categorized as either equipment problems (mechanical or electrical) or procedural problems (including operator errors). Listed below are the primary problems of each type, their effects on the data, and their resolution.

4.4.1 Equipment problems

Transducer sensitivity

The pressure transducer used originally for the testing had a working range of 0-300 psi of pressure. But when it came to measuring smaller pressures below 2 psi, as was required for the soft clay, there was a high amount of oscillation in the readings and a steady pressure would not be maintained over a long period of time. The data points in certain cases varied by more than 1 psi which was very high and would not give accurate readings for the marine clay to be tested. With the transducer reading incorrect values of pressure, the feed back loop on the cell PVP would continuously change the cell pressure applied on the sample trying to match the required pressure. This resulted in the cell PVP applying unsteady pressure on the sample. The old transducers were replaced with pressure sensors having a working range of 0-100 psi of pressure. The new pressure sensor was able to measure constant lower pressures over time which was important for the kind of testing in this research. To compare the sensitivity of the two transducers, a pressure of 10 psi was applied in the triaxial chamber using the cell PVP and the pressure was measured using both the old and new pressure sensors. The plots displaying the comparison between the readings of the pressure sensors are shown in Figure 4.2.

The force transducer used initially in this research was rated for a maximum load of 2000 lbf. The maximum load required to be applied on this clay was approximately 30 lbf. As shown in Figure 4.3, the precision of the force transducer is around 2 lbf which was

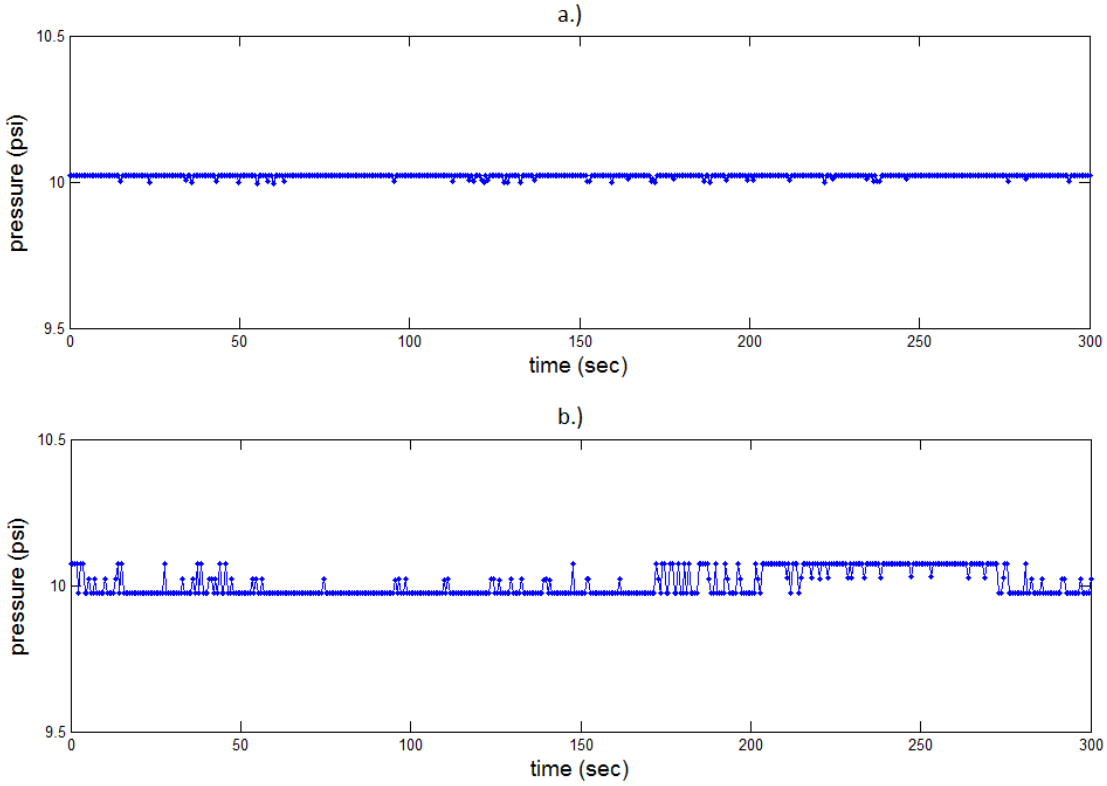

Fig. 4.2. Comparing pressure transducer sensitivity: a) New pressure transducer ; b) Old pressure transducer.

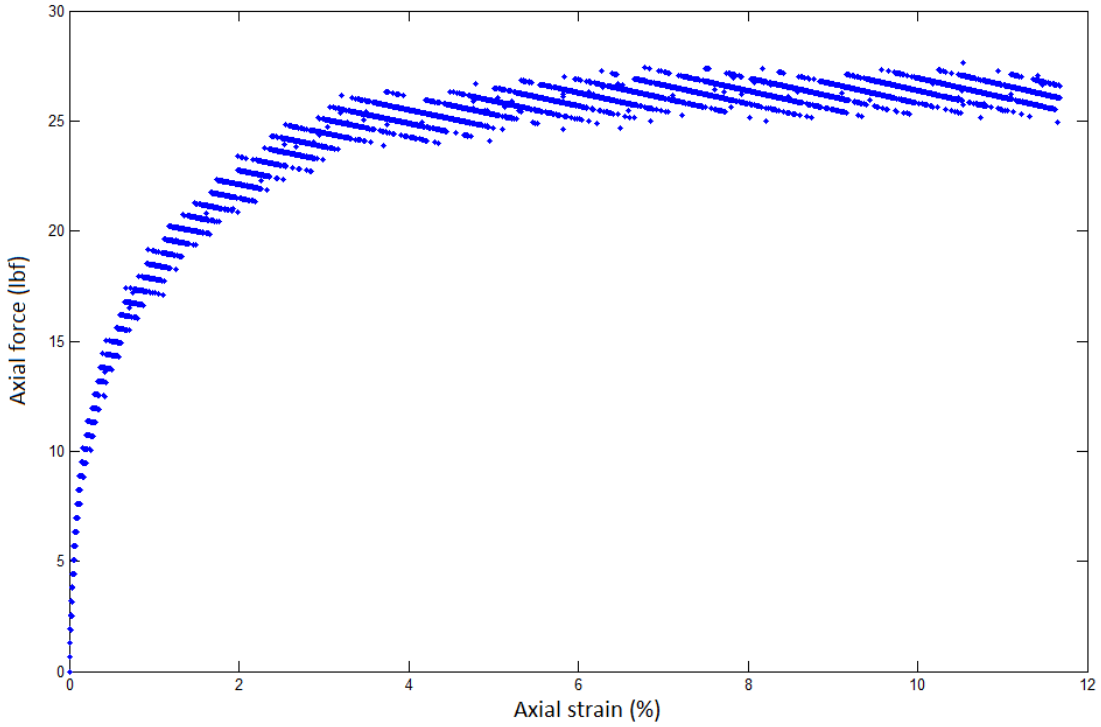

Fig. 4.3. Axial force vs axial strain using old load cell.

not suitable for testing soft clays. A new load cell with a rating of 200 lbf was substituted for the old 2,000 lbf load cell resulting in increased sensitivity.

The linear strain conversion transducer or LSCT was used only for test control and monitoring, and not for the analysis of the test data.

Leaks

Leaks are always a concern during triaxial tests, and particularly so for tests which are carried on for extended periods of time, as the $\mathrm{CK_oU}$-C/E tests. The two possible types of leaks are internal (i.e. cell fluid leaks into the sample), or external (i.e. pore fluid leaks out of the system, outside of the cell). While there were no detectable internal leaks in the

cells during the research program, a few tests were affected by external leaks. This caused an error in the pore pressure reading.

Software limitation

One problem with regard to using the Truepath software was the limit on the number of data points that could be recorded in a single data file during the test. This was observed during the longer tests such as CK_oU tests with OCRs of 4 and 8. Once the limit on the maximum number of recorded data points was reached, the data recording would stop even though the test would keep running well. Data from some good tests went unrecorded before the problem was discovered. A way to work around this was to start a new data file with a reading schedule towards the end of the test. This way the data although is not recorded in the original file can be extracted from the new data file and appended during the data reduction.

4.4.2 Procedural problems

Setting reading schedules

The default reading schedule that was used by the software took very few data points. To increase the number of readings taken during any phase a reading schedule should be created to set the data collection to a user defined rate. The early tests at the beginning of the program were carried out using the default reading schedule. This was changed and the new schedules have been used for all the tests ever since.

Incomplete consolidation

Consolidation was allowed until the end of primary consolidation, this causes pore pressure to be built up when the drain values are closed even before shear begins. Which is why the procedure was modified and the specimen was allowed to sit for 24 to 48 hours

at the final stress state, depending on the height of the specimen, to allow some secondary compression to take place and restore a bit of the structure of the clay which was altered during consolidation.

4.4.3 Overall quality of test data

Despite the problems mentioned above, the overall success rate of the tests was considered reasonable. Once the major problems were resolved the data resulting from this test program were of extremely high quality. In particular the 1D compression curves obtained from the $\mathrm{K_o}$ consolidation phase of the SHANSEP triaxial tests were exceptional. They provided the primary means for estimation of the in situ σ'_p of the marine clay. The consolidation phase also provided the most extensive and reliable estimates of the $\mathrm{K_o}$ of the samples.

5. TEST RESULTS ON GULF OF MEXICO CLAY

This chapter presents the results of all the consolidated undrained triaxial tests carried out on gulf of Mexico clay samples along with the analysis of the data. The first part of the chapter is devoted to the results obtained from the $\mathrm{CK_oU}$ compression and extension tests. Then the results obtained from the conventional CIU laboratory tests are presented.

5.1 $\mathrm{CK_oU}$ tests

5.1.1 Stress-strain characteristics

The stress-strain relationships from $\mathrm{CK_oU}$ compression tests are presented in Figure 5.1. The data include both normally consolidated samples and over consolidated specimens with OCRs of 1.5, 2, 4 and 8 normalized by the pre-shear vertical stress (σ'_{vc}). The stress strain curve for the sample tested at OCR 4 stops at 5.5% strain, because of the initial limit on the number of data points which can be recorded by the software (section 4.4.1.3). This test unfortunately stopped recording data at a time when the user was not available to start another data file.

Figure 5.2 presents normalized stress-strain relationships from $\mathrm{CK_oU}$ extension tests, including data from both normally consolidated samples and over consolidated specimens with OCRs of 1.5, 2, 4 and 8. The problem of the software's limit on recording data occurred with the specimen tested at OCR 4 in extension due to which the data points collected stop at a strain level of 5.5%.

The specimens tested in compression fail at very low axial strains, especially the samples at low overconsolidation ratios. The failure strains increase with increasing overconsolidation ratio as shown in Figure 5.3, which plots the failure strain versus OCR for both $\mathrm{CK_oU}$ compression and extension. As compared to the samples in compression, the $\mathrm{CK_oU}$ extension specimens failed at much larger strains, usually larger than 6%. There is no strain softening visibly seen in the marine clay specimens.

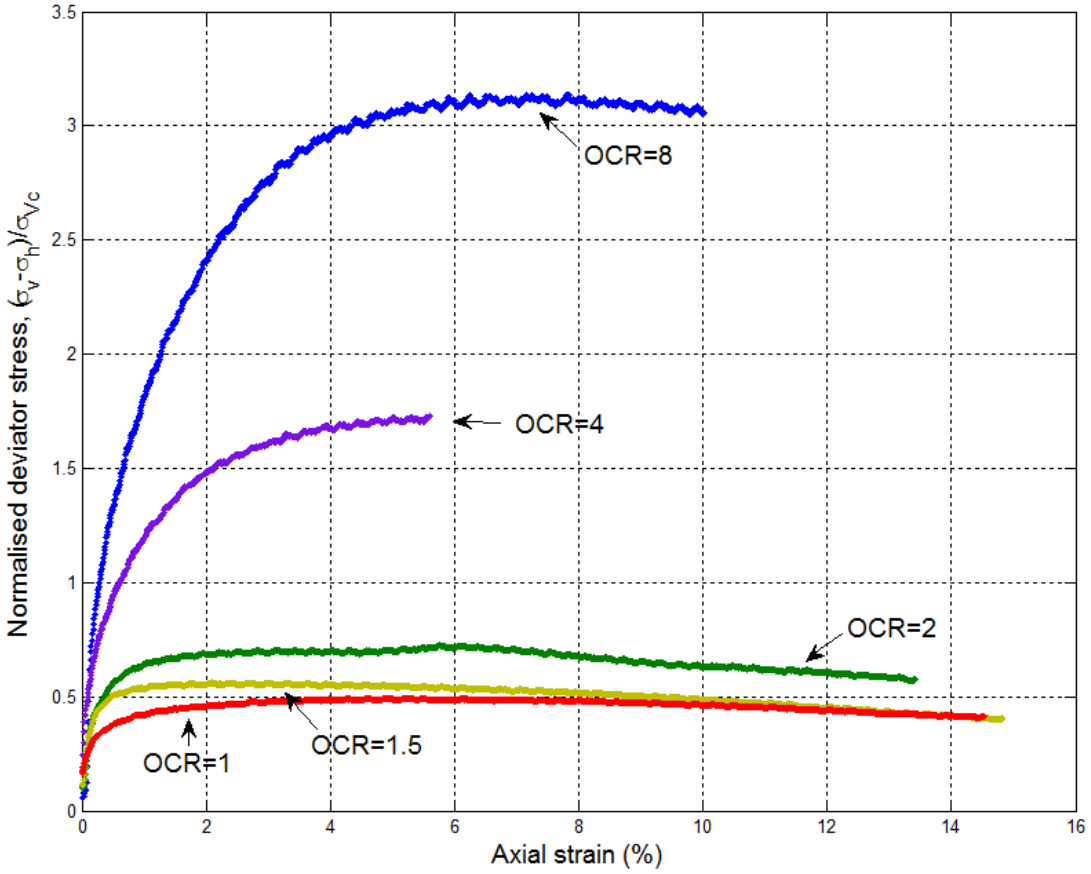

Fig. 5.1. Stress-strain relations for CK_oU-C tests.

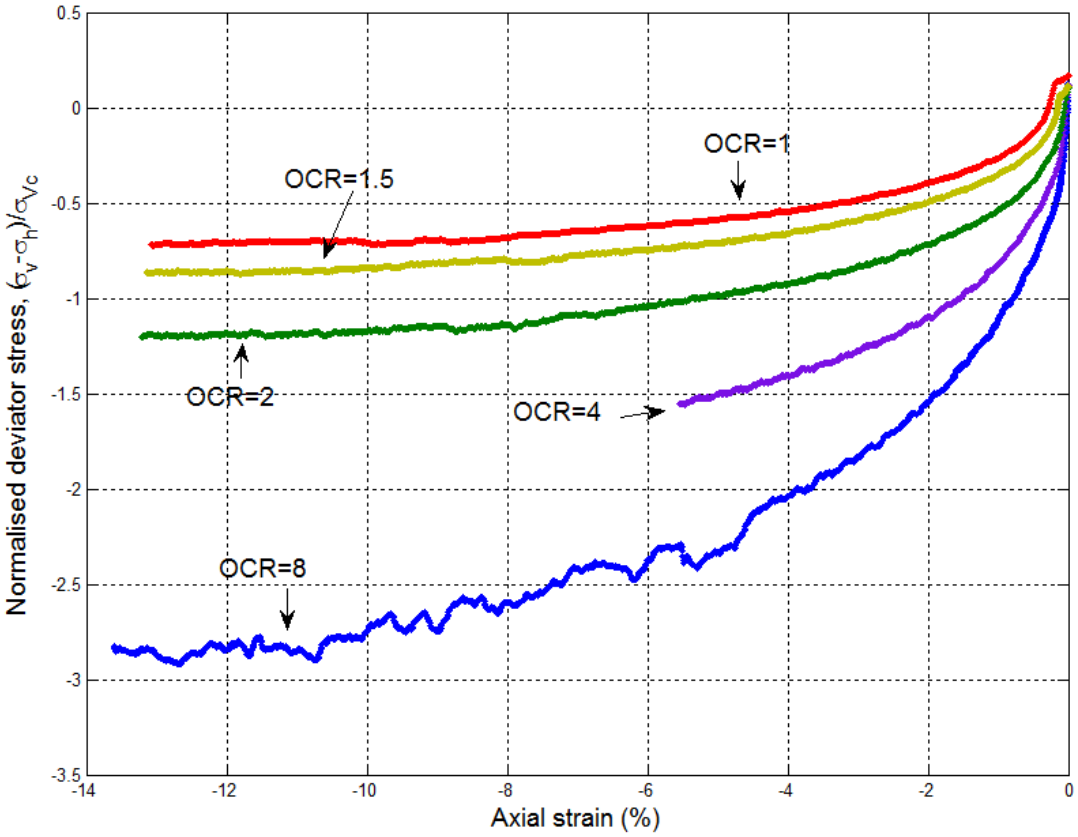

Fig. 5.2. Stress-strain relations for CK_oU-E tests.

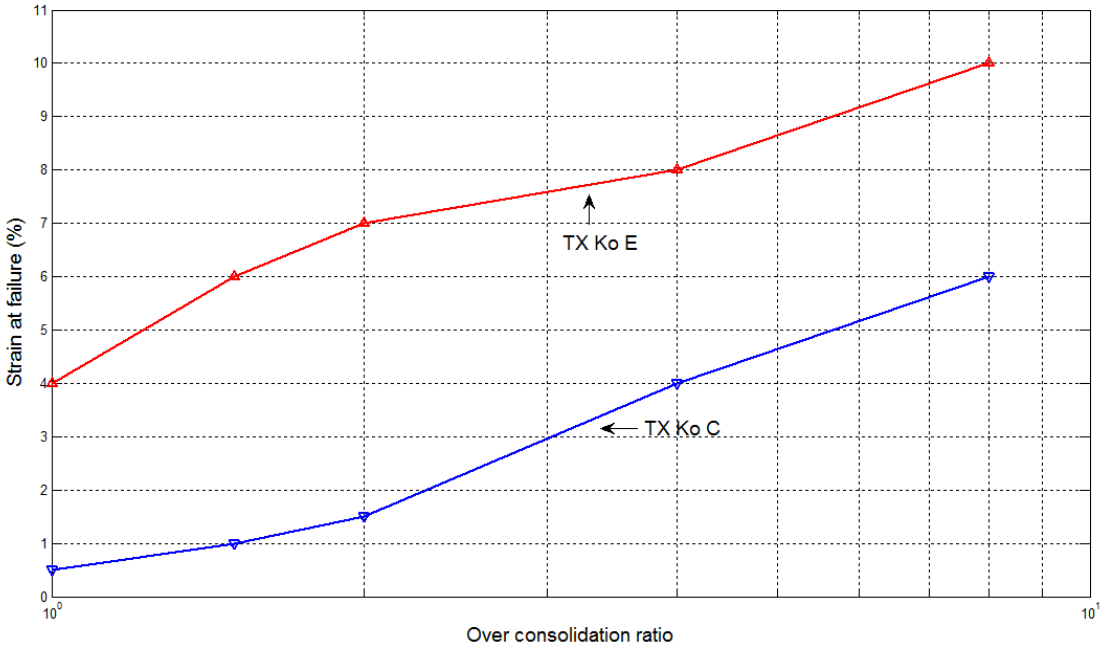

Fig. 5.3. Failure strain with overconsolidation ratio.

These observations are important in the selection of appropriate shear strengths to be used in stability computations. Henkel (1970) pointed out that strain compatibility along a potential failure surface must be considered and that the shear strengths selected for stability analysis must correspond to the shear strain levels developed within the soil along the potential failure surface.

5.1.2 Normalized undrained shear parameters from $\mathrm{CK_oU}$ testing

This section focuses on results of normalized undrained strength ratios versus OCR relationships obtained from the $\mathrm{CK_oU}$ shear tests in order to quantify the degree of undrained strength anisotropy between the compression and extension tests and its variation with stress history. Recommended normalized strength parameters for undrained stability analysis were also developed following Ladd (1991).

Table 5.1
Normalized undrained strength parameters

CK_oU **test**	**n**	**S**	**m**	**COV**
TC	5	0.327	0.697	0.128
TE	5	0.269	0.442	0.470
n= number of tests COV= Coef. of variation				

From the stress-strain data presented in Figures 5.1 and 5.2 we can see that the normalized undrained strength ratios (S_u/σ_{vc}) increase with increasing OCR. This is true for all types of tests. The undrained strength data are interpreted using the SHANSEP framework (Ladd, 1991)

$$(\frac{s_u}{\sigma'_{vc}})_{OC} = (\frac{s_u}{\sigma'_{vc}})_{NC}(OCR)^m \tag{5.1}$$

$$S = (\frac{s_u}{\sigma'_{vc}})_{NC} \tag{5.2}$$

where S is the undrained strength ratio for normally consolidated soil and m is the strength increase exponent. For these SHANSEP tests, OCR is determined by the laboratory maximum past vertical consolidation stress (σ'_{vmax}) divided by the pre-shear vertical stress or the vertical stress at the end of the consolidation phase (σ'_{vc}).

Values of s and m for SHANSEP tests

Table 5.1 summarizes the values of S and m for shear in triaxial compression (TC) and triaxial extension (TE) and Figure 5.4 plots the measured undrained strength ratio (where $q_f = 0.5(\sigma_v - \sigma_h)_f$ and σ'_{vc} is the pre-shear vertical stress) versus OCR, both on a log scale for SHANSEP CK_oU triaxial tests. The listed coefficients of variation (COV) equal the standard deviation in the measured q_f/σ'_{vc} at any given OCR divided by the mean value computed from equation 5.1.

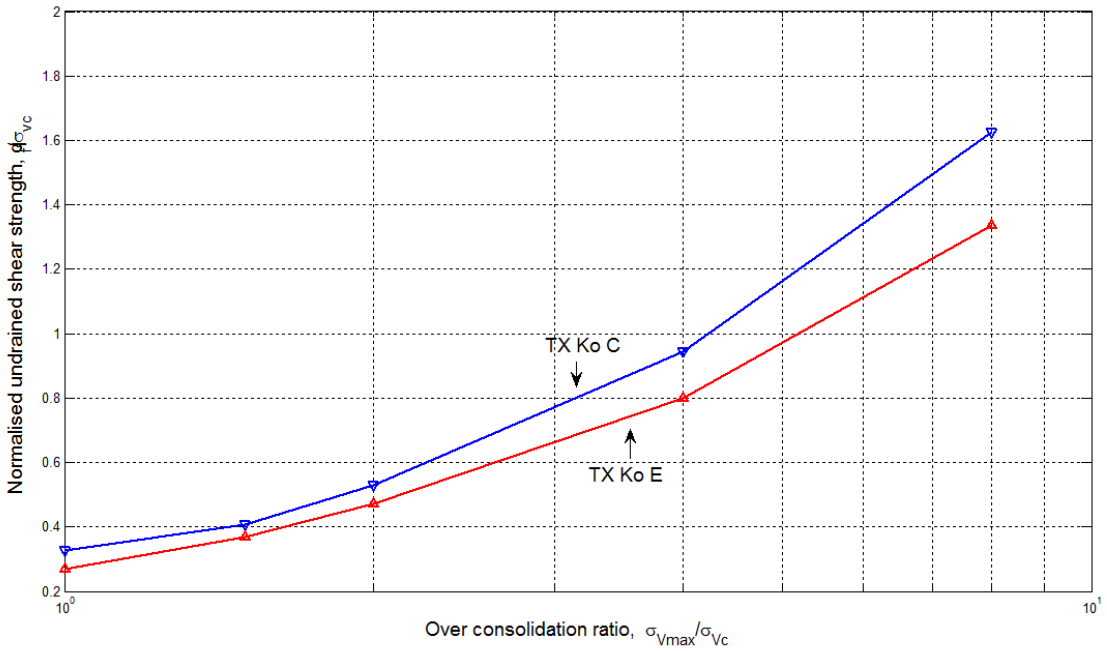

Fig. 5.4. Normalized undrained strength data from SHANSEP $\mathrm{CK_oU}$ tests.

Table 5.2
Degree of anisotropy

OCR	K_s
1	0.822
1.2	0.906
2	0.890
4	0.846
8	0.821

The m-values for the data shown ranges from 0.56 to 0.77, the average of which is reported in the table. It is interesting to note that Ladd et al. (1977) reported m-values ranging from 0.62 to 0.78 from five different clays.

Undrained strength anisotropy

The normalized undrained shear strength ratios are higher for the compression tests than the extension tests. This observation shows that the marine clay exhibits some undrained strength anisotropy. The ratio of peak strength in extension to that in compression has been used to quantify the degree of anisotropy. The parameters in table 5.2 give the values of Ks as defined by the equation.

$$K_s = q_f(TE)/q_f(TC) \tag{5.3}$$

Figure 5.5 plots the normalized undrained shear strength (q_f/σ'_{vc}) along with the corresponding Ks values against log (OCR).

The anisotropic strength ratio, K_s, is approximately constant within the range of OCRs 1 to 10. This indicates that the clay is anisotropic not only in the normally consolidated state but also in the overconsolidated state. Koutsoftas (1981) shows a similar trend for silty clay although the extent of anisotropy is more. Ladd et al. (1977) presented K_s ratios for two other clays where K_s was increasing with increasing OCR.

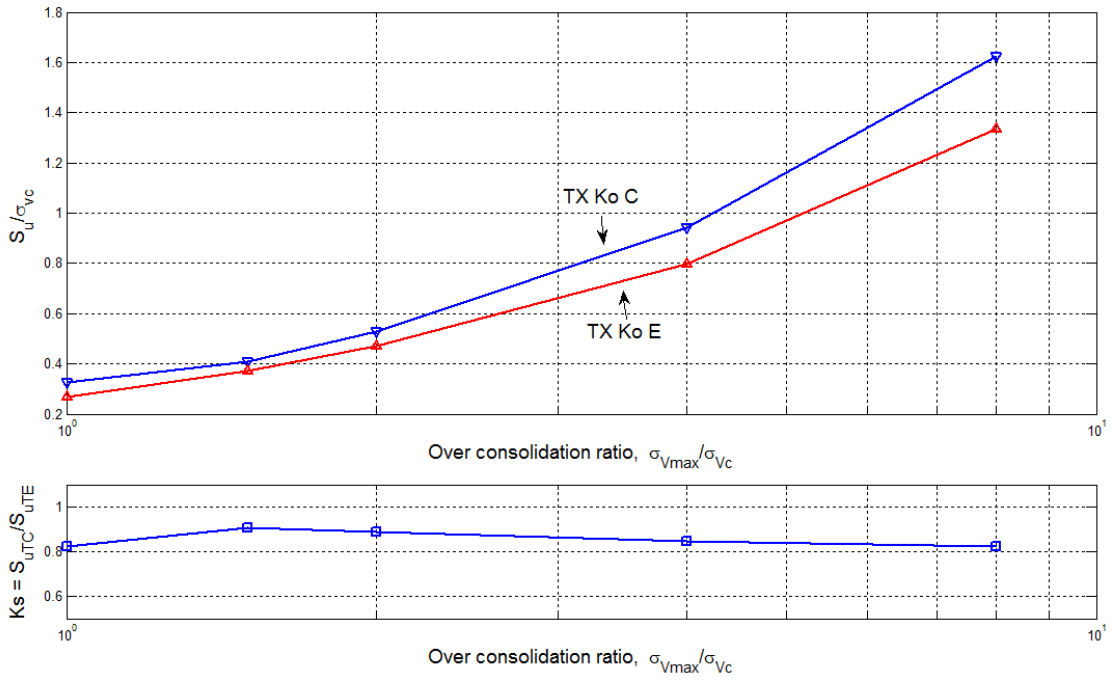

Fig. 5.5. Normalized undrained strengths and Ks versus OCR.

For undrained stability analysis using the method of slices, Ladd (1991) recommends corrections to the peak strengths measured in triaxial tests in order to account for the following factors:

- Increase $q_f(TC)$ by 9% and $q_f(TE)$ by 22% to obtain peak strengths in plane strain compression (PSC) and extension (PSE), respectively (Section 4.6 of Ladd (1991))
- Decrease the average of the peak strengths by 8% ($\pm 4\%$ SD) to account for strain compatibility (Section 4.9 of Ladd (1991))

After selecting $S_c = 0.327$, $m_c = 0.697$, $S_e = 0.269$ and $m_e = 0.442$ to model the peak triaxial strength data, application of the above corrections gives $S_c = 0.356$ and $m_c = 0.697$ for shear in plane strain compression (PSC) and $S_e = 0.328$ and $m_e = 0.442$ for shear in plane strain extension (PSE).

5.1.3 Effective stress behavior

Figure 5.6 presents normalized effective stress paths (ESP) from $\mathrm{CK_oU}$ -compression and $\mathrm{CK_oU}$ -extension. The effective stress paths lead to the following observations:

At failure, the normally consolidated specimen tested in compression shows an increase in excess pore pressure causing the average effective stress, $s = (\sigma_v + \sigma_h)/2$ to decrease, this is also seen in the specimen tested at OCR=1.5 to a lesser extent. The specimens with OCRs over 1.5 show a significant decrease in the excess pore pressure generated, causing the average effective stress to increase. This increase in effective stress becomes more pronounced as the overconsolidation ratio increases. This increase in effective stress during shear is mainly responsible for the increase in s_u/σ'_{vc} ratio as the overconsolidation ratio increases.

The normally consolidated specimen tested in extension showed a reduction in average effective stress, resulting in a low s_u/σ_{vc}. As the overconsolidation increases the reduction in effective stress becomes smaller. At OCRs greater than 2 there is an increase in effective

stresses during shear which again is the reason for the observed increase in S_u/σ_{Vc} with increasing OCR.

Figure 5.6 also shows the effective stress failure envelopes in compression and extension. For the compression tests, the effective stress envelope at critical state is represented by a perfectly straight line at a α of 25.5^o. For the extension tests, the effective stress shear envelope at critical state is not as clear as for compression. It is best represented by a line which passes through the points of maximum shear stress with an α of 26.5^o. The friction angle (ϕ) for the compression failure envelope was found to be 28^o and ϕ for the extension failure envelope was found to be 29.5^o.

The excess pore pressure generation with respect to the axial strain in the $\mathrm{CK_oU}$ compression tests are shown in Figure 5.7. During testing of specimens with OCR=1 and OCR=2 a small leak developed in the tubing of the pore pressure transducer. Although this was noticed and the valve tightened as soon as possible it caused a slight dip in the curves. As seen in Figure 5.7 the excess pore pressure generated decreases with increasing overconsolidation ratio. For the samples tested at higher OCRs especially at OCR=8, the excess pore pressure is negative.

Another important observation that can be made is that for the normally consolidated sample and the sample at OCR=1.5, there is a large increase in excess pore pressure after the peak deviator stress was reached (Figure 5.3).

Figure 5.8 shows the negative pore pressure generated in the $\mathrm{CK_oU}$ extension tests. Here the negative excess pore pressure increases with increasing OCRs. Also an observation is that the maximum negative pore pressure for all samples in $\mathrm{CK_oU}$-E tests develop at the same time when as failure.

The pore pressure coefficients at failure ($\overline{A_f}$) are plotted versus overconsolidation ratio in Figure 5.9 (Schmertmann, 1955). The definition of $\overline{A_f}$ is as follows:

$$\overline{A_f} = \frac{\Delta u - \Delta\sigma_h}{\Delta\sigma_v - \Delta\sigma_h} \qquad \text{(compression)} \tag{5.4}$$

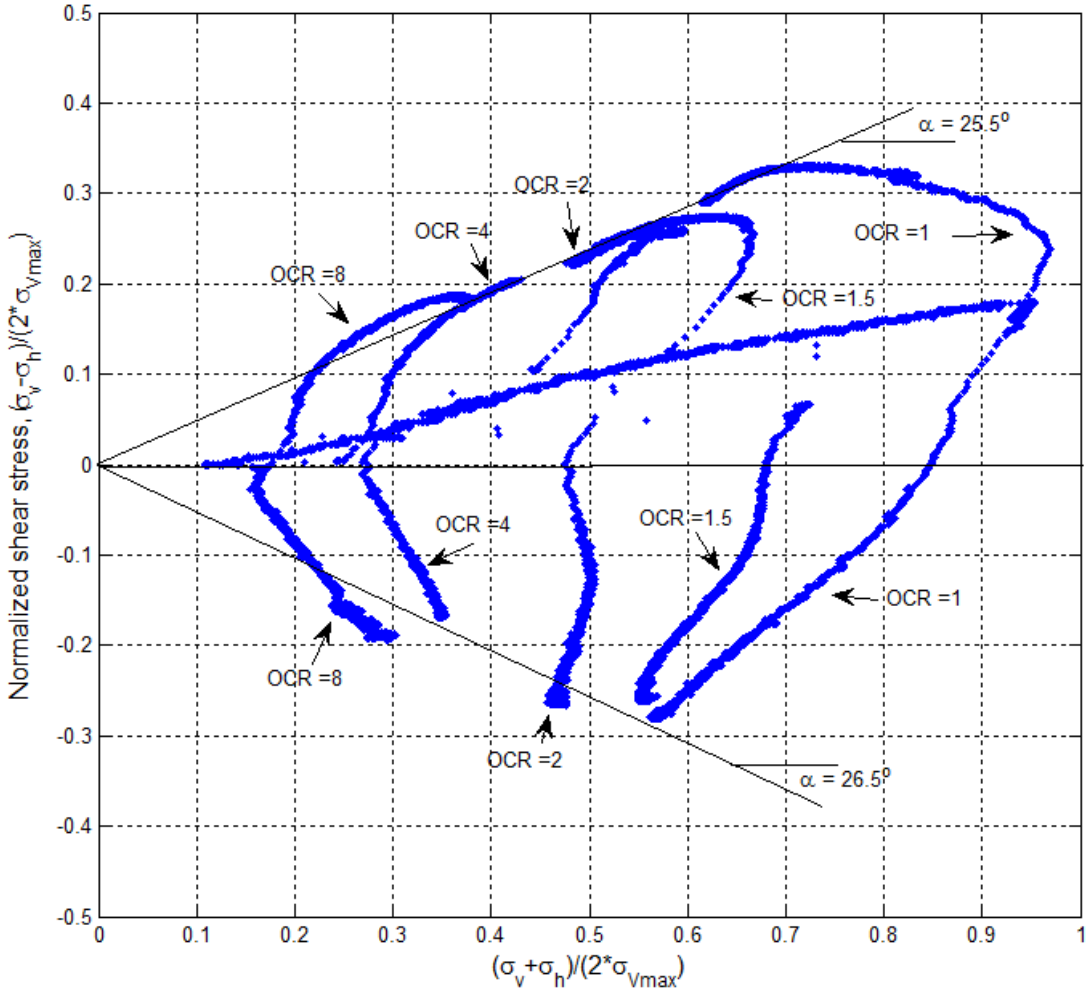

Fig. 5.6. Normalized effective stress paths from CK_oU-C/E testing.

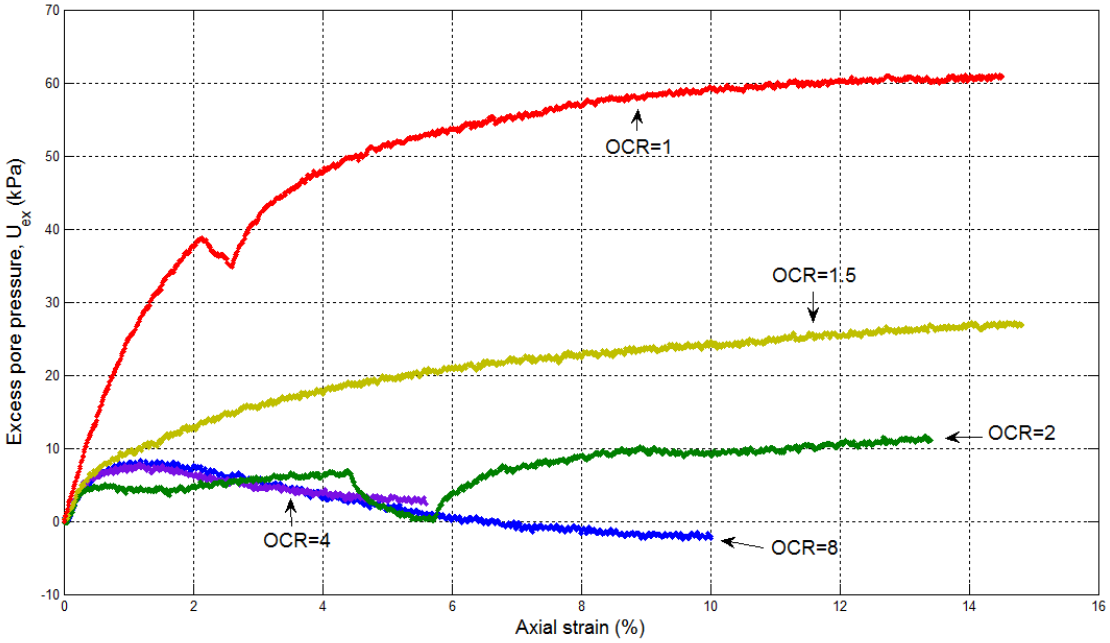

Fig. 5.7. Excess pore pressure generated from CK_oU-C testing.

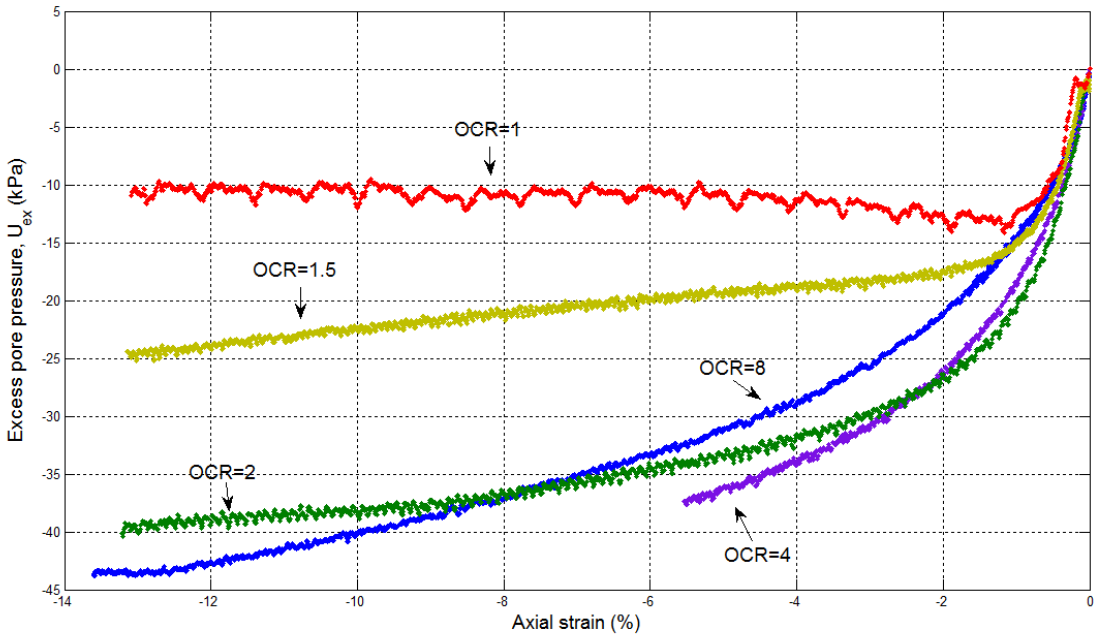

Fig. 5.8. Negative excess pore pressure generated from CK_oU-E testing.

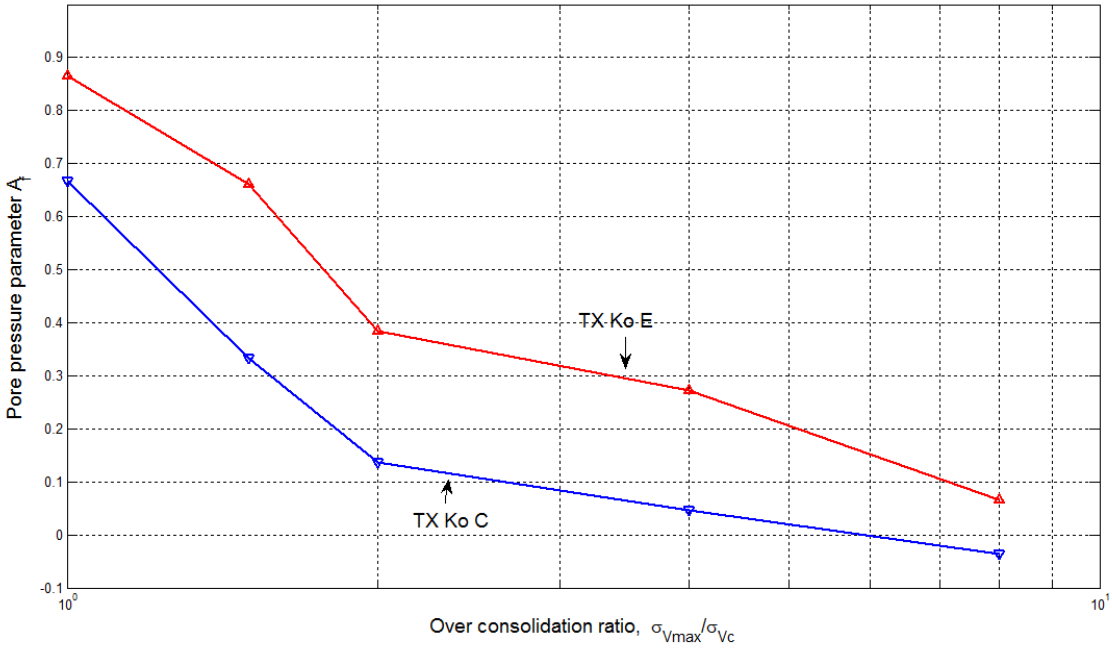

Fig. 5.9. Pore pressure parameter at failure ($\overline{A_f}$) versus OCR from $\mathrm{CK_oU}$-C/E testing.

$$\overline{A_f} = \frac{\Delta u - \Delta\sigma_v}{\Delta\sigma_h - \Delta\sigma_v} \qquad \text{(extension)} \tag{5.5}$$

The pore pressure coefficients in extension are greater than the corresponding values from compression tests. Ladd (1991) and Koutsoftas (1981) reported similar behavior for two different clays and a silty marine clay deposit, respectively. It is important to note however that the pore pressure coefficient became negative at OCR 8 for the compression tests. In this behavior it differs from both Ladd et al. (1977) and Koutsoftas (1981). This behavior however is in agreement with previously published correlations established from triaxial compression tests. Bishop and Henkel (1962) and Duncan and Seed (1967) showed that $\overline{A_f}$ becomes zero at about OCR of 4 and becomes negative at greater OCRs. This difference in pore pressure behavior is significant and would have an important influence on predictions of pore pressures.

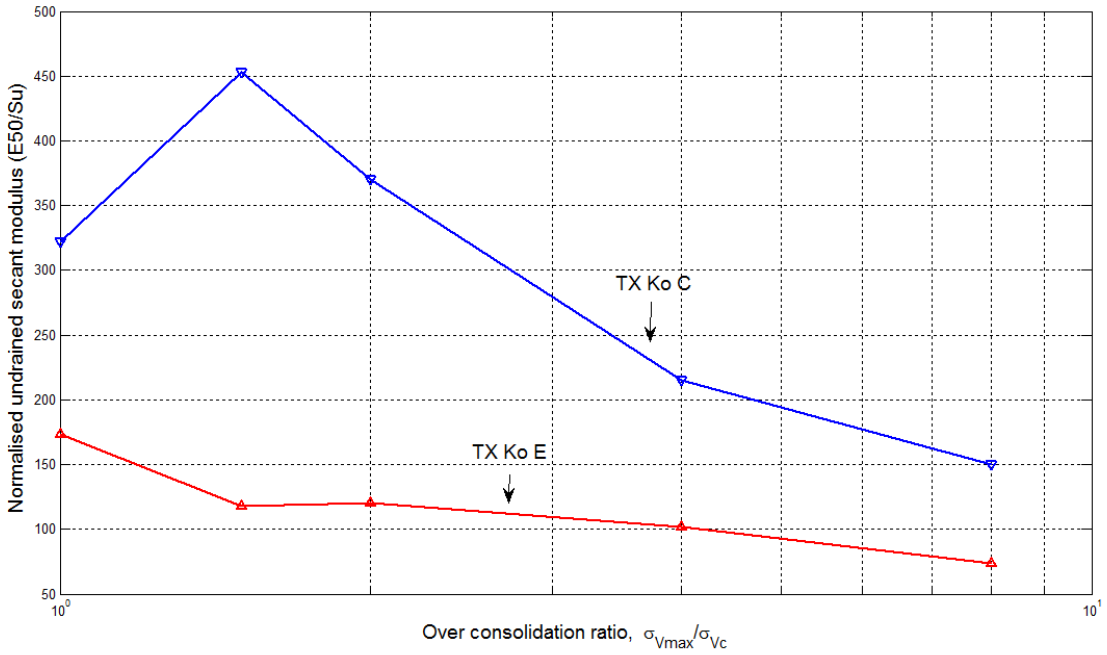

Fig. 5.10. Normalized secant moduli versus OCR from $\mathrm{CK_oU}$-C/E testing.

5.1.4 Undrained moduli

Figure 5.10 plots normalized secant moduli, E_u/s_u, as a function of overconsolidation ratio for both $\mathrm{CK_oU}$ compression and extension. The moduli were determined at an incremental shear stress level of one half of the incremental shear stress at failure. The normalized moduli for the compression tests are almost two times greater than those from the extension tests. This implies that the marine clay is quite anisotropic with respect to its stress strain characteristics.

A better indication of the soil's anisotropy is given by Figure 5.11 which plots normalized secant moduli as a function of OCR but the moduli are normalized with respect to the pre-shear vertical effective stress (σ'_{vc}) rather than s_u. It should be noted that the specimens which were tested in compression and extension were consolidated to maximum vertical effective stresses of 137.9 kPa (20 psi) and therefore specimens with the same

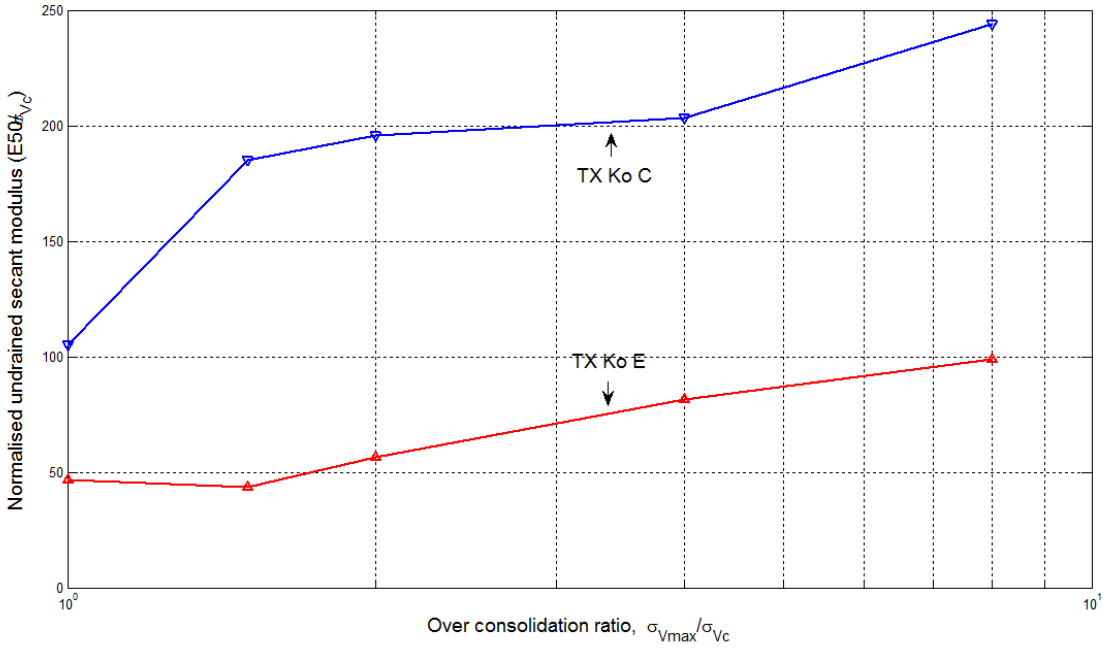

Fig. 5.11. Normalized secant moduli versus OCR from $\mathrm{CK_oU}$-C/E testing.

OCR had similar pre-shear vertical consolidation stresses. Thus, when normalized moduli from compression and extension tests are compared at the same OCR, the comparison reflects realistic differences in moduli since the vertical effective stresses would be very similar.

Small strain secant moduli

Figure 5.12 shows the variation of the secant modulus of the $\mathrm{CK_oU}$ compression tests with axial strain plotted on a logarithmic scale to give a idea of the small strain moduli behavior of the marine clay. The initial part of the curves where the secant moduli appears to increase occurs because of the system's compliance. Although the strain appears to be increasing there is no load applied on the soil due to compliance. The modulus values tend to decrease with increasing OCR ratio for the overconsolidated samples.

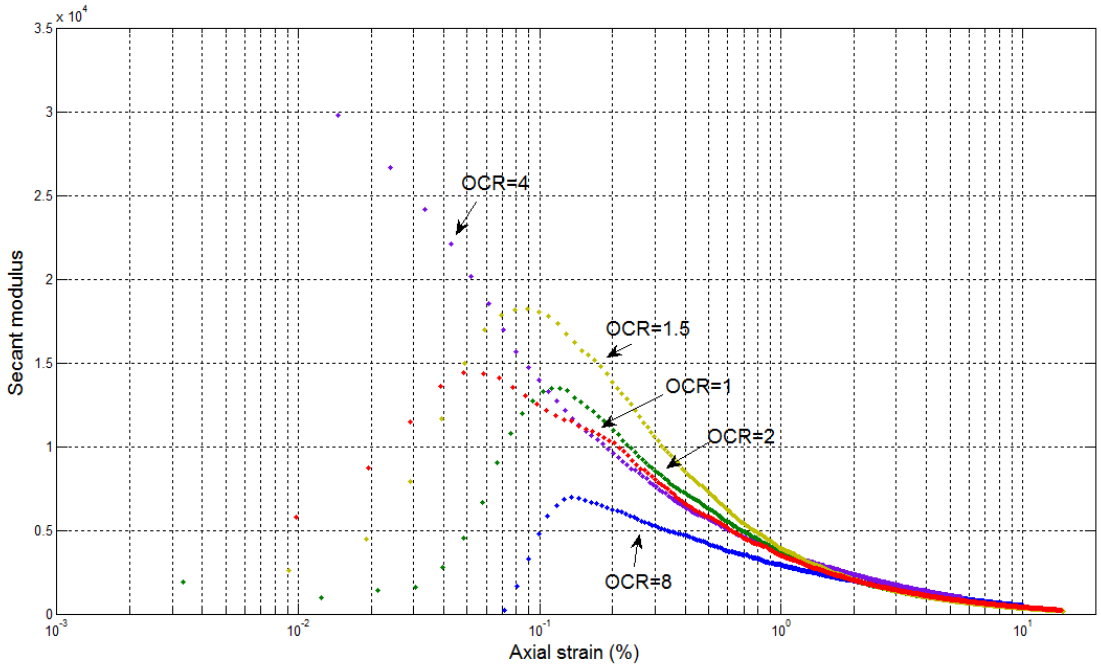

Fig. 5.12. Secant moduli versus axial strain from CK_oU-C testing.

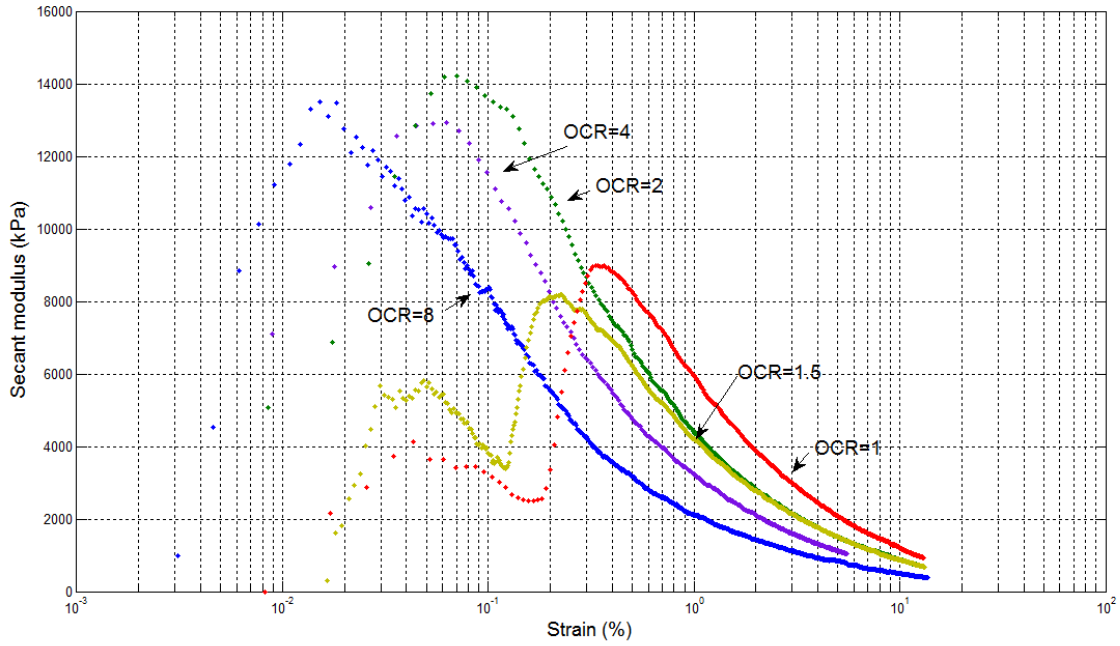

Fig. 5.13. Secant moduli versus axial from CK_oU-E testing.

Figure 5.13 shows a similar variation of secant modulus of the CK_oU extension tests with axial strain plotted on a logarithmic scale. The peak modulus is reached at lower strains as the overconsolidation ratio increases. Also the peak modulus at OCRs 1 and 1.5 lies within 9,000 kPa whereas for OCRs 2 and above the moduli is in the range of 14,000 kPa, this directly suggests that the stiffness of the clay increases with increase in OCR.

Comparing both plots it can be noted that the secant moduli values for the compression tests are an order of magnitude higher that the secant moduli for the extension tests.

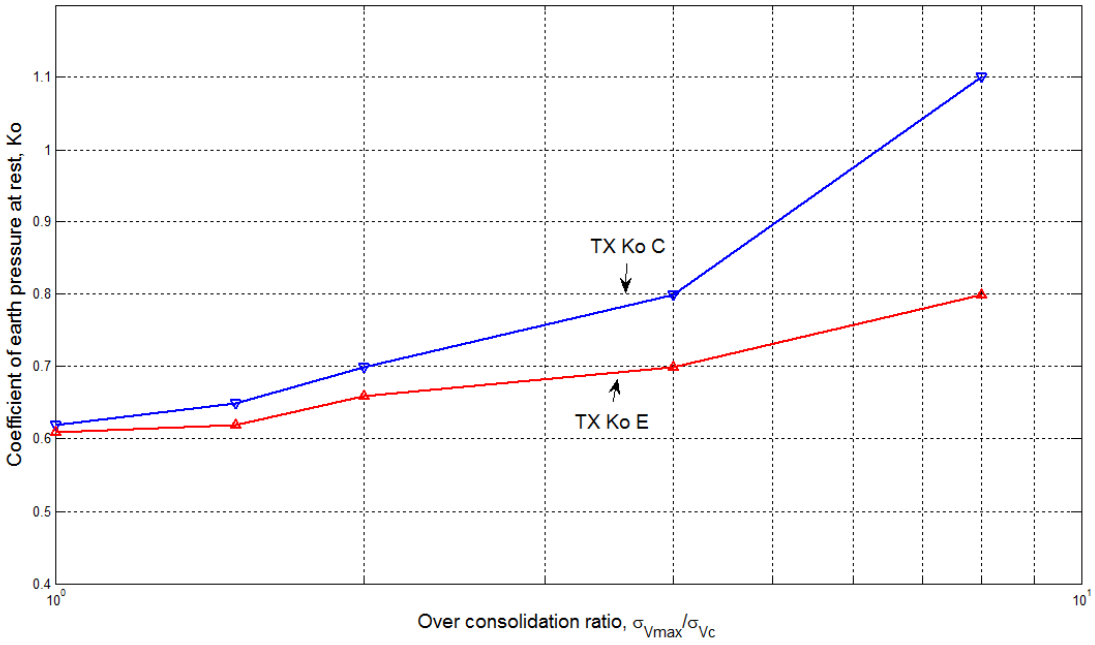

Fig. 5.14. Coefficient of earth pressure versus OCR.

5.1.5 Coefficient of earth pressure at rest

The knowledge of the coefficient of earth pressure at rest (K_o) is often very important for the design of earth retaining structures, excavations and some foundations. Figure 5.14 shows the variation of K_o with OCR (5.6).

$$(K_o)_{OC} = (K_o)_{NC} OCR^{\alpha} \tag{5.6}$$

A plot of the variation of K_o with vertical effective stress (σ_v) is shown in Figure 5.15. The initial curve represents the seating pressure and seating load being applied to the sample. During the K_o consolidation the K_o value first decreases and then remains

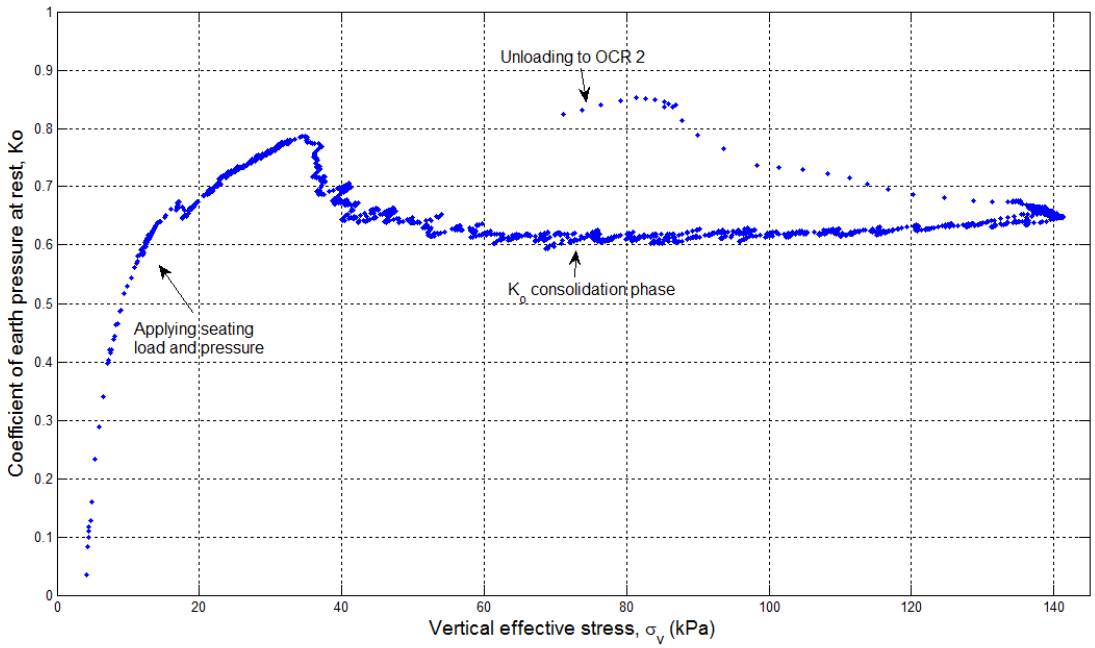

Fig. 5.15. Variation of $\mathrm{K_o}$ with vertical effective stress (σ_v).

constant with the vertical effective stress. The unloading curve, to OCR=2 in this case, shows how the $\mathrm{K_o}$ and σ_v values would change if some form of erosion occurs.

5.2 Results from CIU tests

5.2.1 Stress-strain and excess pore pressure characteristics

Figure 5.16 presents normalized stress strain relationships from CIU compression tests. This data includes both normally consolidated samples and over consolidated specimens with OCR of 2, 4 and 8. As with the $\mathrm{CK_oU}$ tests the data is normalized by the pre-shear vertical consolidation stress (σ'_{vc}).

Figure 5.17 plots normalized stress strain relationships from CIU extension tests for both normally consolidated specimens and over consolidated samples. The specimen

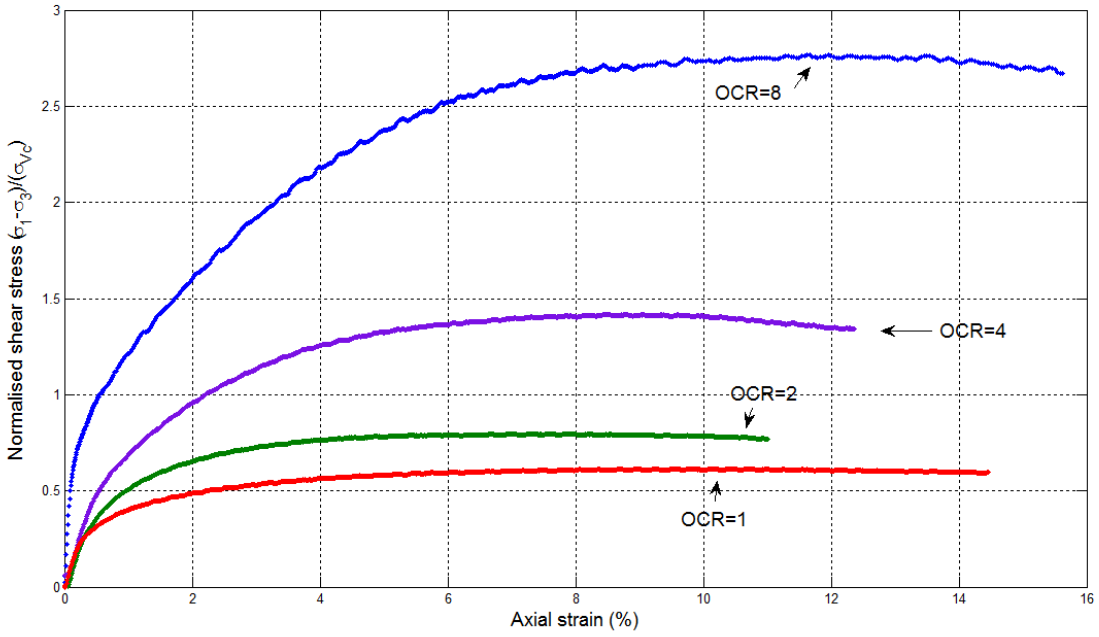

Fig. 5.16. Stress-strain relations from CIU-C tests.)

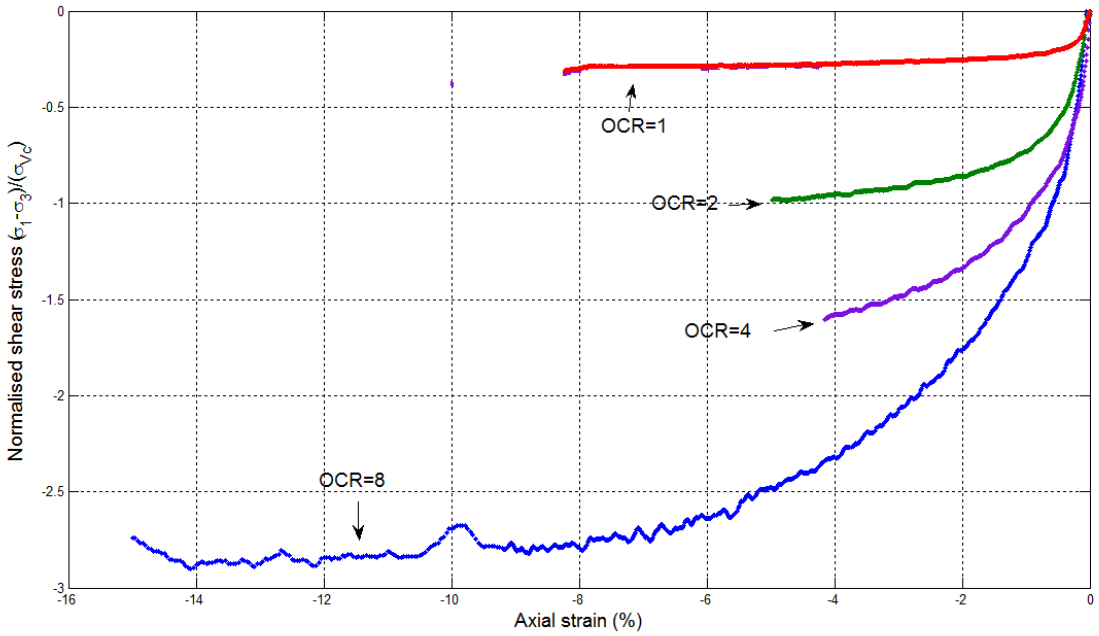

Fig. 5.17. Stress-strain relations from CIU-E tests.

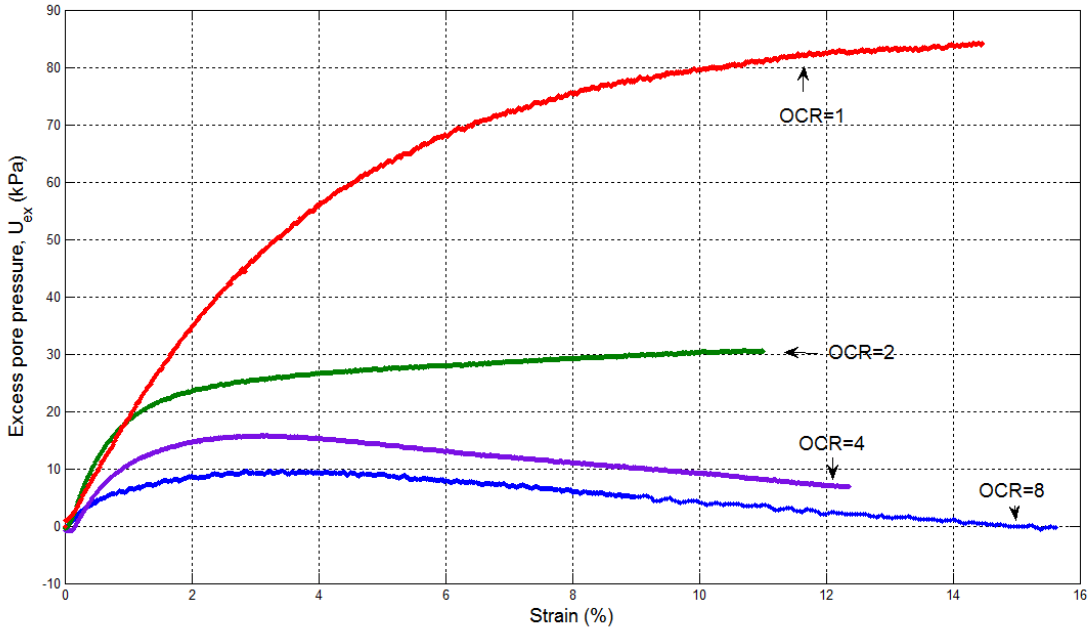

Fig. 5.18. Excess pore pressure developed in CIU compression tests.

tested at OCR=4, developed a shear crack perpendicular to direction of the axial load at a strain of 4.2%, as it was being subjected to axial extension. Since this did not occur in other tests it can be assumed that the shear crack was formed due to the presence of a very thin layer of silt or fine sand in between the clay layers or the presence of a pre-existing crack in the specimen. For both specimens tested in compression and extension the failure strain increases with increase in over consolidation ratio.

Figures 5.18 and 5.19 present the excess pore pressure developed in the CIU compression and extension tests.

5.2.2 Effective stress behavior

Figure 5.20 presents normalized effective stress paths (ESP) from CIU-compression and CIU-extension tests. The figure also plots the effective stress envelopes for both. For

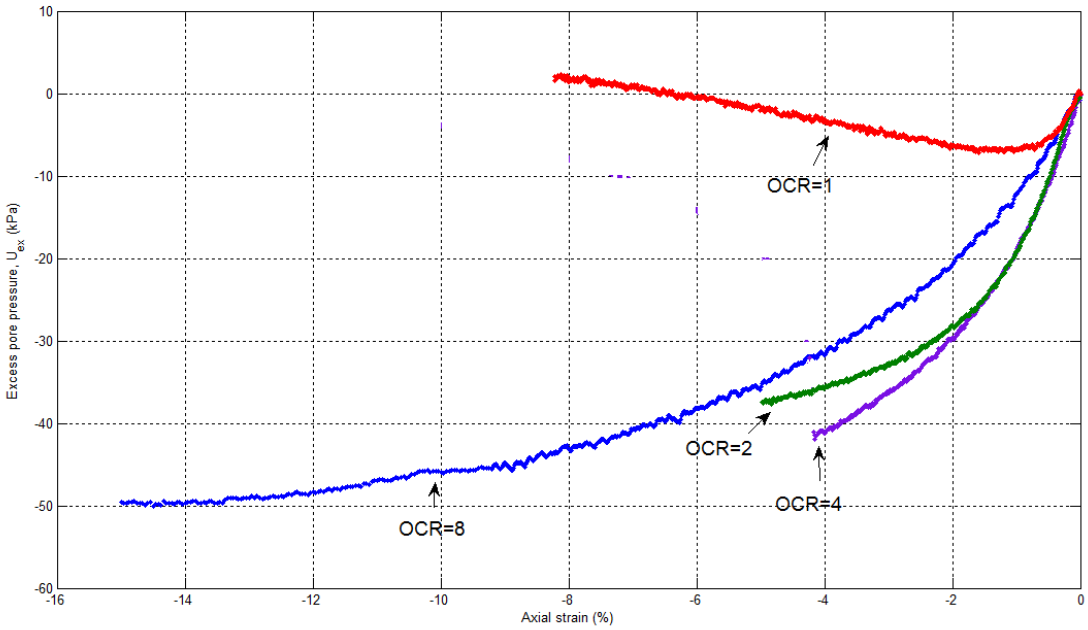

Fig. 5.19. Excess pore pressure developed in CIU extension tests.

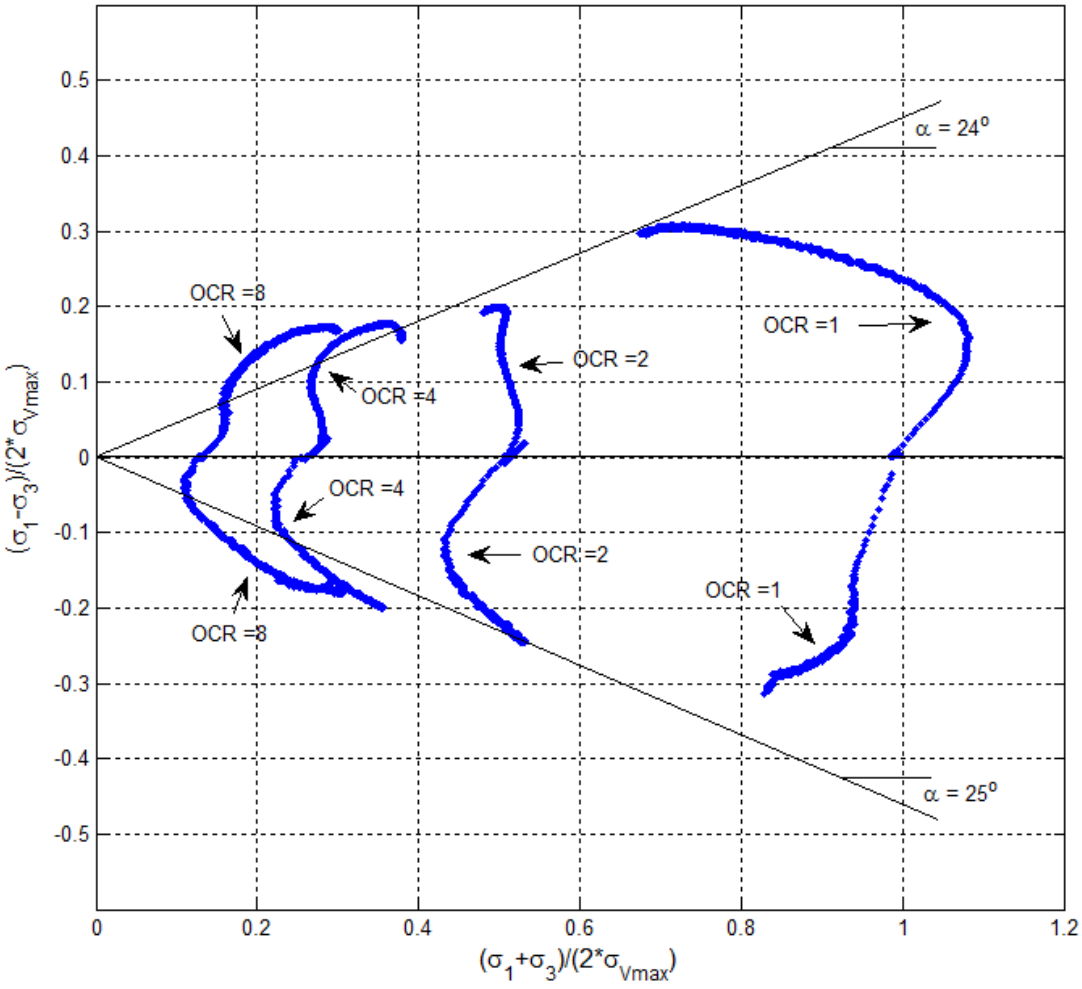

Fig. 5.20. Normalized effective stress paths from CIU-C/E testing.

the compression tests, the effective shear stress envelope at critical state can be drawn as a line which passes through the points of maximum obliquity with an α of 23^o. The effective shear stress envelope for the extension tests is also drawn as a straight line with an α angle of 25^o. The friction angles for the compression and extension tests were found to be 26.4^o and 27.7^o.

Comparing the strengths between the $\mathrm{CK_oU}$-C/E tests and the CIU-C/E tests, it can be seen that the isotropic tests tend to fail at slightly lower strengths than the $\mathrm{K_o}$ consolidated tests. Also the α angle (Figure 5.20) for the isotropic tests in both compression and extension is lesser than the α angles obtained from the $\mathrm{CK_oU}$-C/E tests. This is an important factor to include while designing based on values from conventional CIU-C/E laboratory tests.

6. CONCLUSION AND RECOMMENDATION

This thesis described a research project in which $\mathrm{CK_oU}$ compression and extension, CIU compression and extension triaxial tests were performed on undisturbed samples of Gulf of Mexico clay. The SHANSEP reconsolidation technique was used for the Ko consolidated-undrained ($\mathrm{CK_oU}$) triaxial compression and extension tests at over consolidation ratios (OCR) ranging from one to eight. Eighteen tests were run on jumbo piston core samples from core GOM-core1. This chapter provides a brief summary of the conclusions from the experimental study and recommendations for further research and future work.

6.1 Conclusion

The results of a comprehensive series of undrained shear tests on $\mathrm{K_o}$ consolidated specimens of the marine clay lead to the following conclusions:

The marine clay exhibits some anisotropy with respect to its undrained shear strength behavior. The strengths from extension tests are nearly 80-85% of the strengths obtained in compression. The degree of anisotropy however remains constant with increasing OCR.

The normalized undrained strength ratios increased with increasing OCR primarily because over consolidated specimens showed a significant increase in effective stress during shearing, while the normally consolidated specimens showed a decrease in effective stress.

The marine clay was found to be quite anisotropic with respect to its stress-strain characteristics. Undrained moduli from compression tests are two to three times greater than moduli determined from extension tests at corresponding incremental shear stress levels and OCRs.

The peak modulus at small strains decreased with increasing OCR for the compression tests. In the extension tests the peak modulus was reached at lower strains as the OCR increased.

Strains at failure was very small in compression tests particularly the normally consolidated specimens being on the order of 0.5%. Specimens tested in extension were found to fail at much larger strains of 6% and more. The failure strain was also found to increase with increasing OCR for both $\mathrm{CK_oU}$ compression and extension tests.

Pore pressure coefficients at failure, A_f, were higher from extension tests than from compression tests. Furthermore, the A_f factor was negative for OCR of 8 in the compression tests.

For the compression tests, the excess pore pressure generated continued to increase by a large amount even after the peak deviatoric stress was reached in the normally consolidated and lower OCR specimens.

6.2 Recommendations for future work

Specific testing issues that should be addressed in future work are as follows:

- The triaxial testing apparatus can be set-up with a bender element system and the same SHANSEP $\mathrm{CK_oU}$ tests can be carried out to examine how soil structure evolves during the sampling, trimming and laboratory testing phases.
- SHANSEP $\mathrm{CK_oU}$ tests can be carried out on reconstituted samples of gulf of Mexico clay and compared with the results of the undisturbed samples.

REFERENCES

Alvarado, I. (1996). "Undrained shear behavior of boston blue clay at higher level strain rates. Master's thesis, Northeastern University, Boston, MA.

Baxter, D. Y. (2000). "Mechanical behavior of soil bentonite cutoff walls.," PhD thesis, Virginia Polytechnic Institute, Blacksburg, Virginia.

Bea, R. G. (1971). "How sea floor slides affect offshore structures.." *Oil and Gas J.*, 69, 88–91.

Berre, T. and Bjerrum, L. (1973). "Shear strength of normally consolidated clays." *Proceedings of the Eighth International Conference on Soil Mechanics and Foundation Engineering, Moscow*, 1, 39–49.

Bishop, A. and Henkel, D. (1962). *The Measurement of Soil Properties in the Triaxial Test. 2nd Ed.* Edward Arnold Ltd., London.

Bishop, A. and Wesley, L. (1975). "A hydraulic triaxial apparatus for controlled stress path testing." *Geotechnique*, 25(4), 657–670.

Bjerrum, L. (1973). "Problems of soil mechanics and construction." *Proceedings of the Eighth International Conference on Soil Mechanics and Foundation Engineering*, Vol. 3. 111–159.

Black, D. and Lee, K. (1972). "Saturating laboratory samples by back pressure." *Journal of Soil Mechanics and Foundation division*, 99(1), 75–93.

Casagrande, A. (1936). "The determination of the pre-consolidation load and its practical significance.." *Proceedings of the 1st International Conference on Soil Mechanics and Foundation Engineering, Cambridge, MA*, Vol. 3. 60–64.

Coatsworth, A. and Hobbs, N. (1984). "Computer controlled triaxial equipment in a commercial laboratory." *Ground Engineering*, 17(7), 19–23.

Coulter, H. and Migliaccio, R. (1966). "Effects of the earthquake of march 27, 1964, at valdez, alaska.." *U.S. Geological Survey Professional Paper 542-C*, 36, 1.

Duncan, J. and Seed, H. (1967). "Corrections for strength test data." *Journal for soil mechanics and foundation division*, 93, 121–137.

Germaine, J. and Ladd, C. (1988). "Triaxial testing of saturated cohesive soils." *Advanced triaxial testing of soil and rock.*, 977, 421–459.

Guldur, B. (2010). "Implementation of bender elements in an automated triaxial testing system for measuring clay structure restoration by consolidation. Master's thesis, Northeastern University, Boston, Massachusetts.

Hampton, M., Lee, H., and Locat, J. (1996). "Submarine landslides." *Reviews of Geophysics*, 34, 33–59.

Hance, J. J. (2003). "Development of a database and assessment of seafloor slope stability based on published literature. Master's thesis, The University of Texas at Austin, Austin, Texas.

Hansen, J. B. and Gibson, R. E. (1949). "Undrained shear strengths of anisotropically consolidated clays.." *Geotechnique*, 1(3), 189–204.

Head, K. H. (1998). *Manual of soil laboratory testing. Volume 3: Effective stress tests*. John Wiley & Sons, New Jersey.

Heezen, B. and Ewing, M. (1952). "Turbidity currents and submarine slumps, and the 1929 grand banks earthquake." *American Journal of Science*, 250, 849–873.

Henkel, D. and Gilbert, G. (1952). "The effect of the rubber membrane on the measured triaxial compression strength of clay samples.." *Geotechnique*, 3, 20–29.

Henkel, D. J. (1970). "In proceedings." *ASCE special conference on lateral retaining stresses and earth retaining structures. Ithaca N.Y.* 1049.

Holtz, R. D. and Kovacs, W. D. (1981). *An Introduction to Geotechnical Engineering.* Prentice Hall, Englewood Cliffs, NJ.

Hvorslev, M. J. (1949). "Subsurface exploration and sampling of soils for civil engineering purposes." *Report no.*, Department of the Army, Waterways Experiment Station, Corps of Engineers, Geotechnical Laboratory, Vicksburg, MS.

Jamiolkowski, M., Ladd, C., Germaine, J., and Lancellotta, R. (1985). "New developments in field and laboratory testing of soils.." *SOA Report, Proc. 11th ICSMFE, San Francisco.*, Vol. 1. 57–153.

Karademir, T. (2006). "Use of a computer automated triaxial testing system for assessing and mitigating sample disturbance. Master's thesis, Northeastern University, Boston, MA.

Koutsoftas, D. (1981). "Undrained shear behavior of a marine clay. laboratory shear strength of soil." *ASTM special technical publication*, 740, 254–276.

La Rochelle, P., Lerouleil, S., and Tavenas, F. (1987). "Discussion on strain path method." *Proc. ASCE, J. Geot. Eng. Div*, 113(9), 1088–1090.

Ladd, C. (1991). "Stability evaluation during staged construction.." *Journal of Geotechnical Engineering, ASCE*, 117(4), 542–615.

Ladd, C. and Foott, R. (1974). "New design procedure for stability of soft clays." *J.Geotech. Engng. Div., ASCE*, 100(GT7), 763–786.

Ladd, C., Foott, R., Ishihara, K., Schlosser, F., and Poulos, H. (1977). "Stress deformation and strength characteristics." *Report no.*, State of the Art Report, Proc. of IX ICSMFE, Tokyo.

Lambe, T. and Whitman, R. (1969). *Soil Mechanics*. Wiley & Sons, New York.

Lambe, T. W. (1967). "Stress path method." *J. Soil Mechanics & Foundation Div., ASCE,*, 93(6), 309–331.

Lewin, P. I. (1971). "Use of servo mechanisms for volume change measurement and ko consolidation." *Geotechnique*, 21(3), 259–262.

Lewis, K. (1971). "Slumping on a continental shelf inclined at 1 to 4." *Sedimentology*, 16, 97–110.

Olsen, H., Morin, R., and Nichols, R. (1988). "Flow pump applications in triaxial testing." *Advanced Triaxial Testing of Soil and Rock. ASTM Spec. Tech. Publ., In Donaghe, R.T., Chaney, R.C., and Silver, M.L. (Eds.)*, 977, 68–81.

Rad, N. and Clough, G. (1984). "New procedure for saturating sand specimens." *ASCE J. Geotech. Engng*, 110(9), 1205–1218.

Roscoe, G. A., Schofield, A. N., and Wroth, C. P. (1953). "On yielding of soils." *Geotechnique*, 8, 1–22.

Rutherford, C. (2011). "Development of multi directional simple shear testing device for characterization of the cyclic shear response of marine clays," PhD thesis, Texas A&M University, College Station, Texas.

Santagata, M. C. (1994). "Simulation of sampling disturbance in soft clays using triaxial element tests. Master's thesis, Massachusetts Institute of Technology.

Schmertmann, J. (1955). "The undisturbed consolidation behaviour of clay." *Trans. ASCE*, 120, Issue: 17, 1201–1233.

Skempton, A. (1960). *From theory to practice in soil mechanics.*, chapter Significance of Terzaghi's concept of effective stress. John Wiley & sons.

Trautwein Soil Testing Equipment Co. (2009). *GeoTAC TruePath Users Manual*.

Wright, S. and Rathje, E. (2000). "Triggering mechanisms of slope stability and their relationship to earthquakes and tsunamis." *Report no.*, www.usgs.gov/, United States Geological Survey, Geophysical Long Range ASDIC (GLORIA) mapping project.

APPENDIX A
EQUIPMENT AND PROCEDURES

A.1 Components of the GEOTAC TruePath automated stress path system

The triaxial testing device is a very versatile system and many different implementations exist, both manual and automated, which were developed to solve particular needs. Most of these systems were designed for specific soil characteristics in order to achieve high quality, reproducible results (Coatsworth and Hobbs (1984),Lewin (1971),Bishop and Wesley (1975)). Regardless of its form, the function of a triaxial system remains the same: to apply a three dimensional, axis-symmetric state of stress or strain to a specimen by applying a chamber fluid pressure and an axial load.

The triaxial testing system used for this research was the GEOTAC TruePath Automated Stress Path system (Figure A.1). Its components include the axial load frame, cell and pore pressure flow pumps, the control hardware and software, instrumentation for measurement and data acquisition system.

Table I lists the components and accessories included in the system. Figure A.2 shows the layout of the the triaxial system and how the individual parts were connected (Trautwein Soil Testing Equipment Co., 2009). The triaxial apparatus can be separated into five essential components, each with a basic function in the system.

A.1.1 The triaxial cell

The triaxial cell used for this research is based on device designs stemming from MIT and subsequent research at Northeastern University, including that by Alvarado (1996) and Karademir (2006).

A sketch of the system is shown in Figure A.3. The purpose of each outlet port and the designation of the valve connected to it are as follows.

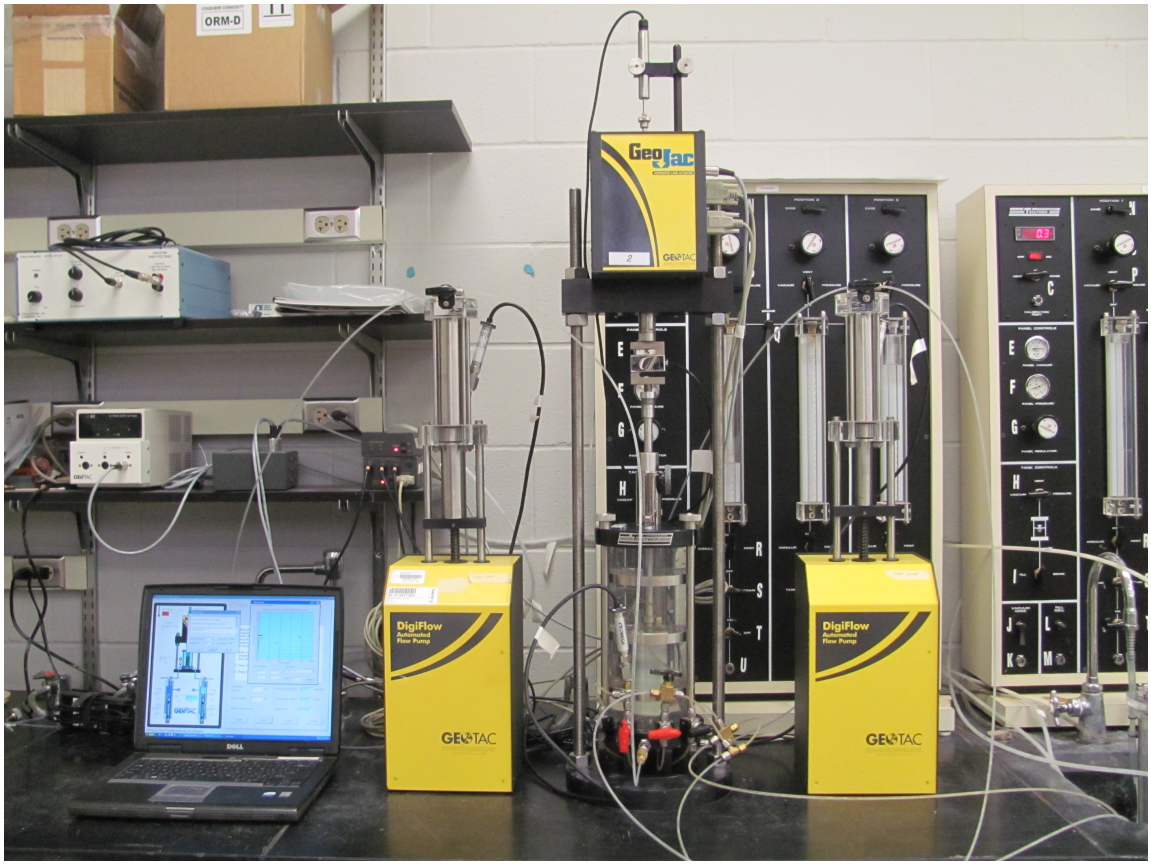

Fig. A.1. GEOTAC Truepath Automated stress path system.

Table A.1
Equipment list

Item	Accessories
GeoJac Load Frame	Power cord Power Brick AD-IO module(4 channels) Serial cables(2) DC power cable Load cell piston adapter Load cell bottom adapter Deformation Sensor Bracket and post
DigiFlow Flow Pumps (2)	Serial Cables(2) DC power cable(2)
Computer	Power cord Keyboard,mouse Serial cable
Variable DC Power supply	Power cord DC power cable
Network Module	Serial cable
Sensors	External load cell Deformation sensor Pressure sensor(3)

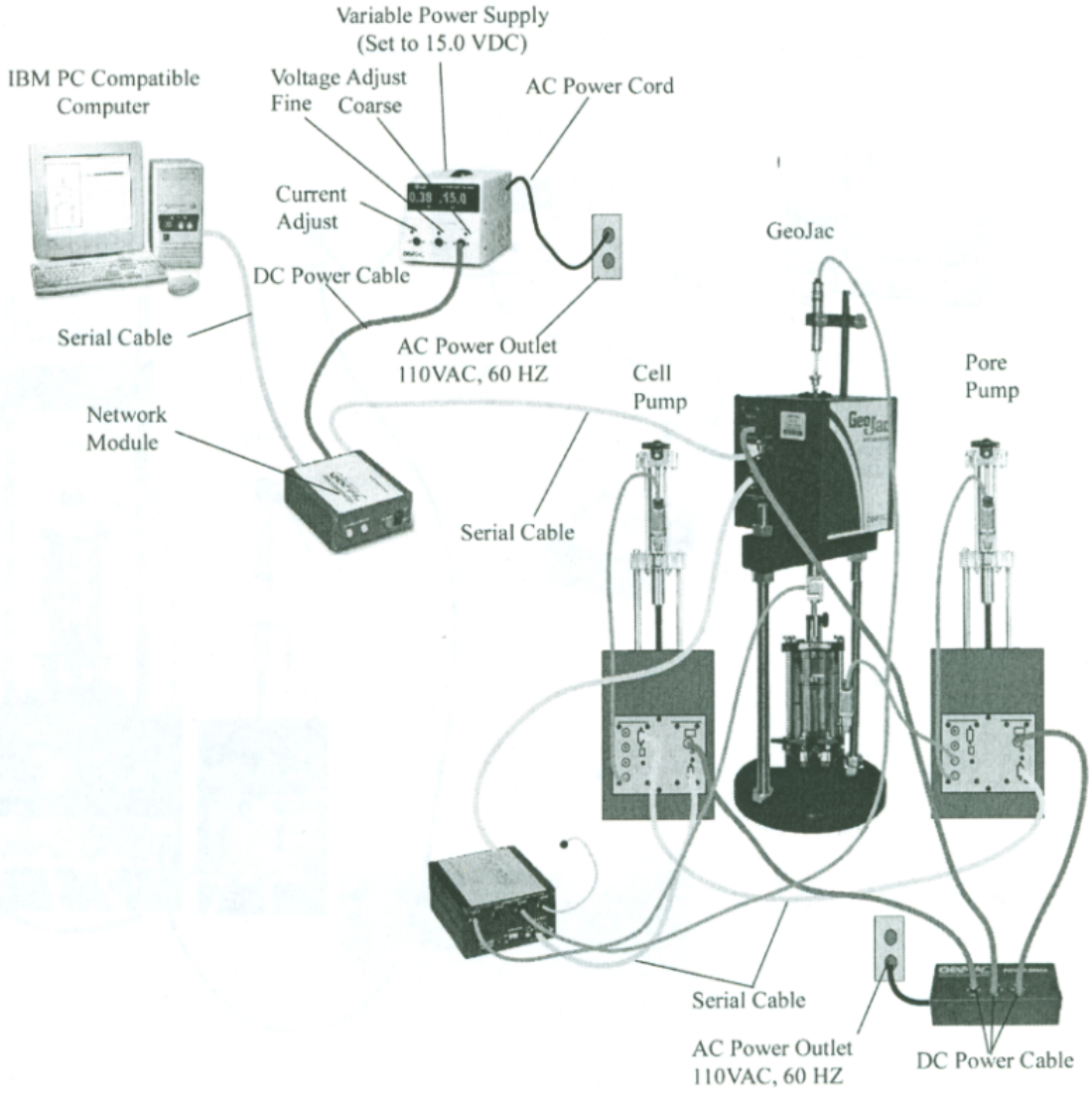

Fig. A.2. Layout of the TruePath Automated stress path system for triaxial testing (Trautwein Soil Testing Equipment Co., 2009).

1. Valves A and B each lead to the top and bottom of the specimen and are connected to each other using a T-junction. The end of the T-junction is connected to a pressure transducer for measuring the sample pore pressure.
2. Valves C and D are connections between the top and bottom of the sample and a switching system controlled by valves F and G, which can be used to alternate the flow, from the sample to the drainage lines or from the back pressure pressure volume pump to the sample.
3. Port E is a quick connect port in the center of the cell base used to fill and empty the pressure chamber of water at the beginning and the end of every test. The quick-connect port is connected to the cell pressure system during the test. This is also a larger bore than the other ports to permit rapid filling and emptying of the cell.

The top cap of the pressure chamber is removable and holds the loading piston that rides through a linear ball bearing bushing, which maintains alignment and eliminates friction. A frictionless rolling diaphragm is connected at its bottom and provides an impermeable seal between the piston and cell chamber. The top plate of the cell is fitted with a quick connect port for venting the chamber while it is being filled or drained. It is also machined so that gas bubbles flow freely out through the vent port when the chamber is being filled. The chamber itself is made of plexiglass.

The top loading cap and base platen are made of a clear plastic material, which was used due to its cost-effectiveness, easy machining, and corrosion resistance. The base platen is inserted in an opening in the cell base, sealed with 2 O-rings, and secured with a large diameter bolt.

A.1.2 Load frame

The triaxial cell is placed in a load frame with a 4.45 kN (1,000 lbf) capacity holding a screw-driven axial loading device (Figure A.4). The threaded support posts are attached to the base of the load frame. The crosshead (which has the external force transducer at-

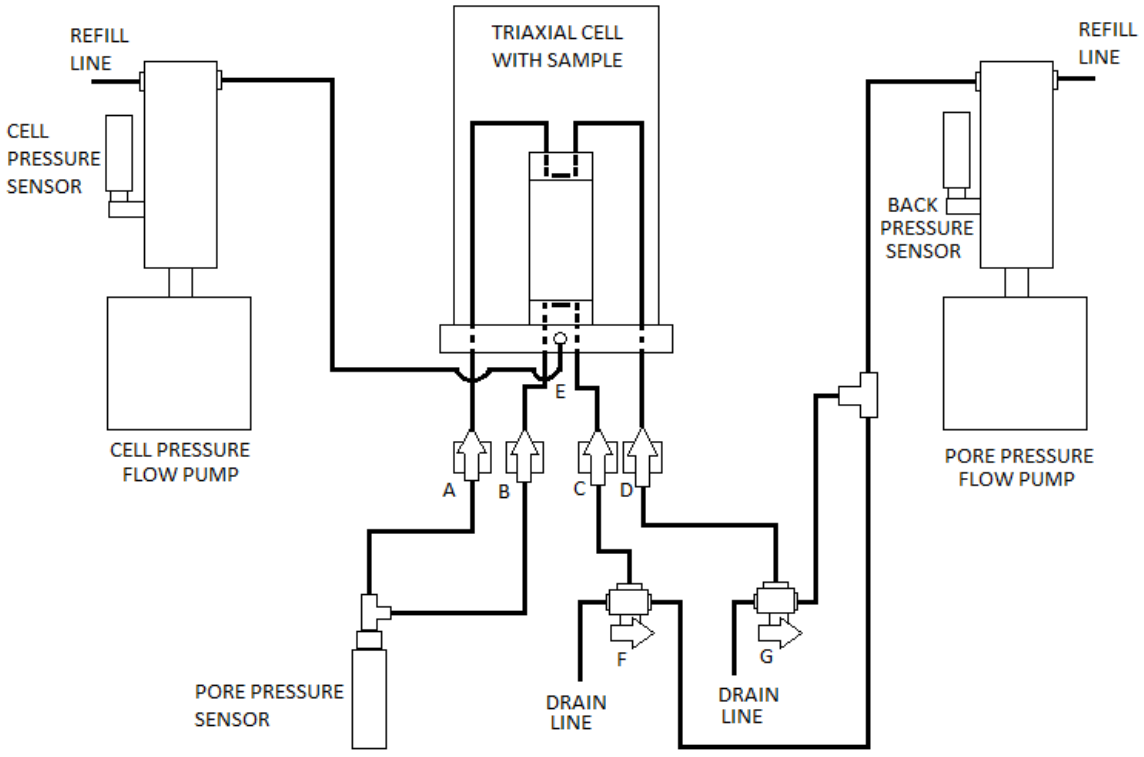

Fig. A.3. Sketch of water entering and exiting the triaxial cell.

tached to it) is connected to both of the support posts with crosshead nuts, which allow for height adjustment and leveling. A main body containing control and actuation equipment (described below) is supported on the crosshead. The platen is attached to the main body via a calibrated screw connected to the servomotor. The external load cell is attached to a piston that rides through the crosshead and is used to apply the axial load.

The load frame motor is controlled by the servo module based on feedback provided from the analog-digital interface (ADIO) module, which in turn converts computer control commands into servo-compatible controls. A built-in encoder computes the values that are displayed in the speed and position fields. The position of the platen is recorded when the test is started and the change in platen position is used to calculate deformation. The encoder information can also be used during the data reduction phase to determine specimen axial deformations inferred from the screwjack rotation.

The load frame ADIO module provides four channels of analog data acquisition. The current setup uses three of the channels: external load cell, pore pressure transducer and deformation sensor (LSCT). The data acquisition system has a 22-bit resolution and can scan 80 readings per second per channel which is more than adequate for most geotechnical testing. The output signal range can be set independently for each channel using the software interface. The excitation for each sensor can be independently set to either 5 VDC or 10 VDC. The total power consumption has an upper limit of 3 A for the entire network, and for the individual sensors the upper limit is 500 mA from each ADIO module (Trautwein Soil Testing Equipment Co., 2009).

Figure A.5 shows the side of the load frame where the servo module is located, and Figure A.6 shows the external ADIO module. The calibration factor for load frame is given by the manufacturer (Table A.2), with a maximum error given as 0.03%.

A.1.3 DigiFlow pressure-volume pumps

Figure A.7 shows a schematic of one of the system's pressure-volume pumps (or flow pumps) with the trade name DigiFlow. The flow pump consists of a piston-cylinder assem-

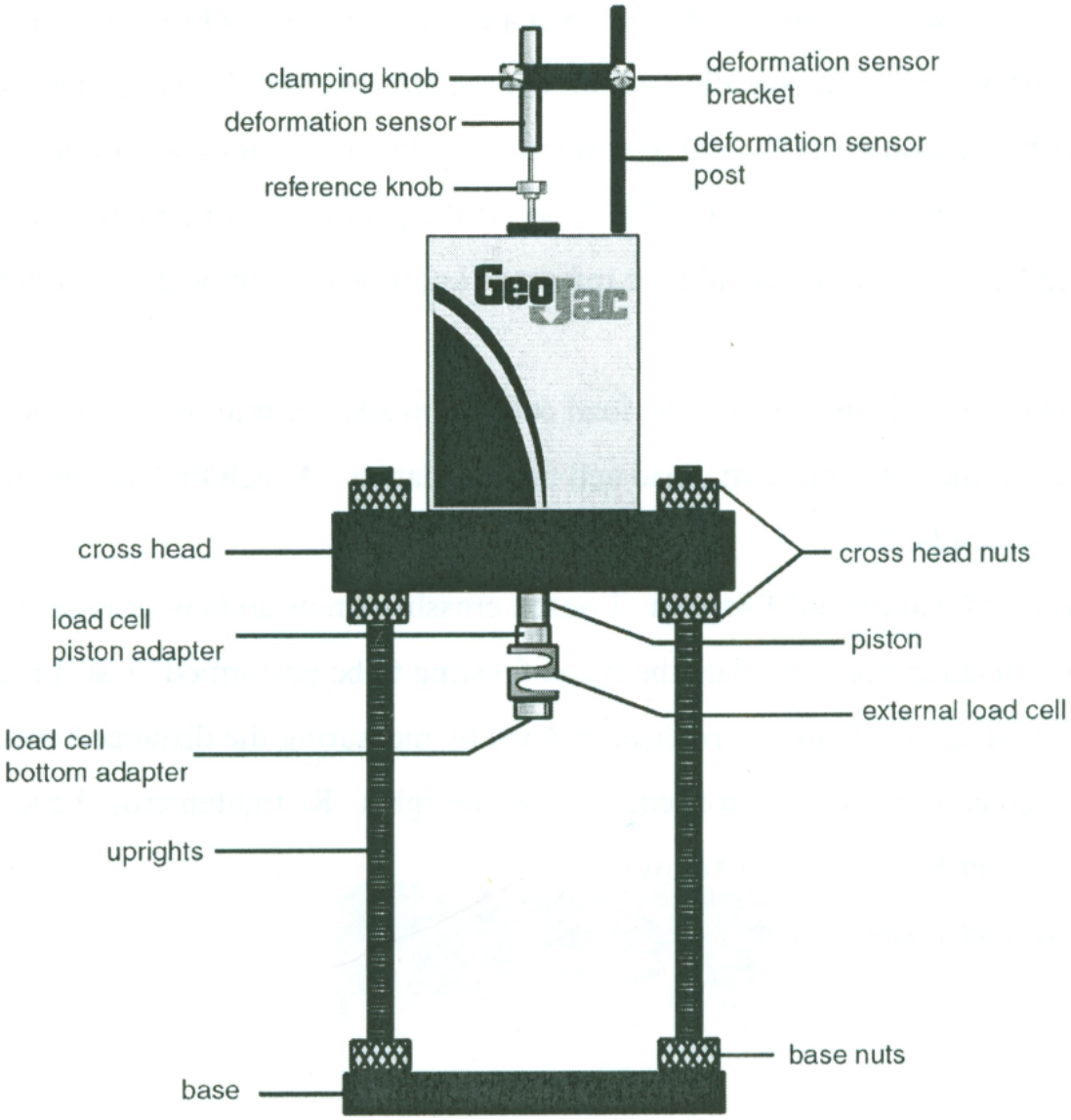

Fig. A.4. Load frame with triaxial cell inside.

Fig. A.5. Servo module on the side panel of the load frame.

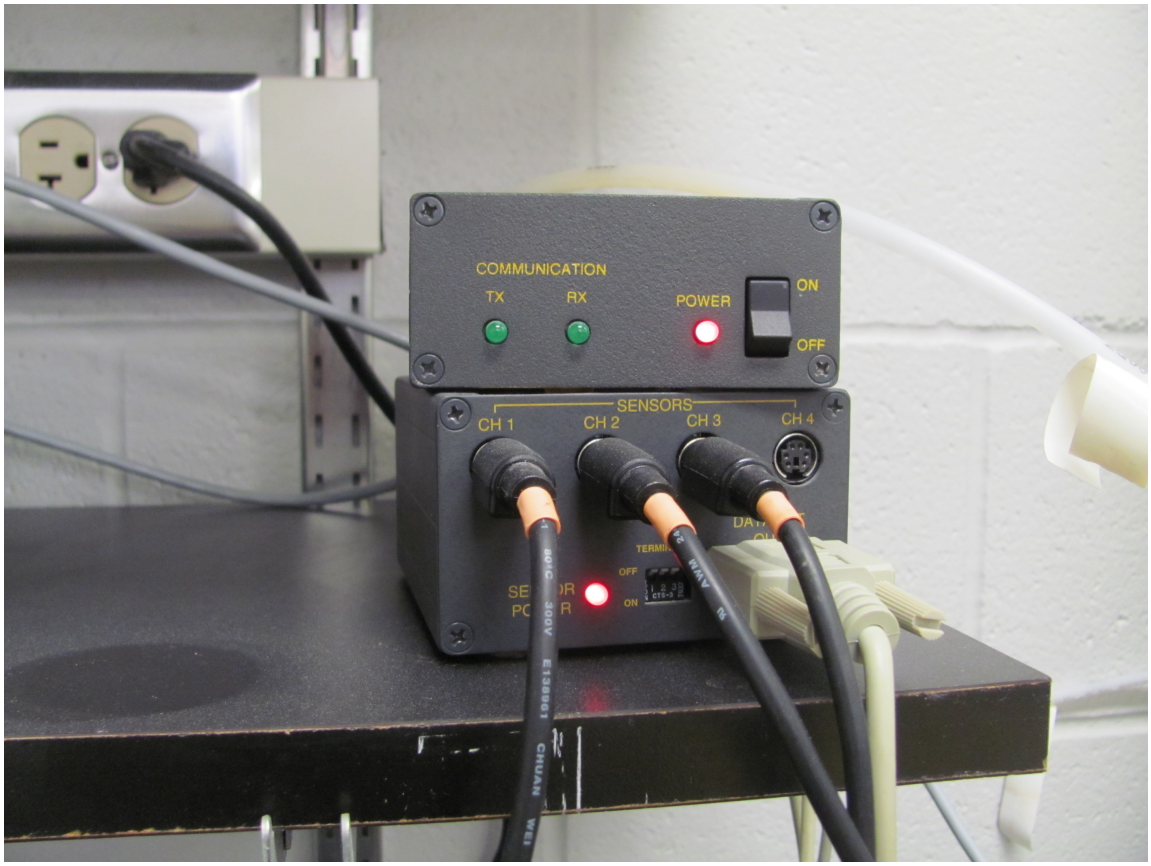

Fig. A.6. External ADIO module for the load frame.

bly attached to the main body unit, where a motor, control circuits and a manual interface is housed. As shown in Figure A.6, a pressure transducer is located at the top of the cylindrical pump, and a two-way valve at the top of the cylindrical pump controls the flow between the pump and the cell (or specimen pore space in the case of the pore pressure flow pump), or to a fluid source to refill the flow pump. For this setup the refill lines of both the flow pumps are connected to a flow panel which in turn is connected to a water tank containing de-aired water. The flow panel is also used to fill the water tank and apply vacuum to the tank removing the dissolved air in the water. The movement of the pressure volume pumps can be individually controlled by using the "Manual Mode" under the software interface "Tools" menu (refer to GeoTAC TruePath Manual, 2009 for details on how to use the control movement of each flow pump).

Each pressure volume pump has two TestNet modules: an analog-digital interface (ADIO) module and a servo control module. The servo module is for controlling the pump motor and the ADIO module is used as the interface between the flow pump and the computer as well as the onboard flow pump display and control panel. The control on the pressure volume pump motor is based on input from the ADIO module. Both of the flow pumps are operated with 24 VDC provided by the load frame, which in turn is connected to the power supply. The cell pressure pump has a capacity of 170 mL and the pore pressure pump has a capacity of 75 mL. Calibration factors for converting voltage to volume change for both cell and pore pressure pumps are given by the manufacturer (Table A.2).

A.1.4 Instrumentation

An array of instrumentation is used for monitoring and/or controlling the triaxial test and collecting data. The GEOTAC system uses an external axial force transducer and three pressure transducers, one on each flow pump (see section A.1.3) and one on the cell itself (used to measure pore pressure during undrained testing phases). All of the transducers

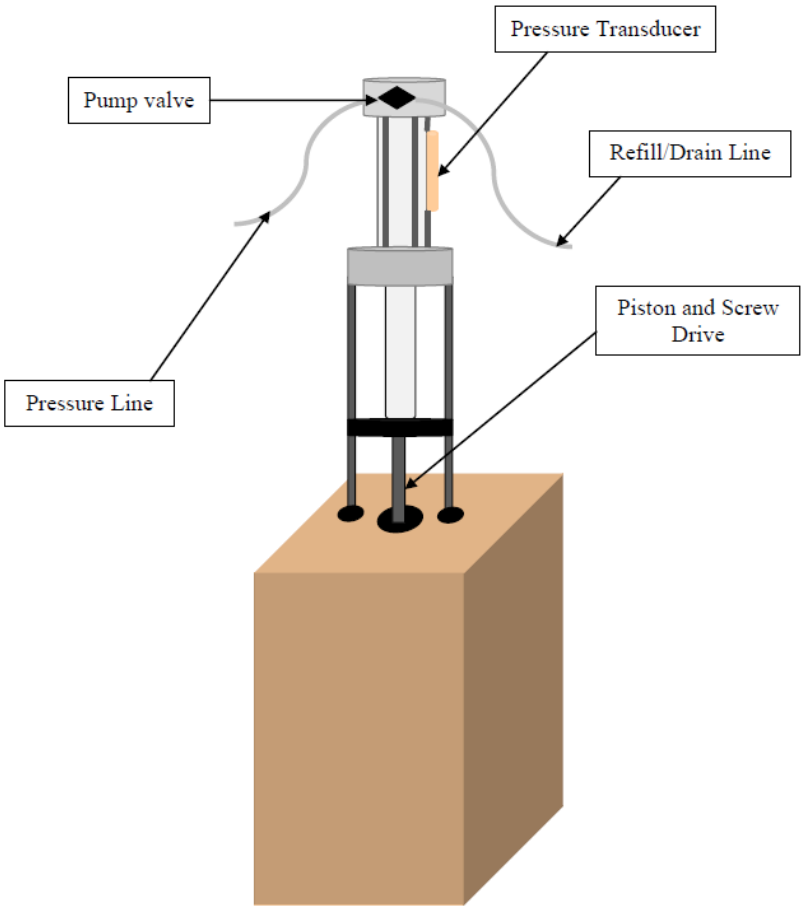

Fig. A.7. Schematic of the DigiFlow pressure volume pump (Guldur, 2010).

use an excitation voltage of 10 VDC. There is a linear relationship between the voltage output signals of these devices and the measured engineering quantities.

$$R_{out} = (V_{out} - V_{zero}) \times C.F./V_{in} \tag{A.1}$$

where

R_{out}= Output in engineering units

V_{out}= Output voltage reading

V_{zero}= Zero voltage reading for transducers

V_{in}= Input excitation voltage reading

C.F. = Calibration factor for that instrumentation device

Transducer zeros need to be set before starting the test. If the zero values are taken after saving the specimen data, new zero values will not be written on the data file. Zero readings for the instrumentation can be taken any time during the test. If the zero readings recorded during the test are different from the one recorded on the data sheet at the beginning of the test, the pressures, temperature, displacement values shown on the display screen are calculated based on the latest zero readings. However, when the data is reduced, care should be taken to use the zero reading appropriate for that particular set of data, as only the initial zero reading is recorded on the data file taken at the beginning of the test. This can result in incorrect values when reducing data. Zeroing procedures are described in Appendix A.3.2.

The external force transducer on the system is an Omega 200 lbf capacity load cell. It is set after the triaxial cell is placed in the load frame. The GEOTAC TruePath system uses three pressure transducers from Omega Engineering, Inc. with pressure ranges of 0 to 100 psi. The system names and the calibration factors related to each transducer are given in Table A.2.

The pore pressure transducer (Figure A.3), bridging valves A and B, is used to measure the specimen pore water pressure during two test phases: the undrained testing phase when the drainage lines to the flow pumps are closed and no back pressure reading is avail-

able; and the K_o consolidation phase, when it is used for comparison with back pressure transducer readings.

The cell pressure transducer is attached to the cell pressure pump and is used for measuring the cell pressure within the triaxial cell (Figure A.1).

The back pressure transducer is attached to the pore pressure flow pump and measures the water pressure inside the flow pump. It is important to check if both pore water and back pressure transducers are reading the same value after the drain lines are flushed. Zero values for these three transducers are taken by using the sensor control of the testnet system. Air trapped in the pressure sensor can cause volume change errors. Air should be released before starting a test. This is done by saturating both the pressure transducer and the pressure lines. Detailed explanation of the zeroing and the saturation process is given in Appendix A.3.2.

As mentioned before, the GEOTAC system load frame uses a calibrated screw-jack to determine displacement. Axial deformation was also measured externally by using an auxiliary linear strain conversion transducer (LSCT) manufactured by Omega Engineering, Inc (Model no. TAMU 008; Table A.2). This LSCT is attached to the load shaft. As the specimen deforms, the shaft moves during the test and the transducer records these movements. The linear range of the transducer is 2.5 VDC for accurate signal measurements. Its working range is +/-25.4 mm (+/-1 inches) and its maximum usable range is +/-38.1 mm (+/-1.5 inches).

A.1.5 Computer, data acquisition system and control software

Computer

The computer used to run the GEOTAC TruePath system should have the following minimum specifications. It should be PC compatible with a Pentium CPU running at 120 MHz or faster, Windows 95 operating system, minimum 16 MB RAM, 3.5 inch floppy drive, 1.2 GB hard drive, and a Super VGA card with a monitor offering 800 x 600 or

Table A.2
List of Instruments and calibrating factors

Instrument	Calibration factor	Units
Cell pressure transducer	9764.99	psi/V/V
Pore pressure transducer	-9800.37	psi/V/V
Back pressure transducer	-9708.31	psi/V/V
Linear displacement transducer	-137.81	inches/V/V
Force transducer	-65159.0	lbs/V/V
Cell pressure-volume pump	136057.56	counts/mL
Back pressure-volume pump	306129.51	counts/mL
Load frame	3940000.0	counts/inch

higher resolution. The computer should also have at least one free serial (COM) port working properly (Trautwein Soil Testing Equipment Co., 2009). The computer used in the TAMU geotechnical laboratory has a 3.2 GHz processor and 1 GB of RAM. It has Windows XP operating system with 512 MB of RAM, and a monitor with 1440 x 900 resolution.

External System modules

The data stream between the computer and the load frame is regulated by the network module. The network module is the first of seven testnet modules in the TruePath system There are two serial ports and one power port on it. The module is connected to the computer through first series port and connected to the load frame with the second series port with two separate series cables.

Precision variable power supply

The testnet module excitation voltage is provided by a linear regulated DC power supply which is connected to an AC outlet (110 VAC, 60 Hz). During the tests, the power supply should be set to 14.9 +/-0.1 VDC. If the DC power input exceeds the 15 V limit, the testnet module can be permanently damaged. The front panel of the power supply and the rear panel of the network module are connected by a DC power cord terminated with a 3-pin DIN connector.

GeoTAC truepath system software

The system is operated by a Windows-based, true 32-bit control and data acquisition software, which has a graphical user interface to enable the user to input test parameters and monitor the test. A standard Windows-style menu is located at the top of the main user

interface window. The available menu items enable users to enter and edit test parameters, sensor calibration information, reading schedules, and hardware settings and constants.

The graphical user interface (Figure A.8) has three main components: the status panel, menu bar and tab panel. The Status panel is located on the left half of the screen and stays there until the end of the test. This panel provides the graphical representation of the physical conditions of the specimen at any point in the testing. It displays instrumentation readings on the screen as follows: temperature (C), position of axial load platen (inches), specimen displacement (inches), axial force (lbs), fluid pressure (psi), and platen deformation rate (inches/min) values. If any of the instrumentation readings go beyond the minimum or maximum limits set by the user , the corresponding display field turns red, an alarm sounds, and the relevant device component stops moving (Trautwein Soil Testing Equipment Co., 2009). Detailed instructions on how to use the software is given in the next section.

A.2 Control algorithm

A.2.1 General operation

Before beginning a test, the operator must enter some input parameters in the TruePath software depending on the kind of test being run, sensor calibration information, reading schedules and hardware settings and constants. This can be done by selecting ‘Setup’ on the menu list and entering each option.

The testnet option opens a module list dialog box that contains all the information on ADIO modules that are connected to the network and the system automatically assigns addresses, which cannot be changed, to the modules according to the order of the list. The gain factor for each ADIO module should be checked before starting any test.

All the sensor information is stored in a configuration file automatically. This information can be viewed by using the ‘Sensors’ option, which contains a summary of the recorded sensor information. It is very important to enter the calibration factors associated

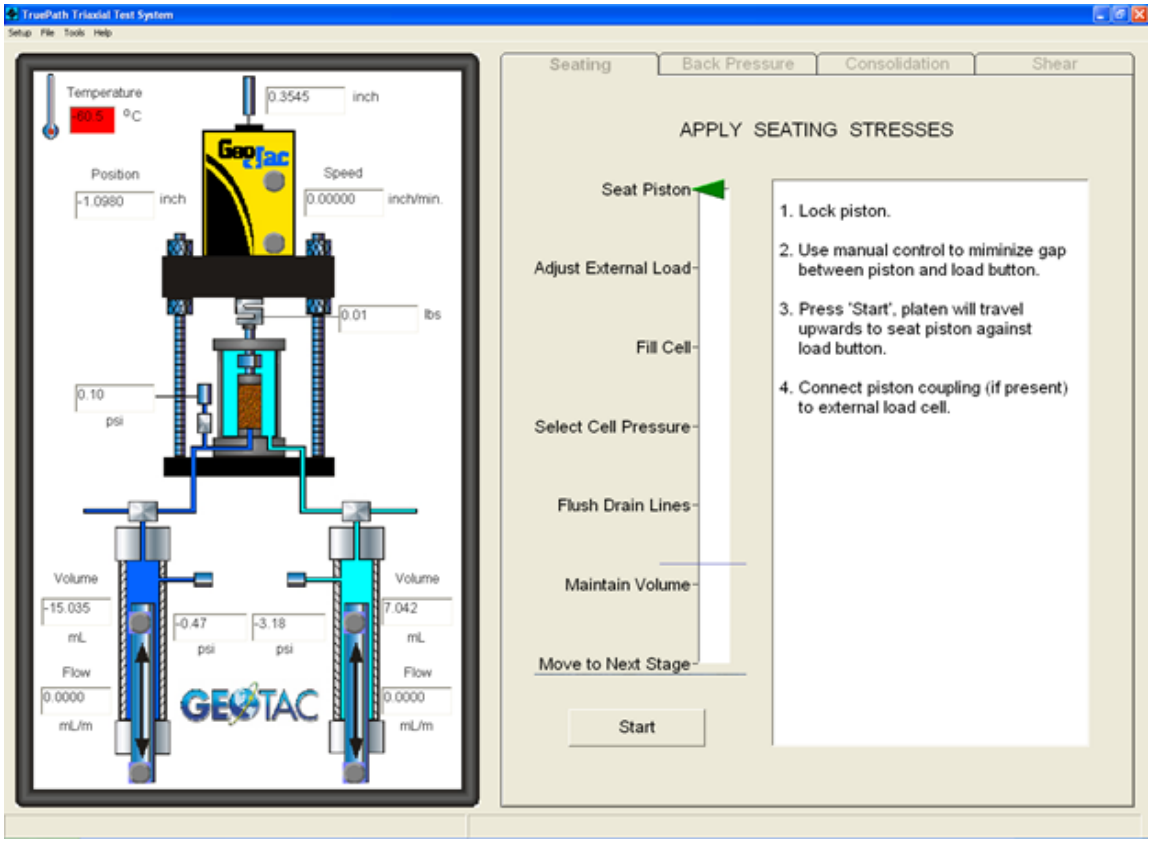

Fig. A.8. Graphical user interface of the GeoTAC TruePath before starting a test.

with each sensor before the system file is operated. Depending on how the sensor is wired, an appropriate excitation voltage has to be chosen (either 5 or 10 VDC). Minimum and maximum limits which are used for detecting overloading of the system are also entered in this menu option.

Other data required includes specimen related information, such as the insitu depth of the sample, initial height and cross sectional area, and test data such as target pressures for the various phases of the test along with their reading schedules, type of consolidation, strain rates, all of which can be changed during each individual phase.

A.2.2 Reading schedules

The software provides a convenient means for storing and recalling various sets of reading schedules used for different stages of the triaxial test. The schedules can be time based or strain based and can be customized according to the rate at which the user wants to collect data.

For this research different reading schedules were used for different phases. One data point was recorded every two minutes for the seating and back pressure phases, which was the default reading schedule. But for consolidation and shear, the default reading schedule was not adequate and had to be modified.

The reading schedule for the consolidation phase was set so that one reading was taken every six seconds for the first ten minutes, one reading every 12 seconds for the next hundred minutes and, lastly, one reading taken every 30 seconds for the next five thousand minutes. The reading schedule allows a long time because $\mathrm{K_o}$ consolidation tests takes up to five days to complete. The reading schedule for the shear phase was based on strain, with a reading taken every 0.01% strain.

A.2.3 Pump saturation

Air trapped in the pumps, pressure sensor, tubing or specimen drains can cause errors in system volume calculations, when pump pressure is raised and air trapped in the pump compresses and slowly dissolves. The resulting volume change due to air compression or dissolution is recorded as flow in or out of the specimen.

Turning the pump valve to the refill port, the pump should be filled with de-aired water. Several cycles of filling and emptying the pump may be required before water can flow out of the drain/refill line continuously without any air bubbles. Lowering the piston with the valve closed causes a small vacuum to build up and air bubbles rise to the top. Once all the air bubbles have risen to the top, the drain valve should be opened and the piston moved up to remove the air from the pump. This should be done for both the flow pumps to make sure no air bubbles remain.

A pressure test should be performed to check for leaks or air in the pumps, pressure sensors or lines. First any visible water should be removed around all the fittings, so that any water found later can be attributed to a leak. Next the pump valve should be switched to the refill/drain line and using the manual mode the piston should be moved to the lower limit. Reverse the piston direction by moving it up approximately one inch. The pump valve must be closed and the pump flow should be reset by clicking on the reset box in the manual control window. The pressure should be ramped to 100 psi in 0.5 minutes, the volume reading should stabilize after a few seconds. If the reading slowly increases with time and does not stabilize, there is most likely a leak. All the connections and fitting should be checked.

A.2.4 Uplift calibration

The load measured using an external load cell is the sum of both the load on the specimen and the piston uplift load. An uplift calibration is needed to correct for the piston uplift load. The calibration is performed by filling the cell with water, placing it in the load

frame, unlocking the piston, and then applying a small cell pressure such that the piston rises and makes contact with the external load cell. The cell pressure is then raised at a slow rate and the uplift load is measured by the load cell as a function of pressure. The target cell pressure should be selected such that it covers the entire range of pressure which will be used during testing. The uplift values are stored in the configuration file and used to adjust the load measured to obtain the correct stress on the specimen.

A.3 Triaxial testing procedure

A.3.1 Specimen preparation and setup

This section describes in detail the testing procedure of the triaxial tests carried out on Gulf of Mexico clay. The marine samples (Chapter 3) are cut from sections of 4" diameter jumbo piston cores. Specimens for testing are selected with the help of MSCL data among the sections within the core liner that have a minimum amount of disturbance. The ends of each core section are not used because of possible disturbance, oxidation and change in the water content during the storage period.

Core cutting and extrusion

The samples were prepared by cutting the one meter long PVC jumbo piston cores into 4 in sections using a telescopic pipe cutter. Once the plastic was cut all the way through, the soil inside was cut by running a thin steel wire through the cross section to make sure it was as undisturbed as possible. Each section was labeled, sealed with wax paper and capped on both ends for storage in a moisture room until testing. The plastic caps were secured with electrical tape.

The sample to be tested was extruded from the pipe using a soil sample ejector. In the TAMU geotechnical laboratory, the ejector combined with a hand operated hydraulic pump (ENERPAC; Model P-80) with a capacity of 10,000 psi, was used to extrude the

soil (Figure A.9). Before mounting the PVC sections in the soil sample ejector, the wax seal and caps at both ends of the core sections were removed. The ejector has three vertical, threaded support posts that hold a steel plate with a 100mm (4 in) diameter opening in the middle through which the sample is pushed out. The core section is placed on a platen which is on the pump piston and this is forced up into the bottom of the tube sample section. The soil sample is then extruded out through the top of the steel plate. The hydraulic jack is actuated by a pumping arm. The bleed valve is used to control the hydraulic pressure and the piston retracts under its own weight.

Sample trimming

After extrusion the specimen should be handled carefully to minimize disturbance, changes in cross section or change in water content. The clay sample is then trimmed into a cylinder with a diameter of 1.5 inches and the height between 2 and 2.5 times the diameter (ASTM D4767 - 04). It is important to maintain the orientation of the sample.

The trimmed specimen should be prepared in a controlled high humidity room where the soil's water content change is minimized. The sample should be lined up vertical, in the shaper whose ends need to be secured into the sample, so it keeps the same axis the entire time it is being trimmed. The wire saw should be directly lined up with the sides of the shaper and then slowly moved downward to shave off the outside of the clay. It should be turned periodically using the top handle on the shaper to prevent corners in the sample. The sample should first be trimmed using the two inch diameter side, as this allows lesser shearing and disruption of the sample. Once the sample is a 2 inch diameter cylinder, it can be trimmed again using the wire saw on the 1.5 inch diameter side, giving rise to a uniform minimally disturbed cylinder of 1.5 in diameter. The sample should then be carefully laid on its side and cut to a length between 3 to 3.75 in. Keeping the orientation of the sample in mind the dimensions should be measured with a digital calliper. The trimmings of the sample should be kept for the water content determination.

Fig. A.9. Hydraulic hand pump along with the extruder.

Setup in triaxial apparatus

Once the sample is cut and ready to be tested, it is very important that the sample is not left out in the open for very long. It should be prepared just before placing on the triaxial base.

Rubber membranes are used to seal the specimen and also carry part of the axial and lateral load. For this reason, very thin membranes are preferred. A correction is applied to the data to account for the stress on the membrane (Appendix B).

Two porous stones are required, one on each end of the sample. These stones are cleaned using an ultra sonic device and placed in de-aired water to remove all the fine particles and air bubbles from the pores.

Other materials required for the test are: two filter disks cut to 1.5 in diameter, two O-rings slightly smaller than 1.5 in diameter. The setup and placement of the specimen is given in the following steps.

1. The O-rings are slid over the bottom half of the membrane extender, they should be placed without any turns. The membrane is placed inside the membrane extender with the two ends of the membrane coming over the edges of the extender.
2. The membrane should be checked to make sure it is not twisted or unevenly taut. A vacuum is applied on the extender to remove the air in between the membrane and the extender. Once the air is removed the vacuum is turned off.
3. The sample is sandwiched between the two porous stones with the filter disks working as a barrier between the porous stones and the soil, it is then assembled on the triaxial base by placing the bottom of the specimen on the base pedestal and then the top cap over the top porous stone.
4. The sample should be sitting vertically on the triaxial base. The membrane extender should slowly be brought down through the sample close to the bottom; the membrane on the bottom side is then slid over the bottom porous stone and the base

pedestal. One of the O-rings is pulled on to the base cap sealing the bottom of the sample.

5. The membrane extender should now slowly be removed, simultaneously sliding the top part of the membrane over the porous stone and top cap. The second O-ring is then pulled over the top cap, sealing the sample within the membrane.
6. The tubes coming from the triaxial base should be fixed onto the top cap, completing the pore pressure connections to the sample.
7. The cell base along with the sample should now be placed within the load frame. The plexiglass cell chamber is placed in the groove on the base of the triaxial cell. The loading piston in the top of the pressure chamber should be locked when it is brought down on the chamber.
8. The load button should be unlocked and brought down slowly to make contact with the sample. If the load button does not easily go into the top cap of the sample, it indicates that the sample is not set upright and should be corrected.
9. The cell chamber can then be secured to the base using the three silver rods. While screwing these rods into the cell base, none of them should be tightened until all three rods are in place. Alternating between the rods while tightening helps in maintaining the top of the test chamber to be level.

The sample is now ready to be tested (Figure A.10).

A.3.2 Starting a test

The triaxial system software should be started and the program's display window opens automatically. The software has four separate stages for a typical triaxial test: seating, back pressure, consolidation and shear. Tabs on the right hand side of the display screen of the software program represent each stage.

Before starting a test file, all the calibration factors of the transducers should be entered and all the sensors that are connected in the system should be zeroed. This is carried out

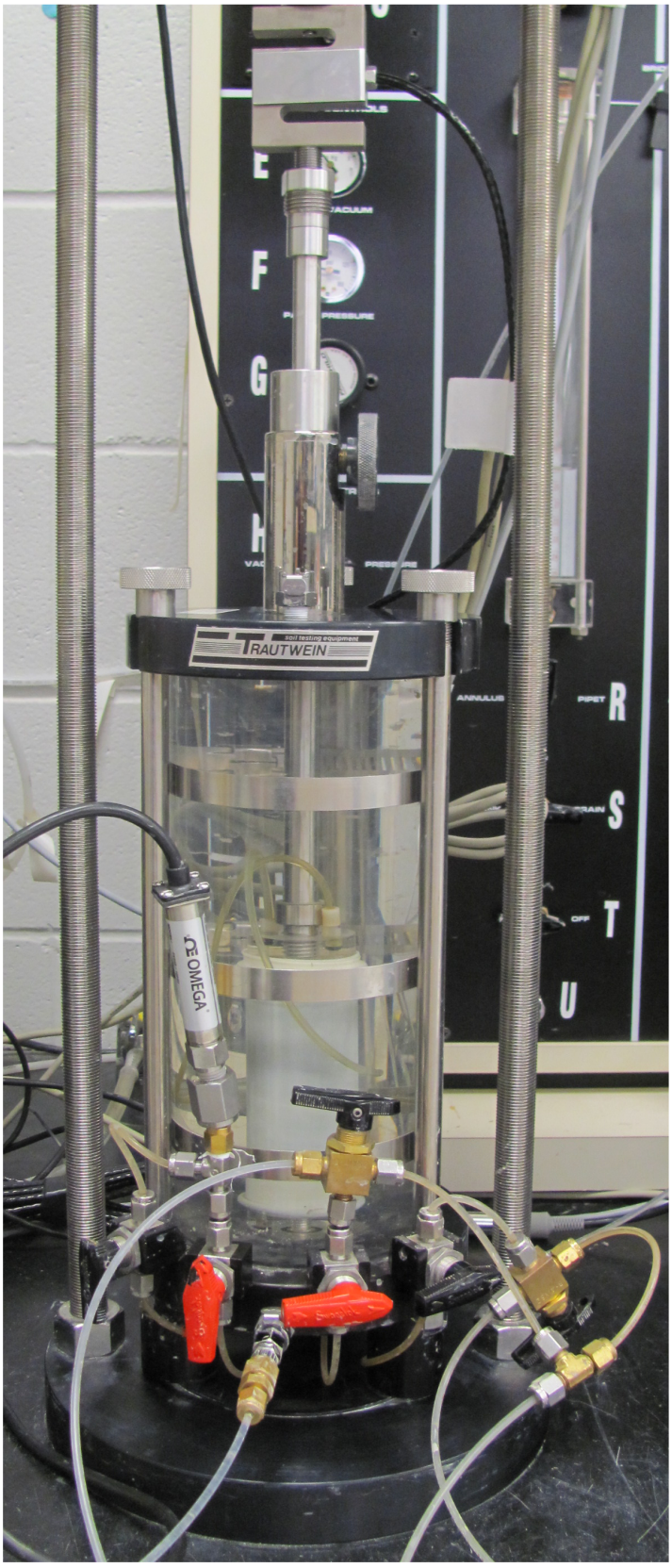

Fig. A.10. Sample placed in the triaxial chamber and ready to be tested.

by using the ‘Sensors’ option in the ‘Setup’ menu. By opening up the ‘Sensor list’ window and selecting a sensor the calibration factors and other parameters for the sensor can be entered. The other parameters that should be checked include the channel that the sensor is attached to, the excitation voltage and the maximum and minimum values (in units) that the sensor is rated for. Additional sensors can be added to the software if required by using the ‘Add sensor’ button in the ‘Sensor list’ window.

The pressure transducers should be left open to atmospheric conditions while taking the zero reading. The load cell should be left free, without any load applied before taking the zero reading. The other parameters can be set once before running the first test (if the sensors used do not change), however the zero reading should be taken before each test. The values entered can now be saved by going to the ‘Setup’ menu and clicking on the ‘Save’ option.

A test data file is created by choosing ‘Specimen Data’ under the ‘File’ menu item and filling in the appropriate details of the sample to be tested. The sample dimensions should be entered here and this is important as all of the calculations based on the dimensions of the specimen use this information as a reference point. This creates a data file which can be saved in the truepath folder. The details of the type of test which will be performed should be entered by clicking on ‘Test Data’ in the ‘File’ menu item. The test parameters are controlled at the beginning of the test and can be changed later on as well. The test data records information on the seating pressure, type of the consolidation including limiting values for effective stress, and information on the shear phase including the rate of loading and its maximum strain.

Once the data file is created, the tabs on the right of the screen become available. At each stage throughout the test, the display screen provides guiding instructions for users. It is important to record zero readings before creating the data files; as any zero values recorded after creating these files will not be saved.

A.3.3 Seating

The first stage of the test is the seating process which involves filling the cell, applying seating confining pressure, flushing specimen drain line and adjusting the cell pressure to maintain the initial specimen volume. A screen shot of the steps involved is shown in Figure A.8. The loading piston is seated by closing the gap between the load shaft and the external cell by using the manual control. With the load shaft locked in place, the 'Seat piston' phase is started by choosing the downward option. This moves the piston attached to the loadframe down until the external force transducer makes contact with the spherical top button of the cell piston and the program automatically stops the process in response to a compressive stress on the external force transducer.

The 'Adjust External Load' phase is initiated by clicking on 'Start' and releases any excess load acting on the load cell to result in a 4 to 8 lb load applied to the piston after which it is unlocked. The cell is then filled with de-aired water from the water tank. The cell chamber should be vented while filling.

A small cell pressure is required to keep the membrane pressed against the specimen during the drain line flushing. The cell seating pressure depends on the specimen tested, the softer the specimen the smaller the pressure. For this research a cell pressure of 13 kPa(2 psi) was used. The cell pressure line from the cell pressure flow pump is connected to the chamber using a quick connect valve at the bottom of the cell. A target pressure is entered in a window that opens on pressing the 'Start' button.

Once the seating pressure is applied, the back pressure pump is used to flush water through the top and bottom of the specimen drain lines. The 2 way switching system (Figure A.3) is used for this purpose. Valves A, B, C and D are kept open, valve F directs water from the back pressure flow pump into the sample and valve G directs water from the sample into the drain. The direction of valves F and G are then reversed to force the water in the pore pressure lines to change direction. This switch is carried out a few times to remove all the air bubbles from the pore lines. The back pressure pump should be refilled as required after this step.

The last phase of the seating stage is the maintain volume step, where a confining pressure is applied to the specimen such that it does not swell. It allows the system to equilibrate. Since this research deals with soft marine clays the time taken in this phase is very short as the response time for the volume change is short. Once data is recorded for 10-15 min, the testing can be moved to the next stage which is applying back pressure to the sample.

A.3.4 Back pressure saturation and B value

The back pressure saturation process involves raising the specimen pore pressure (back pressure pump) while simultaneously maintaining a constant difference (effective stress) between the cell pressure and pore pressure. Maintaining constant effective stress is required so as to not allow the specimen to undergo a volume change. An important criterion for this process is that the pore pressure should be increased at a rate slow enough to allow pore pressure equalization throughout the specimen.

The saturation occurs by two processes. The first process involves compressing air bubbles due to the pressure increase (Boyle's law). This occurs in a matter of seconds. The second process is the dissolving of air into the solution (Henry's law). This is time dependent.

Back pressure saturation is started by entering a 'Target Back Pressure', an 'Effective Stress' and then clicking 'start'. The progress of the saturation can be viewed by clicking on the 'Graph' button. The sample was allowed to saturate for 12-15 hours.

The degree of saturation is given by the 'B' coefficient which can be measured at any time during the saturation process. The B value can be checked by suspending saturation and closing the drain lines. Clicking on 'Check B' opens a window where the cell pressure increment, 34.45 kPa, (5 psi) can be entered. The 'B' coefficient is displayed and the pore pressure increase versus time can be viewed by clicking 'Graph'. Once the B value reaches 0.95 or the sample is 95% saturated the 'B' check can be terminated and the cell pressure

returns to its pre 'B' check value. The top and bottom drain valves can be opened and the software moved to the consolidation phase.

A.3.5 Consolidation

Three different methods can be employed to consolidate specimens. Isotropic consolidation is accomplished by increasing the confining pressure while maintaining constant back pressure. Anisotropic consolidation is achieved by increasing both the axial load and confining pressure such that the ratio between the vertical and horizontal stress remains constant. K_o consolidation is accomplished by increasing the vertical load while adjusting the cell pressure such that lateral deformation is prevented.

Before the start of the consolidation phase the flow pump pistons should be adjusted so that the expected volume change can be accommodated. Depending on the type of consolidation different parameters need to be entered.

For isotropic consolidation, the values of 'Target Effective Stress' and 'Effective Stress Rate' need to be entered and the 'loading' direction must be specified. The 'Unloading' direction is used to achieve an overconsolidated condition. The confining pressure is increased on a linear ramp based on the stress rate provided. Once the target effective stress is reached the system enters a creep mode, where the cell pressure and back pressure are maintained while the specimen volume change can continue. The time for primary consolidation is dependent on the height of the sample typically ranging from 24 hrs to 30 hrs for Gulf of Mexico clay. Specimen equilibrium is determined by viewing the plots available through the 'Graph' button. The program provides access to the following graphs: compression curve, p-q stress path plot, principle stresses versus strain, back pressure versus time and volume change versus time. All of these graphs can be viewed during the consolidation phase at any time.

If K_o consolidation was selected, the values for 'Target Vertical Effective Stress' and 'Strain Rate' should be entered. The target vertical effective stress for Gulf of Mexico clay was set as 140 kPa (20 psi). The aim was to one dimensionally consolidate the specimens

to a target effective stress value which is approximately 1.5 to 2 times larger than the estimated in situ preconsolidation pressure (SHANSEP). The strain rate applied on the specimens was set to 1%/hr. Here consolidation is achieved by subjecting the specimen to a constant rate of deformation and extracting pore water at a rate equal to the specimen area times the deformation rate while adjusting the confining pressure to maintain an excess pore pressure equal to zero. The time taken for the specimen to reach equilibrium in the case of $\mathrm{K_o}$ consolidation is a lot more than isotropic. The process can be monitored by viewing the same available plots.

Before ending the consolidation phase, the drain valves are closed to check if the pore pressure increases. If the pore pressure increases with time the sample should be left to consolidate for another 12-24 hrs. If the pore pressure reading is stable and does not increase, the consolidation phase can be ended.

A.3.6 Shear

The software allows for drained or undrained conditions, compression or extension modes of loading during the shear stage. The shear tab gives all the instructions to carry out this test phase. The input information for this stage is recorded in the 'Test' file. These values can be altered during the test with the exception of drainage conditions, which cannot be changed during the test. Cell pressure is kept constant at the value observed at the end of the $\mathrm{K_o}$ consolidation for that test.

The drainage valves are closed and shearing was started with predefined maximum effective stress and maximum strain value. The strain rate was set to 1%/hr and the limiting strain value set to 15% on the $\mathrm{CK_oU}$ compression and extension tests. The strain rate was set to 5%/hr with 15% limiting strain for the CIU compression and extension tests. A maximum vertical effective stress value of 482 kPa (70 psi) was entered, but the test was always governed by the maximum strain. The test was stopped when either the limiting strain or limiting stress was reached.

The extension tests required a coupling to be screwed on from the top of the piston to the load cell coupling. The reading on the load cell should be constant before and after the coupling.

A.3.7 Test tear down

Test tear down involves removing loads and pressures from the specimen and removing the sample from the chamber all carried out using manual controls. Any coupling between the piston top and external load cell should be undone. The LSCT is removed. The cell chamber should be emptied by connecting the bottom quick connect to the drain and venting the chamber from the top. Once the cell is drained the specimen should be removed without distorting the specimen excessively or losing soil. Final water contents of the sample should be recorded.

APPENDIX B
DATA REDUCTION AND CALIBRATION OF SENSORS

B.1 Calculation

Table 1 lists the formulae used by the data reduction program to calculate the various parameters which are obtained from each test. The parameters directly obtained from the data file are:

- Force
- Cell pressure
- Back pressure
- Pore pressure
- Platen position or current height

The output data file displays the time in a date-time format, which is converted from date-hr:mm:ss to seconds on microsoft excel. The data file is then imported into matlab which computes all the results and plots each graph.

B.2 Corrections

An area correction and membrane correction were applied to all triaxial tests conducted on Gulf of Mexico clay for the testing program described in Chapter 4 and Appendix A. A standard area correction was used, assuming the sample deforms as a right circular cylinder. Details of the corrections applied to the observed data from the triaxial tests are given in this appendix.

The combined area and membrane correction used on the triaxial data is the Baxter and Filz correction explained below (Baxter, 2000).

Table B.1
Formulae used for data reduction

Conversion from volts to engineering units	**Units**=$CF\times$ ($V_{reading}$-V_{zero})/V_{in}	$V_{reading}$= **Transducer reading** V_{zero}= **initial reading** V_{in}= **Excitation voltage**
Axial strain	ϵ_a=H/H_o*100	H_o= Initial specimen height H= Current specimen height
Volumetric strain	ϵ_v=V/V_o*100	V_o= Initial specimen volume V= Current specimen volume
Deviatoric stress	σ_d=F/A_c - M_c	F=Force A_c= Corrected area M_c= Membrane correction
Horizontal effective stress	σ'_h= cp	cp= Cell pressure
Vertical effective stress	σ'_v= σ_d + σ'_h	
Total stress path coordinates	T_s=(σ'_v + σ'_h)/2 T_t=(σ'_v - σ'_h)/2	
Effective stress path coordinates	E_s=(σ'_v + σ'_h)/2 - U_b E_t=(σ'_v - σ'_h)/2	U_b= Back pressure
Lateral stress ratio	K_c=σ'_h/σ'_v	
Friction angle	Φ= $\tan^{-1}$(T_t/T_s)	
A parameter	A= (ΔU - $\Delta\sigma'_h$)/($\Delta\sigma'_v$ - $\Delta\sigma'_h$)	ΔU= Change in pore pressure

B.2.1 Area correction

For this triaxial data the cross sectional area of the specimen was corrected during consolidation and shearing phases assuming that the specimen deforms as a right circular cylinder (barreling failure). This correction is used in the standard test method (ASTM D4767) for consolidated undrained tests and is recommended by La Rochelle et al. (1987) for bulging type failure. The area correction is given in equation B.1.

$$A_c = A_o \times (1 - \epsilon_{vol})/(1 - \epsilon_a) \tag{B.1}$$

where:

A_c = corrected area of specimen

A_c = initial area of specimen

ϵ_{vol} = volumetric strain of sample

ϵ_a = axial strain of sample

B.2.2 Membrane correction

The rubber membrane surrounding the specimen transmits the radial effective stress to the soil particles and also establishes the boundary between the cell fluid and pore fluid. It is well established in the literature that the membrane provides resistance to the applied loads and that it is necessary to correct for its contribution. Henkel and Gilbert (1952) originally developed a membrane correction applied to the deviatoric stress for undrained compression tests, Duncan and Seed (1967) extended their work to include the effect of both axial and volumetric strains. The ASTM standard D4767 provides a membrane correction and recommends correcting for the strength of the membrane if the error in deviator stress due to strength of the membrane will be greater than 5%.

During shearing, a correction was made to the major principal stress in the specimen using equation B.2.

$$\Delta\sigma_v = 4\epsilon_a t_o E/D_o(1-\epsilon_{vol}) \tag{B.2}$$

where:

ϵ_a = axial strain measured from the beginning of shear

t_o = thickness of the membrane at the beginning of shear

E = young's modulus of the membrane

ϵ_{vol} = volumetric strain measured from the beginning of shear

B.3 Calibration of transducers

All the sensors used in this research were soldered and calibrated before use.

B.3.1 Axial displacement transducer

A linear strain conversion transducer (LSCT) was used for measuring the axial deformation in the specimen. It has a total displacement range of 1 in. This measurement should be distinguished from the calibrated screwjack used by the system during the test to determine magnitude and rate of axial displacement. The data from the LSCT was not used for data analysis of the test. The LSCT was calibrated with a depth micrometer calibration device, every 0.05 in a voltage reading was recorded. This process was applied in two cycles, to perform a linear regression analysis and to test the repeatability of the cycle. The linear regression curve is shown in Figure B.1 for the LSCT used.

B.3.2 Force transducer

The force transducer (Omega; LCCA-200) with a range of 200 lbs was incorporated in the system to increase the accuracy of force measurements. The transducer has a voltage range of 3.004 mV/V and a signal resolution of 0.1 mV.

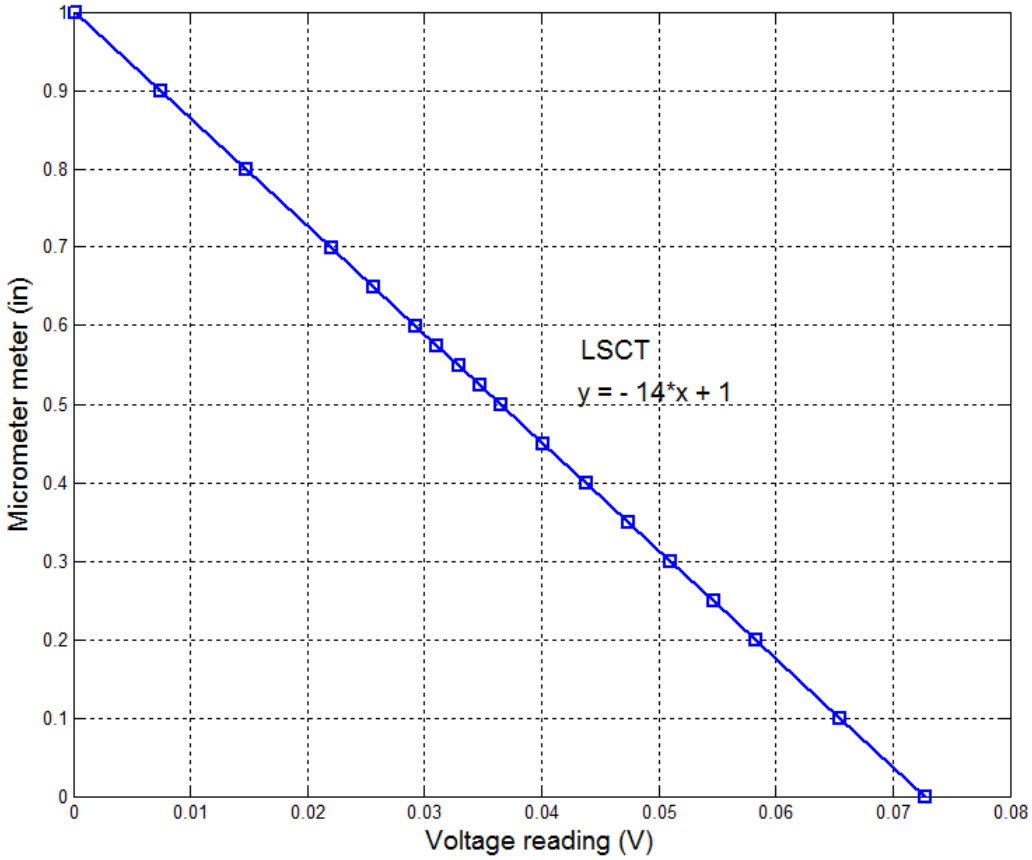

Fig. B.1. Calibration of the LSCT used for this research.

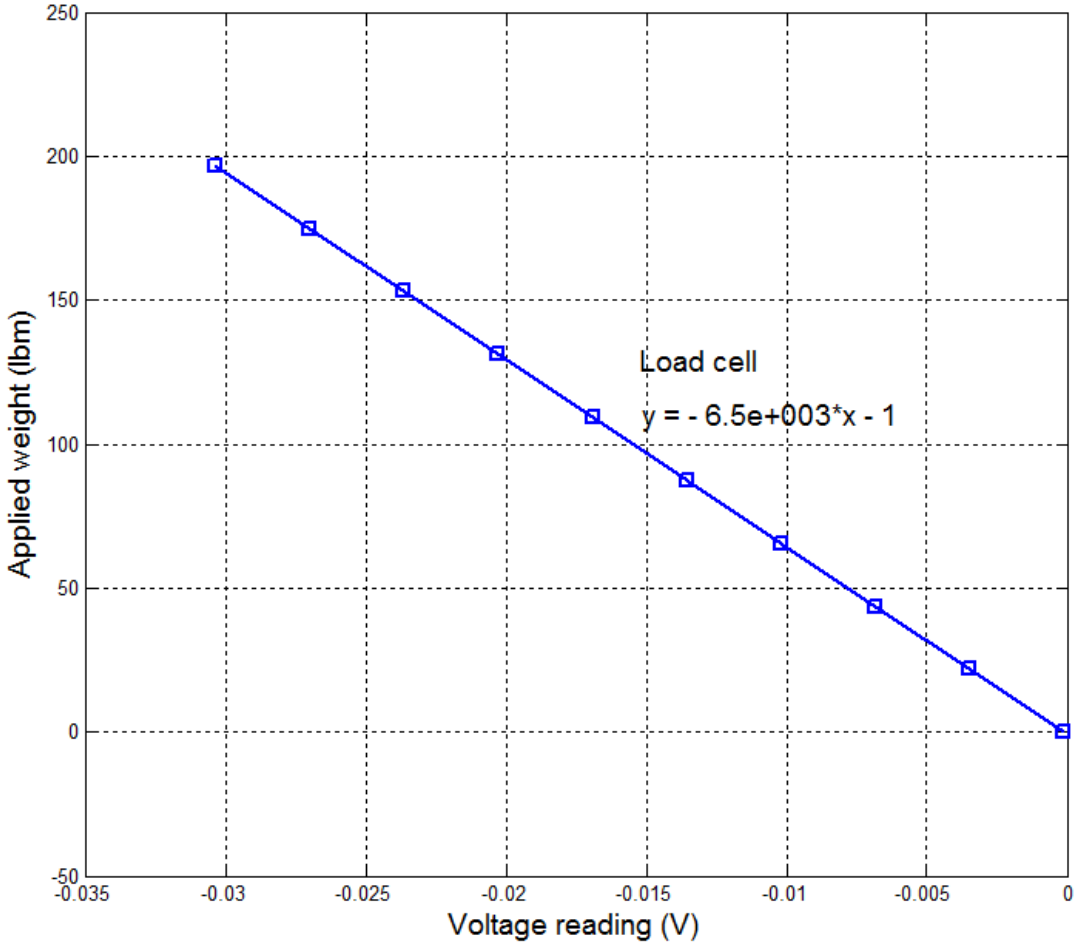

Fig. B.2. Calibration of the load cell LCCA-200 used for this research.

A mechanical calibration device was used to calibrate this force transducer. The transducer was connected to a power supply and a digital multimeter. A physical weight was applied on the mechanical device which transfers the load to the force transducer through a lever arm, the voltage was recorded for each load increment. This process was repeated in two cycles, and a linear regression analysis is performed (Figure B.2). The upward and downward cycles test the repeatability of the calibration.

B.3.3 Pressure transducer

A total of three pressure transducers were used for this research (Omega; PX602 series). Each has a working range of 100 psi. These lower range transducers were preferred as more sensitivity was required for the soft clay.

A hydraulic pressure calibrating device was used to calibrate the pressure sensors. Similar to the force transducer the pressure sensor is connected to a power supply and a digital multimeter to take voltage readings. A hydraulic piston was used to apply pressure to the transducer, known weights were placed in increments to increase the pressure carried by the hydraulic piston. The voltage was recorded with each increment in pressure in both the upward and downward cycles with a linear regression analysis giving the calibration factors.

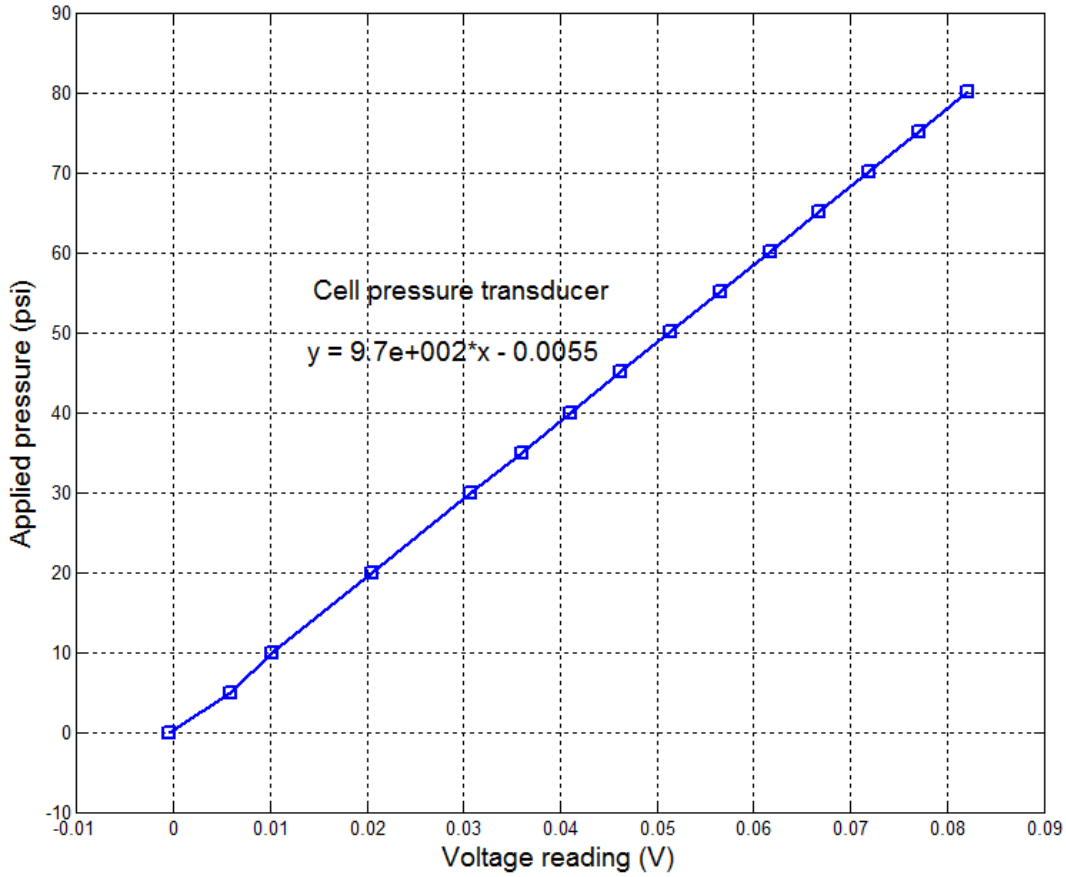

Fig. B.3. Calibration of the cell pressure transducer used for this research.

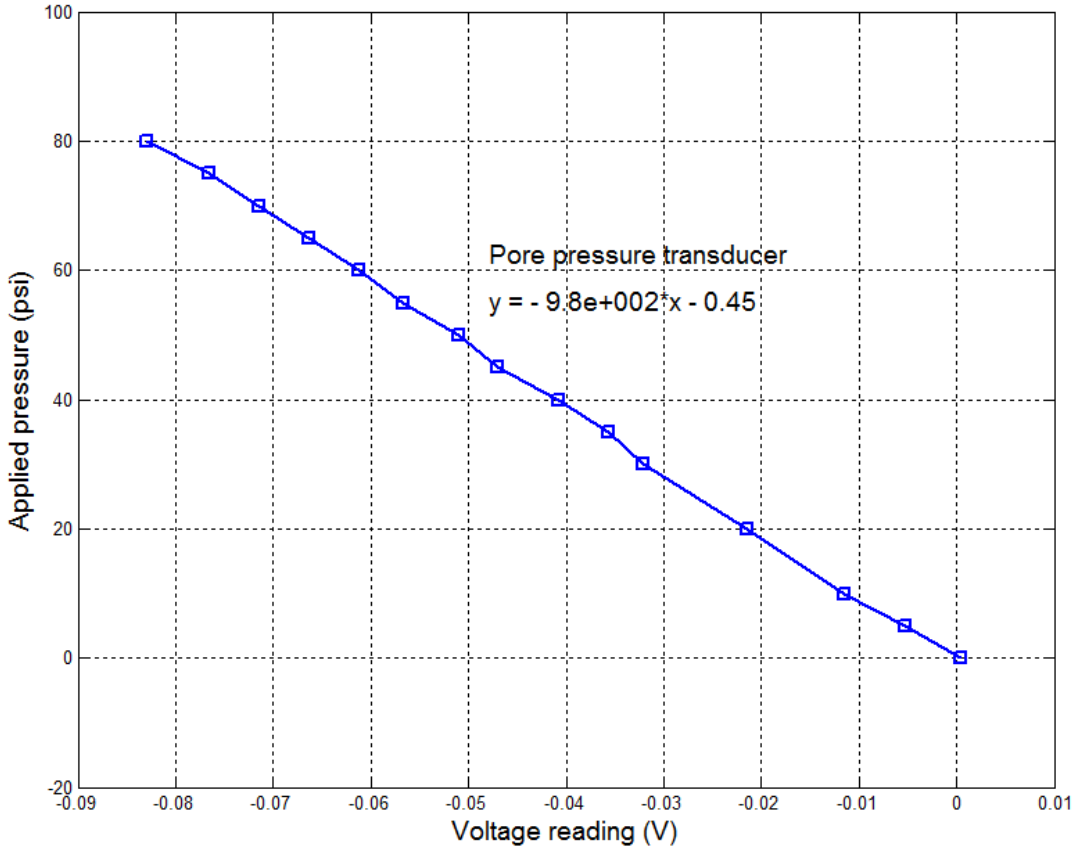

Fig. B.4. Calibration of the pore pressure transducer used for this research

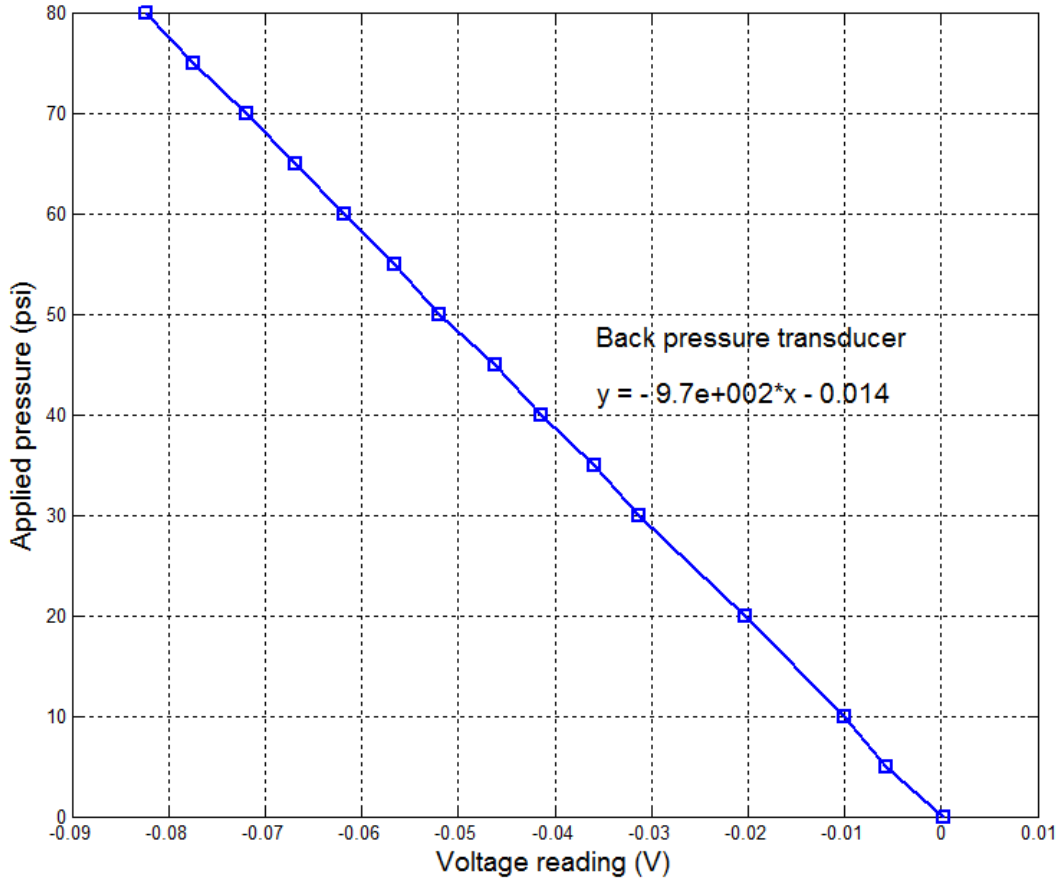

Fig. B.5. Calibration of the back pressure transducer used for this research

VITA

Name: Madhuri Murali

Address: Civil Engineering Dept
c/o Dr Giovanna Biscontin
Texas A&M University
College Station, TX-77840

Email address: madhuri.x.murali@gmail.com

Education: B.Tech, National Institute of Technology, Tiruchirapalli
M.Sc, Texas A&M University, College Station